Delft University of Technology

Wave hydrodynamics in ports

Numerical model assessment of XBeach

A.L.Z. (Andrew) Wong

MSc Thesis

October, 2016

DEME
Dredging, Environmental & Marine Engineering

Wave Hydrodynamics in Ports

Numerical model assessment of XBeach

by

A.L.Z. (Andrew) Wong

to obtain the degree of Master of Science in Civil Engineering

at the Faculty of Civil Engineering and Geosciences of Delft University of Technology,

to be defended publicly on November 9, 2016 at 10AM.

Student number:	4092848	
Project duration:	February 1, 2016 – November 1, 2016	
Thesis committee:	Prof. dr. ir. M.J.F. (Marcel) Stive	TU Delft, Chairman
	Dr. ir. M. (Marcel) Zijlema	TU Delft
	Ir. C. (Coen) Kuiper	TU Delft
	Ir. A.C.S. (Arjan) Mol	DEME Group
	Ir. C.M. (Kees) Nederhoff	Deltares

Final version

An electronic version of this thesis is available at `http://repository.tudelft.nl/`.

TU Delft

Preface

This MSc thesis concludes the Master of Science Civil Engineering curriculum with the specialization Hydraulic Engineering at Delft University of Technology, the Netherlands. The thesis work has been carried out at DEME Group in Belgium as a part of the JIP XBeach initiated by Deltares.

I would like to acknowledge all the members of the graduation committee for their constructive meetings and feedback. Their insights and knowledge in this topic were extremely valuable. Individually, I would like to thank Kees Nederhoff for being my XBeach guru throughout the journey. Our endless discussions were indispensable and it contributed greatly to my process. Arjan Mol, I am grateful for your knowledge on hydrodynamics and numerical modelling. Your guidance, the discussions and the 'trips' to Belgium are much appreciated. Coen Kuiper, your office was always open whenever I had questions about my research, writing or just for a talk. You steered me in the right direction whenever I thought I needed it. Thank you for that.

I gratefully indebted to Marcel Zijlema for your accessibility, knowledge and enthusiasm in wave penetration study with XBeach. Finally, it gave me great pleasure in acknowledging the constructive feedback of Professor Marcel Stive during our meetings. Your comments were very valuable.

Furthermore, I would like to thank my parents, sister and my loved one for their unconditional support.

Deltares is especially acknowledged for providing all the necessary data obtained from their laboratory experiments.

A.L.Z. (Andrew) Wong
Nijmegen, October 2016

Abstract - English

Wave climate in harbours determines for a significant part the efficiency of harbour operations. A good prediction of the hydrodynamics is therefore regarded as indispensable, which is often done by means of advanced numerical modelling. This study is a part of the Joint Industry Project XBeach. The goal of this research is to determine the application limits of the numerical model XBeach (both non-hydrostatic and surfbeat) for the purpose of modelling hydrodynamics in harbours.

XBeach non-hydrostatic, a phase-resolving model where the waves are resolved on the individual wave scale, is theoretically able to predict the hydrodynamics because relevant short and long wave processes are resolved. To this end, the depth-averaged nonlinear shallow water equations are solved. Further, the application range for phase-averaged models is smaller, because the waves are averaged and no phase information is considered to include the dominant wave processes in harbours (e.g. diffraction). XBeach surfbeat *(Roelvink et al., 2009)* is a mix between phase-resolving model (long waves) and phase-averaged model (short waves). This indicates that the long wave processes (e.g. harbour oscillations) are included in surfbeat. This mode uses the energy balance equation, which is coupled to the nonlinear shallow water equations for the long waves.

To be able to examine the applicability of XBeach, two simplified harbour layouts are considered which are subject to a variety of wave conditions. The considered governing wave processes are reflection, diffraction and harbour oscillations. These laboratory experiments are reconstructed in XBeach and its results are compared to the measurements. Wave-structure interaction is not further considered, because the XBeach model does not have the possibility to define structure properties.

Comparison between the simulation results and measurements have shown that periods and wave heights of the short waves ($f > 0.04$ Hz) are only well calculated by XBeach non-hydrostatic. Wave conditions with a relatively large wave height over depth ratios (up to 0.3) are still accurate. XBeach surfbeat gave inaccurate results for the wave heights of the short waves, because diffraction is not considered in the calculation model.
With respect to the long waves ($f \leq 0.04$ Hz), both modes in XBeach are able to reproduce the wave heights, wave periods and the resonant frequencies. The accuracy of the phase-resolving and phase-averaged modes is comparable. However, more confidence is placed in XBeach non-hydrostatic, especially when long-crested waves are involved. The accuracy of XBeach surfbeat for the wave heights is higher if the long waves are still bounded to the wave groups inside the harbour. Without the presence of these short waves, the long waves are free which can freely amplify resulting in an overestimation.

摘要 - 简体中文

港口内的波浪环境在很大程度上决定了港口的运转效率，因此很好的预测水动力条件是必不可少的，而这一过程往往需要借助先进的数学模型。作为JIP XBeach的一部分，本课题的首要目标是确定“XBeach non-hydrostatic”模型和“XBeach surfbeat”模型在模拟港湾水动力条件时的适用范围。

“XBeach non-hydrostatic”模型是一个相位识别模型。其中，波浪被分解成一个个独立的波单独进行分析。通过预测相关的单个长波浪和单个短波浪的波要素，该模型在理论上能够预测出港内的水动力条件。为此，该模型需要解水深平均非线性浅水方程。相比于“XBeach non-hydrostatic”模型，相位平均模型的适用范围较小，因为波浪要素被取了平均值而且港湾内主要的波浪类型（如衍射波浪）的相位信息并没有被考虑。
“XBeach surfbeat”模型结合了针对于长波的相位识别模型和针对于短波的相位平均模型，这表明对长波的预测被完全囊括于该模型中，而且重要的港内波浪振荡作用也得以求解。能量平衡方程的结果可以导出长波的非线性浅水方程。

为了能够验证XBeach模型的适用性，本文还列举了两个包含多种波浪条件的港口设计案例。实验数据通过在XBeach模型中的重新构建出的结果需要与原始测量数据相比对。其中，波浪反射、波浪衍射以及港内波浪振荡作用是本课题中主要考虑的因素。然而，结构、波浪之间的相互作用并未予以考虑，因为XBeach模型不具备定义结构特性的功能。

最终，通过比较模拟结果和测量结果，短波（波频大于0.04 Hz）的波周期和波高只能借助“XBeach non-hydrostatic”模型很好的计算。当相对波高（波高 / 水深）较大（达到0.3）时，“XBeach non-hydrostatic”模型依然适用。当模拟短波的波高时，“XBeach surfbeat”模型运算结果并不准确，因为波衍射并未予以考虑。
对于长波来说（波频小于0.04 Hz），两套模型均能够很好的模拟波高、波周期以及共振频率。相位识别模型的准确性和相位平均模型是具有可比性的。但是，“XBeach non-hydrostatic”模型能够给出更为可信的结果，尤其针对于长峰波。如果长波仍然被限制在港内的波群中，“XBeach surfbeat”模型在模拟波高时具有更高的准确率。如果没有短波，长波能够被自由的放大，从而导致对结果的高估。

Contents

List of Figures

List of Tables

Introduction, Literature Review & Case Description

1 Introduction

1.1. General framework

Further development of XBeach *(Roelvink et al., 2009)* has drawn the interest of contractors and engineering firms who use this open-source advanced numerical model for consultancy, research and design works. These activities have resulted in requests and questions by them about the use and its applications.

Therefore, Deltares has initated the *JIP XBeach* (acronym: Joint Industry Project XBeach) to create a community consisting of engineering companies, contractors and public parties joining together to address the shortcomings, share experiences and further development of the numerical model for other purposes than it was initially developed for. This thesis is a part of the project *JIP XBeach* for the topic **Hydrodynamics in ports** carried out at DEME Group. The Belgian marine contractor DEME Group is especially interested in predicting wave motions in harbours as they are often involved in the design and construction worldwide.

Recently, XBeach has been developed to predict the impact of storms on coastal areas, where the long waves (i.e. surfbeat, infragravity waves) dominates the wave field. These long wave motions are also relevant in harbours, because it can interrupt harbour operations or causes hazardous situations for vessels. XBeach surfbeat (hereafter: SB) could be an alternative for the existing calculation models because of its reasonable computational time and the ability to fully resolve long waves. For example, it *might* serve as a first estimate to predict possible resonance in the harbour. If short waves are not to be neglected, a switch is easily made to the more complete non-hydrostatic mode within XBeach (hereafter: NH). This is also of interest because it is able to compute both the primary and (second order) long waves, but at the expense of the computational ease.

Therefore, the main aim of this thesis is to examine the ability of XBeach SB and NH in predicting wave climates and the determination of application limits for hydrodynamics in harbours in general. In order to assess the performance of XBeach, the numerical results will be compared to measured wave data. These are obtained from laboratory experiments and provided by Deltares.

1.2. Problem description and motivation

The efficiency of a harbour is determined by many factors, such as infrastructure, (local) economy, terminal equipment and downtime during operations. The latter is caused by inefficient cargo handling which is in turn often the consequence of severe hydraulic conditions. Extreme wave conditions, strong cross-current, harbour oscillations or wave period that coincides with the eigenperiod of a vessel could hamper harbour activities and can last for days. In addition, unwanted wave motions are not only a nuisance during the operational phase, but it may also affect the workability of the floating equipment during construction. Therefore, a good overview of the wave climate in a harbour is indispensable.

A priori, it is not easy to determine which hydrodynamic processes are pronounced. To assess the hydrodynamic impact on the harbour operations, prediction of the hydrodynamics is often done in two ways (or combination of both):

- Physical scale model tests.
- Advanced numerical modelling.

Both methods have its advantages and challenges. Laboratory experiments are time-demanding and require facilities such as a basin, wave generator, measurement equipments and several scaled-prototype harbour geometries. On the other hand, almost all the wave processes are involved and good insight is often gained in the hydrodynamics.

Numerical models are less 'labour-intensive' and relatively time -and cost efficient compared to physical modelling. Up to now, few numerical models are tested and validated for wave agitation in harbours. SWASH, MIKE21 BW, TRITON and PHAROS are examples of models that are extensively tested for this purpose and they show promising results in terms of accuracy (e.g. *Boeyinga (2010)*, *van Mierlo (2014)*, *Alabart et al. (2014)* and *Monteban (2016)*). However, the computational time of the current calculation models is quite lengthy and therefore not always attractive to use for initial design.

Recently, attempts are made to use phase-averaged models, e.g. SWAN *(Reijmerink, 2012)*. These type of simulation models are able to do simulations within an acceptable time, but accuracy issues arise especially in situations where processes of the short waves are important.

The above identified issues are the motivations, especially within the *JIP XBeach*, to look for alternative numerical models that:

- have higher accuracies than phase-averaged models (e.g. SWAN).

- are faster than phase-resolving models (e.g. SWASH, MIKE21 BW).
- are cheaper and more time efficient than physical modelling.
- can be used for a quick assessment of hydrodynamics in harbours.

Of course, improving phase-resolving models in terms of computational efficiency is an option, but in this study we seek for an intermediate solution with SB. The NH mode is also of interest, since model set-up is done easily and resolving fully the total water elevation which is relevant for the short waves in harbours.

1.3. Objectives

The aim of this research is to examine the ability of XBeach SB and NH for the purpose of wave hydrodynamics in harbours in general and determine the application boundaries. Data sets obtained from laboratory experiments are available and serve as a case study for the assessment of the model performance.

The research question is as follow:

'To what extend is XBeach (Surfbeat & Non-hydrostatic) able to simulate hydrodynamics in harbours and under which circumstances and conditions can the numerical model be used?'

The objectives are:

- To identify (theoretically) the possibilities and limitations of XBeach for harbour applications.
- To examine the XBeach model (surfbeat and non-hydrostatic) by comparing the results with the measurements, as well as inter-model comparison. The focus is on accuracy and computatonal efficiency.

1.3.1. Study approach

The study consists of roughly three main parts. The study procedure consists of the steps as indicated in Figure 1.1.

1. **Literature review:** as XBeach is the main focus of this study, it is important to understand the model and the governing equations. Insight in the possibilities and shortcomings of the calculation models are studied in more detail. Further, wave processes that may occur in and near harbours that may affect shipping activities are discussed. Based on the literature study, the study limits to and within the possibilities of the XBeach model. The literature review is discussed in

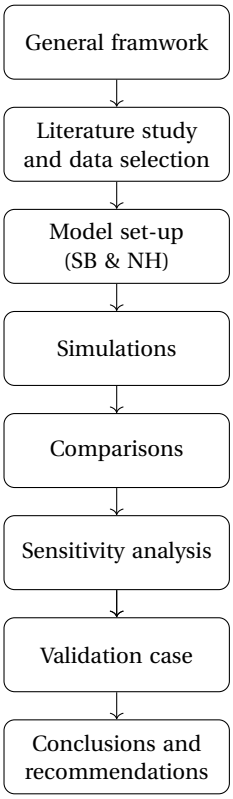

Figure 1.1: Overview research approach in a nutshell.

Chapters 2 and 3. In Chapter 4, the laboratory experiments are briefly discussed. Chapter 7 introduces a methodology to compare the results as well as some terms that are used later on in the study.

2. **Numerical modelling:** This part of the study consists of two parts. Firstly, data from the physical model tests in the Vinjé directional basin with a simple harbour geometry is used in this study to compare the results. To this end, realistic wave conditions are selected. Further, comparisons are made between measurements - models and model - model. This part of the study is elaborated in Chapter 6 for the non-hydrostatic mode and in Chapter 7 for the surfbeat mode.

   The second part uses the same approach and methodology, but with a different harbour layout and wave conditions. It serves as an additional case in order to determine whether the findings in the first part are also applicable under slightly different conditions. The results are presented in Chapter 8.

3. **Model recommendations & practical applications:** The study is concluded in Chapter 9 with recommendations and conclusions regarding the capability and applicability of XBeach.

2

Literature Overview

2.1. Introduction

Harbours are subject to various hydrodynamic processes simultaneously. It is not easy to predict which wave processes cause nuisance, because it depends on many complex factors. This chapter provides a general overview of the most common wave processes found near and in harbours that potentially cause hindrance to harbour operations. Firstly, Section 2.2 presents the basic fundamental theories required for proper understanding of the succeeding matter. The application of the theory in XBeach is further discussed in Chapter 3 where the model capabilities are discussed. At the end of this chapter in Section 2.3, a brief description is given of the existing calculation models for wave and flow in coastal areas that have been used for simulating hydrodynamics in harbours. The discussion on the calculation model aims for a better understanding of possibilities and limitations as well as alternatives for XBeach.

It should be noted that most of the theory is described based on the linear wave theory. A description of the linear wave theory can be, for example, found in *Holthuijsen (2007)*.

Finally, the terminology in this study is as follow: short waves are defined as the waves above a certain split-frequency, whereas the long waves are below that frequency. Generally f > 0.04 Hz and 0 Hz ≤ Hz ≤ 0.04 Hz are the short and long waves, respectively.

2.2. Wave hydrodynamic processes in harbours

1. ***Shoaling*** occurs when waves propagate towards the shore in water that becomes gradually shallower. Consequently, wave speed and wavelength decrease according to the frequency dispersion relationship (Equation 2.1):

$$\omega = \sqrt{gk\tanh(kh)} \tag{2.1}$$

where:

ω	radial frequency	[rad/s]
g	gravitational acceleration	$[m/s^2]$
k	wave number	[-]
h	water depth	[m]

When a stationary situation is considered, the energy flux (Ec_g) is constant along the wave rays (i.e. no energy loss). Wave energy that propagates towards the shore increases per horizontal surface area and hence the wave height ($E \propto H^2$). The shoaling coefficient described by Equation 2.2 indicates that wave height will grow to infinitely when approaching shoreline:

$$K = \frac{a_{nearshore}}{a_{offshore}} \tag{2.2}$$

where the numerator and denominator are the nearshore and offshore wave amplitude, respectively. However, wave breaking or any depth-induced processes ensure that wave height will approach zero at the waterline.

Generally, shoaling is less relevant in a harbour. The water depth is often sufficient large such that there is hardly any interaction of the wave and the bed. In case shoaling does occur however, this process is still negligible for harbour operations, because the wave height was already small and will not increase that much due to shoaling. Shoaling is more pronounced at the foreshore and near the coastline.

Conversely, de-shoaling is a process that occurs. It happens when waves propagate from shallow water towards deep water (e.g. turning basin, access channel). Wave amplitude decreases and the negative impact on harbour operations is much less.

2. ***Refraction***, also a depth-induced process, is turning of waves towards shallower water depth due to the velocity gradient along a wave crest. Consider a wave that is travelling obliquely towards the shoreline. That part of a wave closest to the waterline is in an area of smaller water depth. As the wave speed decreases ($c = \sqrt{gh}$) with decreasing water depth, it then travels with a lower velocity compared to the part of the wave that is in deeper water. The fast-travelling part of the wave propagates faster than waves in shallow water which causes the waves to bend.

The effect of refraction in harbours is noticeable at places with non-uniform bed, for example at the entrance channel or places with heavy sedimentation. Generally, refraction in the basin is not very pronounced since the bed is fairly flat and the water depth is sufficiently large.

3. ***Diffraction*** is the process in which wave height decreases abruptly along the wave crest due to the presence of obstacles. Waves propagate into the shadow zone while the amplitude is progressively decreasing due to the lateral transfer of wave energy resulting in a concentric-circle-like pattern. Generally, further away from the obstacle the wave height decreases as a function of space. The effect is more pronounced for long waves than short waves and is also related to the length of the breakwater. A very long wave, say tidal wave, does not 'feel' the breakwater and a typical diffraction pattern is absence.

   Diffraction is often observed in harbours due to the presence of breakwater or side basin. It is considered that this type of wave transformation - among others - contributes significantly to the energy penetration. Additional effects due to diffraction should be controlled (e.g. reflection of wave energy which may induce unwanted oscillations) by blocking the energy penetration sufficiently.

4. ***Reflection*** occurs when hard boundaries are present and cause (partial) reflection of wave energy. Theoretically, when waves interact with a vertical impermeable wall, all the wave energy will reflect off the wall with almost 100% reflection. In case of a sloping boundary a fraction of wave energy will bounce back.

   Reflection of waves can be expressed with the so-called reflection coefficient K_r which is simply the ratio between the reflective wave height and the incoming wave height (Equation 2.3):

$$K_r = \frac{H_r}{H_i} \tag{2.3}$$

   The actual amount of reflective wave energy depends, among others, on structure characteristics and wave conditions. This process occurs mainly at the inner side of the basin and therefore it is important to have measures to dampen out the wave energy, such as higher friction.

   If too much energy is being reflected, it may generate unwanted effects such as oscillations. Often, reflection characteristics are unknown and then it can be more convenient to express the reflection coefficient in terms of local bed slope and hydraulic conditions, with the surf similarity *(Battjes, 1974)*, indicating the type of wave breaking:

$$\xi_0 = \frac{tan\alpha}{\sqrt{H_{m0}/L_0}} \tag{2.4}$$

   The surf similarity ξ is the ratio between the bed slope and the wave steepness. Roughly speaking, for ξ_0 values smaller than 3, the breaking is associated with the spilling type where much of the wave energy is dissipated. Values larger than 3 indicate surging or collapsing type of breaking. For higher values, it shows characteristics of reflective rather than breaking wave. As it is related to energy dissipation, the amount of reflective energy on a sloping impermeable beach or structure can be estimated via the reflection coefficient. For the short waves, the coefficient is determined by:

$$K_r = 0.1\xi_0^2 = 0.2\pi\beta_H^2, \quad \text{where } \beta_H = \frac{h_x}{\omega}\sqrt{\frac{g}{H}} \tag{2.5}$$

   β_H is the normalized bed slope parameter as a function of the bed slope h_x, radial frequency

ω and the incoming wave height H. Obviously, a steep bed slope results in a higher reflection coefficient. In harbours, steep impermeable structures are present indicating that the reflection coefficient is almost equal to 1.

N.B.: Equation 2.5 is also valid to characterise the shoaling behaviour of long waves *(van Dongeren et al., 2007)*.

5. ***Nonlinear wave-wave interactions*** occur both in deep and shallow water and is the transport of energy to and from higher and lower frequencies. Extra peaks are to be seen in the spectra: subharmonic and superharmonic for lower and higher frequencies, respectively (and is often a multiple of the peak frequency). The level of nonlinearity increases with decreasing water depths; the peaks in the wave spectrum become more obvious.

   These interactions exist when wave components collide. In deep water, called quadruplet wave-wave interaction, one pair of wave component has to interact with another pair. In contrast to the shallow water conditions, where 3 wave components are sufficient, deep water requires at least 4 components. The reason is that resonance of 3 components cannot be induced with the dispersion relation. If wave number, direction and wave frequency of pair 1 coincide with those of pair 2, then energy is transferred amongst the wave components by resonance. The process in shallow water is called *triads wave-wave interaction*. This wave-wave interaction can already be induced if one pair interacts with a third, freely propagating wave component with similar characteristics.

   In a harbour it is not always clear which of those two processes occur because of the intermediate water depth. It can be best assessed by looking at the wave spectra whether secondary (or tertiary, quaternary and so on) peaks of the harmonics are present or absence. Undesired water motions may occur when peaks in the lower frequencies of the wave spectrum become significant.

6. ***Dissipation*** is associated with decrease of energy in a wave field. It is a complex process where turbulence and other nonlinear effects are involved and are therefore still poorly understood. Many attempts are made to describe dissipation with the linear wave theory and the results are quite satisfying. The *common* dissipation processes that are observed nearshore are elaborated briefly.

   (a) Friction: bottom friction is dominant in shallower waters where orbital motions create a very small turbulent boundary layer at the bottom. Essentially, it is a transfer of momentum and energy from the orbital motions to that layer. In deep water, the interaction of orbital motions with the bed are negligible.

   (b) Breaking: breaking waves are often described as depth-induced or steepness-induced breaking. In deep and intermediate water depth, white-capping is the dominant process which is steepness-induced breaking. Many formulations exist to describe wave breaking and are derived empirically. For example, wave steepness in shallow water is limited according to the Miche-criterion. Equation 2.6 shows the upper limit wave breaking:

$$H_{max} \approx 0.14 L \tanh(\frac{2\pi h}{L}) \tag{2.6}$$

where:

H_{max}	Maximum individual wave height	[m]
L	Individual wave length	[m]
h	Local water depth	[m]

In deep water, Equation 2.6 is reduced to $H/L = 0.14$. Essentially, breaking occurs when the wave speed exceeds the horizontal orbital velocity.

In shallow water, wave breaking is associated with the water depth. *Battjes and Janssen (1978)* modified the Miche-criterion and indicates that wave breaking is proportional to the local water depth:

$$H_{max} \approx h\gamma_b \tag{2.7}$$

where γ_b in Equation 2.7 is the breaking coefficient and lies between 0.5 - 0.6 and 0.6-0.8 for regular and irregular waves, respectively. Note that various wave processes can enhance wave breaking by increasing the steepness (shoaling) or may induce an opposite effect (e.g. diffraction, refraction). Note that both Equations 2.6 and 2.7 are determined empirically and the formulations are not very theoretical sound.

7. ***Long waves*** become significant in shallower water, especially when short waves are less relevant or dissipated. Several theories (*Watson and Peregrine (1992), Symonds et al. (1982) and Longuet-Higgins and Stewart (1964)*) have been developed to describe the generation of the long waves. The reader is referred to these papers about the generation mechanism. Below, we will discuss three types of long wave phenomena that are relevant for harbour.

   (a) Long waves forced by wave groups: this phenomenon is the focus of the numerical model XBeach where long waves are fully resolved. They are generated by wave groups due to the difference in radiation stresses under high and low waves. Radiation stresses are defined as the mean value of the momentum flux. In its simplest form, the water level elevation forced by the wave group energy variation is described as *(Longuet-Higgins and Stewart, 1964)*:

$$\frac{\partial^2\eta}{\partial t^2} - gd\frac{\partial^2\eta}{\partial x^2} = \frac{1}{\rho}\frac{\partial^2 S_{xx}}{\partial x^2} \tag{2.8}$$

   where the space and time varying radiation stress:

$$S_{xx}(x,t) = (2n-0.5)E(x,t) = (2n-0.5)(\bar{E} + \hat{E}cos(\Delta\omega t - \Delta kx) \tag{2.9}$$

   The overbar in equation 2.9 indicates the mean energy and the hat the energy modulation due to the wave groups. The long wave elevation in shallow water is calculated according to:

$$\eta_{l,b}(x,t) = -\frac{S_{xx}(x,t)}{\rho(gd - \frac{\Delta\omega^2}{\Delta k^2})} \tag{2.10}$$

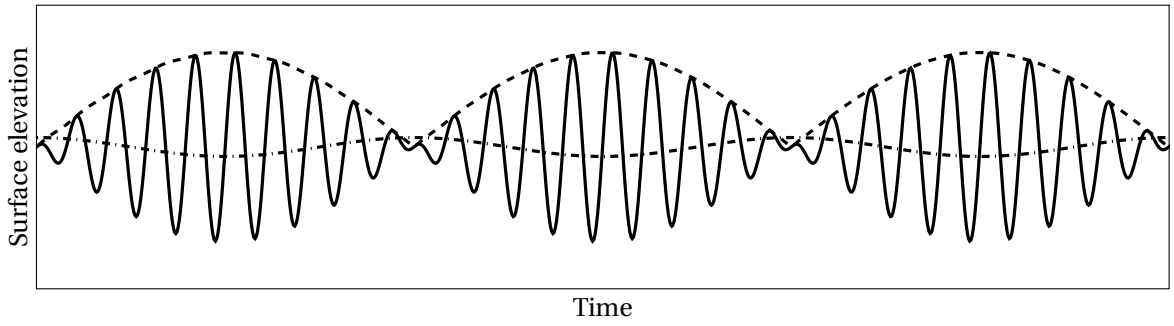

Figure 2.1: Short wave groups and the associated bound long wave. Solid line (−) shows the primary waves with the corresponding bound wave (dash-dotted line −.−) and wave group envelope (dashed line −−).

This water level variation is called bound waves and it travels with the speed of the short wave groups. Equation 2.10 shows that under high short wave envelope (high radiation stresses, high energy) a local water level depression is induced and vice versa. The perfect bound wave in figure 2.1 is phase-locked and in anti-phase (180 degrees) with the short wave envelope indicating that there is energy transfer from the high to the low frequency component. As a result of that, the surf zone is dynamic and moves up and down as function of time and arriving wave group; this is called **surfbeat** and may induce oscillations in the harbour (see below). Once the short wave group structure is lost, the long wave is no longer forced and propagates with its own non-dispersive wave speed $c = \sqrt{gh}$.

(b) Harbour oscillations: when an open sea is connected to a semi-closed basin, **forced** oscillations may occur in the longitudinal direction (direction perpendicular to the harbour mouth) due to penetration of long wave energy such as surfbeat. These long wave oscillations are notorious when the period of the motion equals the natural frequency of the confined system. The first resonance harmonic is called the *Helmholtz mode, fundamental mode or pumping mode* where the water elevation inside the harbour follows the movement of the open sea and is a function of time. In a harbour this may result in excessive vertical and rotational motions of large vessels. This is very likely since the resonant periods of vessels, generally between 30 seconds to 10 minutes, fall into the same range of the eigenperiod of a harbour. Decay of this energetic harbour mode is predominantly due to radiating of the energy out of the harbour via the entrance. If the entrance of the harbour is relatively large, it is obvious that wave energy can propagate in and out the harbour basin easily. This means that narrowing the entrance will reduce the potential incoming wave energy. On the other hand, the restricted harbour mouth leads to amplification of the resonant modes. This is called the *Harbour Paradox* named by Miles and Munk *(Rabinovich, 2009)*.

(c) Seiches: the main difference between seiches and harbour oscillations is the forcing which is said to be **free** for seiches. The schematised basin is fully closed. Seiches arise mainly from external forcing such as nonlinear interaction between short and long waves, wind waves, seismic activities or atmospheric pressure and their impact is in the same manner as harbour oscillations. These oscillations are effectively dampened out by friction and the impact can be minimised by adding sufficient damping and proper port lay-out.

2.3. Numerical models for wave hydrodynamics in harbours

Great variety of numerical models exists that are suitable for modelling the hydrodynamics in coastal waters. When choosing a calculation model, the user should have knowledge about the limitations of the models. Therefore, in this section, we will discuss the 2 main types of models that have been extensively tested for wave agitation in harbours. An overview of the available types is given in Table 2.1. From top to down, the computational effort increases and more hydrodynamic processes are resolved rather than parametrized. In this study, we often refer to the term *complex geometry* and for the remainder of this study we define this term as situations where diffraction of the short waves are not to be neglected.

Numerical models can be distinguish in two main categories: *wave-averaged* and *wave-resolving*:

- ***Wave-averaged*** (or phase-averaged) models are based on energy or action balance equation. The hydrodynamics are described as an averaged process in both time and space (of a wave group) in a statistical way. Therefore, much of the wave information is lost. Processes that need to be resolved on the scale of the individual waves and in complex geometries are therefore less suitable with this model type. Moreover, the numerical implementation is often explicit indicating that numerical stability is subject to a stability criterion. This implies that there is a restriction in the time and spatial resolution. On the other hand, the computational time is relatively small compared to wave resolving models and is therefore very suitable if a vast area is of interest.
- ***Wave-resolving*** (or phase-resolving) models are used where phase information of a wave field is required. Moreover, the model domain of interest is relatively small and the computational grid must be fine enough to solve all the relevant wavelengths. This indicates that short wave processes such as dispersion, diffraction, refraction and shoaling are fully resolved. In complex geometries wave-resolving models are more suitable than wave-averaged models.

Table 2.1: Types of wave models. Adapted from *van der Hout et al. (2015).*

Type	**Calculation model**	**Example**
Wave-averaged	Spectral	SWAN, TOMAWAC
	Wave group forcing shallow water models	XBeach Surfbeat, Delft3D Surfbeat
Wave-resolving	Potential flow - *Mild slope*	PHAROS, MIKE21 EMS
	Boussinesq-type	MIKE21 BW, TRITON
	Non-hydrostatic	SWASH, XBeach Non-hydrostatic
	Free-surface Navier-Stokes	IH2VOF, OpenFOAM

2.3.1. Wave-averaging models

- ***Spectral models***
  Spectral models such as TOMAWAC and SWAN (developed by Delft University of Technology) are computationally very efficient. Although phase information is lost, this often does not present a problem in open ocean where engineers are more interested in the wave climate rather than the behaviour of an individual wave. These models are suitable when conversion of spectral information from offshore to nearshore is needed.

  SWAN model uses the *wave-action balance* which computes wave energy propagation, redistribution and dissipation in the spatial, time, directional and frequency domain. It also includes wave generation by wind (source) and dissipation by friction, white-capping and breaking (sink). Redistribution of energy by quadruplet nonlinear wave interaction is approximated. Further, spectral models provide information in the form of 2D-wave spectrum which describes the energy distribution over frequencies and directions. The relevant wave parameters can be derived from the wave spectrum.

  Recently, efforts are made to include diffraction in approximate form. It remains doubtful whether such models are applicable to predict hydrodynamics in sheltered areas due to their (in)accuracy and numerical instability *(Enet et al., 2006)*.

- ***Shallow-water models forced on wave-group-scale***
  This type of model is a combination of phase resolving and phase averaged. The long waves (or low-frequency motions) are fully resolved with the nonlinear shallow water equations whereas the short waves are solved with the wave-action balance equation. The energy transfer from the wave action balance to the nonlinear shallow water equations induces the long waves. Examples are XBeach surfbeat and Delft3D - SURFBEAT (Delft3D - FLOW User Manual, 2014). For the latter, *van der Molen (2006)* showed promising results of the hydrodynamics in harbours. More details can be found in Subsection 3.2.1 of Chapter 3.

2.3.2. Wave-resolving models

- ***Potential flow models***
  Examples of potential flow models are MIKE21 EMS and PHAROS and both can be classified as mild-slope models. The hydrodynamic forcing of the potential flow models are based on the mild-slope equations (derived from the potential flow theory) and is restricted for wave propagation over mild slopes as the name already indicates. Moreover, the linearised numerical model is only valid to describe small amplitude waves, because it is depth averaged and the vertical structure of the flow is described according to the linear wave theory.

  Mild-slope models are steady-state, which means that the governing equations do not depend on time. By considering a selection of waves with different frequencies and directions, an irregular wave field can be well approximated by superposition of the individual components. Consequently, these models are computationally efficient because phase information is obtained and

its relative short runtime. Wave processes such as diffraction and reflection are resolved, which make this type of model suitable for modelling in complex geometries.

- ***Boussinesq-models***
  TRITON and MIKE21 BW are examples of models based on the Boussinesq's theory. Whereas in shallow water the hydrodynamics can be described by the shallow water equations, the wave behaviour in deep water can be explained by the linear wave theory. Linear wave theory is not valid to describe the hydrodynamics at transitional water depth because the depth over amplitude ratio is too small. Shallow water equations are also not very suitable, because both the vertical and horizontal water motions are still important. The Boussinesq's theory can describe this region better. The base of the Boussinesq's theory is also derived from the potential flow theory. The key difference with mild-slope models is that these models are not depth-averaged, but it takes the vertical flow structure into account.

  The hydrodynamics can be resolved in situations with complex geometries with transitional water depths, such as harbours. The challenge remains in the application limit which is governed by the *kh-value*. Moreover, higher order models (higher order derivatives) allow a larger *kh-value* and water depth. In this way higher accuracy can be achieved, but at the expense of computational ease.

- ***Non-hydrostatic models***
  Recently, non-hydrostatic models such as SWASH *(Zijlema et al., 2011)* and XBeach non-hydrostatic *(Smit, 2008)* are gaining popularity. Governing equations are the three-dimensional nonlinear shallow water equations and a momentum equation in the vertical direction. Non-hydrostatic refers to the non-hydrostatic pressure term in the horizontal momentum equation and therefore it takes the vertical hydrodynamic properties of the flow into account. The frequency dispersion is therefore included.

  The uniqueness of multi-layered non-hydrostatic models is that the hydrodynamic properties are also discretised in the vertical direction rather than depth-averaged; the water depth is divided into *vertical layers*. It allows to compute the frequency dispersion to higher accuracy by simply increasing the vertical layers. The resolution in the vertical is a function of the dimensionless waterdepth *kd-value*; the vertical structure is now an integrated part of the solution. In addition, wave breaking is included in the model where mass and momentum conservation still applies. This makes the calculation model suitable in areas before and after wave breaking. Further, the model with only one vertical layer model is called 'depth-averaged'. The depth-averaged variant of SWASH is similar to that of XBeach non-hydrostatic, see Subsection 3.2.2 of Chapter 3.

2.3.3. Final considerations

From a practical point of view, computational efficiency, robustness as well as user-friendly numerical model are preferred in engineering applications. Obviously, accuracy is important as well. Generally speaking, hydrodynamic modelling in harbours are often done with phase-resolving software as short

waves are not always to be neglected. However, it does not mean that phase-averaged models should be discarded from the user's considerations. A decision support chart is given in Figure 2.2 of how to select a numerical model for harbour applications in certain situations.

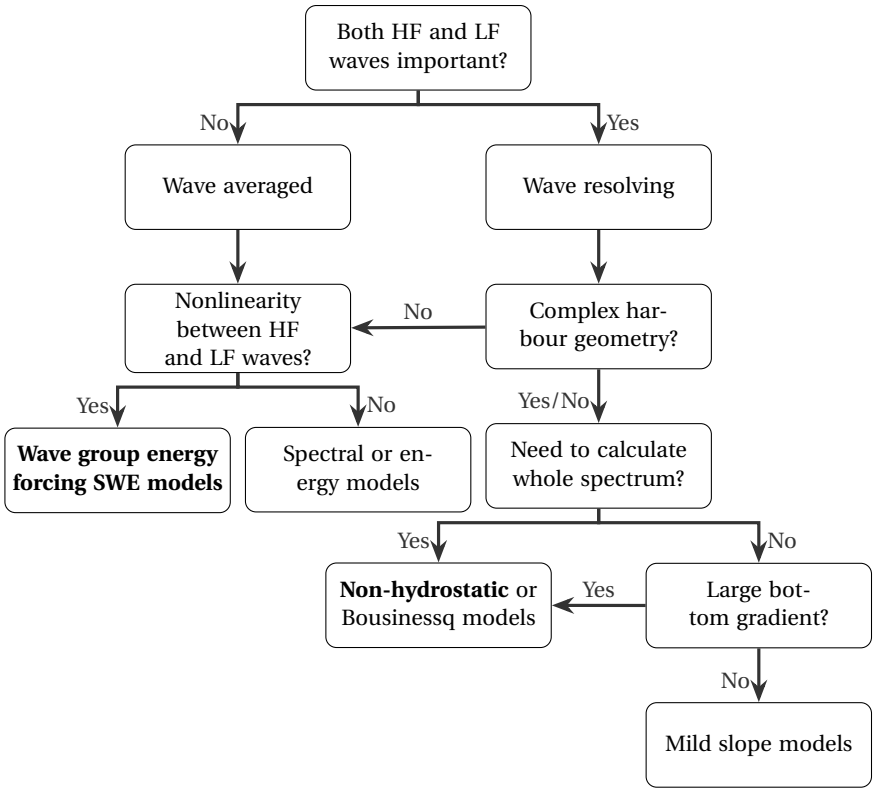

Figure 2.2: A schematic decision support chart. The numerical models indicated in bold are considered further in this research. HF denotes the high-frequency waves, or short waves and LF is the abbreviation for the low-frequency waves, or long waves.

2.4. Conclusion

This chapter has provided a basic overview of hydrodynamic processes in harbours, basics of numerical modelling in ports and the model limitations. Hydrodynamics affect and change each other in the harbour, which makes predictions of the wave climate quite difficult. Obviously, the occurring hydrodynamics may also have impact on the choice for the numerical model. Additionally, if the user is only interested in a specific process, a simpler or cheaper calculation model can be used. The user has to keep the limitations of the calculation model in mind. Some conclusions are drawn with regard to the hydrodynamics in harbours and the current numerical models that are applied in harbour engineering.

- ***Wave processes***
  Reflection, diffraction and harbour oscillations are identified as the most **common** wave processes. Depth-induced processes (e.g. refraction, shoaling) are generally less relevant in the harbour as the bottom topography in the basin is fairly flat and sufficiently 'deep'. Obviously, the occurring hydrodynamics depend on wave conditions, site characteristics and the harbour layout.

- ***Numerical models***

  A great variety of numerical models exists to simulate hydrodynamics in harbours and the choice depends mainly on which process(es) is (are) of interest(s). Wave-averaged models, such as SWAN, are less suitable in situations with complex geometry (e.g. *Reijmerink (2012) and Boshek (2009))* for the reason that phase information is not considered.

  An intermediate solution between the wave-resolving and wave-averaged models are the numerical models that approximate the short waves, while fully resolving the energy on the infragravity band (long waves). In situations where long waves are dominant, it may be interesting to opt for this model type. Examples are Delft3D - SURFBEAT and XBeach surfbeat.

  Finally, phase-resolving models are preferred where short wave processes are important. It fully resolves both the short and long waves, but with the drawback of the long simulation time. Examples of phase-resolving numerical models are TRITON, SWASH and MIKE21 BW.

3

The XBeach Model

3.1. Introduction

XBeach *(Roelvink et al., 2009)* is a two-dimensional process-based numerical model for simulating hydrodynamics, morphology and sediment transport in coastal areas. It has been applied to simulate and predict nearshore morphological processes on a dissipative beach during storms and on the time scale of storms. The XBeach model is tested and validated under these conditions.

Recently, several studies have been carried out with SB to model hydrodynamics where infragravity motions are dominant, such as in reef and atoll environments (e.g. *Quataert (2015)* and *Gawehn (2015)*): the first results are promising. As XBeach is proved to be a robust numerical model and computationally efficient *(Roelvink et al., 2009)*, developers are interested to apply this model outside its 'comfort zone' (e.g. harbours).

This chapter presents a description of the 2 modes of XBeach and discusses the relevant processes and model features related to hydrodynamics in harbours. Based on the model physics, conclusions are drawn about the suitability of hydrodynamic modelling with XBeach in harbours.

3.2. Hydrodynamic modes

The XBeach model has two hydrodynamic modes: hydrostatic and non-hydrostatic *(Smit, 2008)*. In the hydrostatic mode, discussed in Subsection 3.2.1, the user can opt for the stationary or surfbeat variant. The phase-resolving mode (XBeach non-hydrostatic) is further elaborated in subsection 3.2.2.

3.2.1. XBeach hydrostatic

XBeach is developed as a short wave averaged and long wave resolving model. The user can choose, in its hydrostatic mode, between the instationary (surfbeat) or the stationary mode. The main difference is that for the latter one the long waves are not resolved.

Stationary XBeach

This mode is applied during mild wave conditions in combination with tides. It neglects all the long wave (infragravity) motions and wave group variations. Further, wave propagation, shoaling, refraction, directional spreading, bottom friction and energy loss due to wave breaking are resolved. It only solves the wave action balance equation, see Equation 3.1.

Instationary XBeach: surfbeat

Similar to stationary XBeach, the surfbeat mode does not solve the short waves individually. For the initial purpose of the model, this is valid because short waves are often dissipated (e.g. wave breaking, friction) by the time these waves approach the waterline. Instead, the long waves become dominant. An approach that fully describes the short wave is considered to be costly and not necessary. The short wave propagation is described by considering the directionally spread wave group energy that propagates with the group velocity and along a mean direction. The wave action balance given in Equation 3.1 resolves the wave group energy and reads as follows:

$$\frac{\partial A}{\partial t} + \frac{\partial c_x A}{\partial y} + \frac{\partial c_y A}{\partial y} + \frac{\partial c_\theta A}{\partial \theta} = -\frac{D_w + D_f + D_v}{\sigma} \tag{3.1}$$

where c represents the group velocity associated with the peak frequency in the x-direction (cross-shore), y-direction (longshore) and θ -direction (with respect to the x-axis). The terms D at the right side of Equation 3.1 counterbalance the wave energy propagation by dissipation due to wave-breaking (D_w), bottom friction (D_f) and vegetation (D_v). σ is the intrinsic frequency.

The well-known wave action is represented by A in Equation 3.1 and is the ratio between the wave energy density in each directional bin and the intrinsic frequency:

$$A(x, y, t, \theta) = \frac{S_w(x, y, t, \theta)}{\sigma(x, y, t)} \tag{3.2}$$

In SB, there are several options available for wave breaking. Energy dissipation due to breaking, D_w, is by default modelled according to *(Roelvink, 1993)*:

$$D_w = \frac{2\alpha}{T_{rep}} Q_b E_w \frac{H_{rms}}{h} \tag{3.3}$$

where:

$$Q_b = 1 - exp(-(\frac{H_{rms}}{H_{max}})^n) \tag{3.4}$$

the root-mean-square wave height and maximum wave height are obtained from:

$$H_{rms} = \sqrt{\frac{8E_w}{\rho g}} \tag{3.5}$$

$$H_{max} = \gamma(h + \delta H_{rms}) \tag{3.6}$$

where α is a wave dissipation factor , Q_b is a probability function (fraction of breaking waves), E_w is the total short wave group energy and h is the local water depth. The ratio H_{rms}/h in Equation 3.3 is the breaker parameter γ and indicates the point of breaking. Other wave breaking formulation exists and the reader is referred to the XBeach Manual.

The wave group energy dissipation due bed friction is calculated as:

$$D_f = \frac{2}{3}\rho\pi f_w \Big[\frac{\pi H}{T_{rep} sinh(kh)}\Big]^3 \tag{3.7}$$

where f_w is the orbital motion friction factor which is related to the bed roughness. These values are typically in the order of 0.3 for a sand bed. Further, T_{rep} and k are the mean period and wave number, respectively. By default this setting is turned off.

The long wave motions are solved in the time domain using the nonlinear shallow water (hereafter: NLSW) equations which are *coupled* to the wave action balance equation for the wave group variations. The radiation stresses, obtained from the wave energy variation, induce a force on the water column and serve as the input for the NLSW equations. In other words, the long waves are forced by the wave group varying energy.

The wave forces are given by:

$$\begin{aligned} F_x &= -\Big[\frac{\partial S_{xx}}{\partial x} + \frac{\partial S_{xy}}{\partial y}\Big] \\ F_y &= -\Big[\frac{\partial S_{yy}}{\partial y} + \frac{\partial S_{yx}}{\partial x}\Big] \end{aligned} \tag{3.8}$$

The wave forces (Equation 3.8) generate the long waves via the classical nonlinear shallow water equation and consist of the continuity equation:

$$\frac{\partial \eta}{\partial t} + \frac{\partial h u^L}{\partial x} + \frac{\partial h v^L}{\partial y} \tag{3.9}$$

and the momentum equations:

$$\begin{aligned}
&\frac{\partial u^L}{\partial t} + u^L\frac{\partial u^L}{\partial x} + v^L\frac{\partial u^L}{\partial y} - fv^L - \nu_h\Big[\frac{\partial^2 u^L}{\partial x^2} + \frac{\partial^2 u^L}{\partial y^2}\Big] = \frac{\tau_{wx}}{\rho h} - \frac{\tau_{bx}}{\rho h} - g\frac{\partial \eta}{\partial x} + \frac{F_x}{\rho h} + \frac{F_{v,x}}{\rho h} \\
&\frac{\partial v^L}{\partial t} + u^L\frac{\partial v^L}{\partial x} + v^L\frac{\partial v^L}{\partial y} + fu^L - \nu_h\Big[\frac{\partial^2 v^L}{\partial x^2} + \frac{\partial^2 v^L}{\partial y^2}\Big] = \frac{\tau_{wy}}{\rho h} - \frac{\tau_{by}}{\rho h} - g\frac{\partial \eta}{\partial y} + \frac{F_y}{\rho h} + \frac{F_{v,y}}{\rho h}
\end{aligned} \tag{3.10}$$

The considered velocities, u^l and v^L, are the Lagrangian velocity which is defined as the distance a particle travels in one single wave period divided by the corresponding wave period. η is the water surface elevation, $F_{v,x}$ and $F_{v,y}$ vegetation-induced stresses, ν_h is the horizontal viscosity and f the Coriolis coefficient. τ_{wx}, τ_{wy} and τ_{bx}, τ_{by} are the wind shear stresses and bed shear stresses, respectively. Note that the bed shear stresses in Equation 3.10 is related to the long waves only. The short wave energy dissipation is represented with Equation 3.7.

A final remark is made on the computational method. The short and long waves are not resolved on the same computational grid. An advantage of this is that the grid sizes need not be too small; only the long wave motions are solved on the spatial grid whereas the short wave energies are resolved on a directional energy grid. For this reason, the spatial grid size is roughly one order of magnitude larger in contrast to wave-resolving models.

3.2.2. XBeach non-hydrostatic

When short waves cannot be neglected, the user can opt for the non-hydrostatic mode (hereafter: NH) of XBeach. This 2DH mode resolves waves on the scale of the wave itself. It uses the incompressible Reynolds-averaged Navier-Stokes equations as the solver with a non-hydrostatic dynamic pressure term. The governing set of equations are depth-averaged and consists of the the continuity equation:

$$\frac{\partial \eta}{\partial t} + \frac{\partial hu}{\partial x} + \frac{\partial hv}{\partial y} \tag{3.11}$$

and the momentum equations:

$$\begin{aligned}
&u\frac{\partial u}{\partial x} + v\frac{\partial u}{\partial y} + \frac{\partial u}{\partial t} + g\frac{\partial \eta}{\partial x} + \frac{1}{h}\int_{-d}^{\eta}\frac{\partial P}{\partial x}dz = \frac{1}{\rho h}\frac{\partial h\overline{\tau}_{xx}}{\partial x} + \frac{1}{\rho h}\frac{\partial h\overline{\tau}_{xy}}{\partial y} - \frac{\tau_{bx}}{\rho h} \\
&v\frac{\partial v}{\partial x} + u\frac{\partial v}{\partial y} + \frac{\partial v}{\partial t} + g\frac{\partial \eta}{\partial y} + \frac{1}{h}\int_{-d}^{\eta}\frac{\partial P}{\partial y}dz = \frac{1}{\rho h}\frac{\partial h\overline{\tau}_{yx}}{\partial x} + \frac{1}{\rho h}\frac{\partial h\overline{\tau}_{yy}}{\partial y} - \frac{\tau_{by}}{\rho h} \\
&u\frac{\partial w}{\partial x} + v\frac{\partial w}{\partial y} + \frac{\partial w}{\partial t} + \frac{1}{h}(P_\eta - P_{-d}) = \frac{1}{\rho h}\frac{\partial h\overline{\tau}_{xz}}{\partial x} + \frac{1}{\rho h}\frac{\partial h\overline{\tau}_{yz}}{\partial y}
\end{aligned} \tag{3.12}$$

The pressure term P is integrated over the vertical direction and the resulting term is:

$$\int_{-d}^{\eta} \frac{\partial P}{\partial x} dz = \frac{h}{2} \frac{\partial P_{-d}}{\partial x} + \frac{P_{-d}}{2} \frac{\partial(\eta - d)}{\partial x} \tag{3.13}$$

Note that in Equation 3.12 the term τ_b is referred to the bottom friction and $\tau_{x,y}$ to the turbulence viscosity. The reader is referred to the work of *Zijlema and Stelling (2005, 2008); Zijlema et al. (2011)* for detailed derivation and implementation of the equations. In contrast to SB, a big advantage of this NH mode is that the total water surface elevation is calculated. Now, short wave processes such as diffraction and reflection can be solved.

Furthermore, wave breaking is well captured. This process is a difficult phenomenon because it is not only highly nonlinear, but also the additional involvement of air-water interaction makes it complex. Whereas other numerical models (e.g. Boussinesq's) require a separate wave breaking model that initates breaking, this is not needed in the NH mode. The reader is referred to the work of *Zijlema and Stelling (2008)*.

In reality, both nonlinearity of waves and frequency dispersion are important for wave breaking. As the NLSW equations only contain nonlinearity and no frequency dispersion, wave breaking is not always well modelled. However, this NH model includes frequency dispersion, via the vertical gradient of the non-hydrostatic pressure term, which 'counterbalances' the nonlinear behaviour prior breaking and where mass and momentum are (locally) conserved. The actual location of wave breaking is therefore captured. It makes the application of this model prior and after breaking suitable in coastal engineering practises. This feature is considered as revolutionary in terms of robustness and accuracy.

The wave action balance is no longer needed and thus reduction of the simulation time is expected. However, the higher spatial resolution and time restriction make the runtime for a model significantly longer compared to the SB mode.

3.3. Applicability of XBeach

The governing equations of XBeach are discussed in Sections 3.2.1 and 3.2.2 and a relation to XBeach's applicability for harbours is made in this section. This is a continuation of the literature review in Chapter 2. Firstly, we indicate the shortcomings of the numerical model related to hydrodynamics based on the theory discussed. Secondly, an overview is given on how XBeach deals with the common harbour processes.

3.3.1. Limitations of XBeach in general

XBeach makes assumptions to discard or simplifies (irrelevant) processes to reduce computational time. The assumptions made impose limitations and inaccuracies and the user should be aware how that influence the results. Model limitations related to hydrodynamics in harbours are identified below.

Porous structures such as breakwaters and quay walls are an integrated part of the bathymetry. In XBeach, it is not possible to assign a porosity or reflection coefficient to the structure which means that everything is impermeable. This may lead to inaccurate reproduction of the hydrodynamics for a porous (sloping) structure. Because of this shortcoming, porous structures are not considered in this study.

Depth-averaging is applied in the NH mode. The horizontal spatial domain (longshore and cross-shore) consists of grid cells, but the vertical spatial domain only consists of 1 vertical layer, and therefore the vertical profile is said to be depth-averaged. With a single layer, the accuracy of the NH mode is limited by the dimensionless water depth value kd of 1.

The consequence is that the frequency dispersion is less accurately solved, especially in deep water, resulting in phase errors. Moreover, the inaccuracy may impose in an overestimation of the short wave heights, because the characteristics of the vertical structure of the flow is not taken into account explicitly (e.g. energy dissipation due to breaking is underestimated). If the vertical flow structure is also discretised in the vertical direction, frequency dispersion becomes more accurate *(Zijlema and Stelling, 2008)*. Vertical structure of the flow is important for example in situations with wave breaking and flow variation in the vertical dimension.

Wave-averaging of the short wave in SB results in loss of phase information and the surface elevation cannot be obtained. The assumption is considered as a good assumption for the purpose SB was initially developed for: dissipative beaches where long waves are dominant. For some short wave processes, XBeach is able to approximate the physics by taking certain processes parametrically into account (e.g. *Van Geer et al. (2012)*). In the phase-resolving mode, the total surface water elevation is computed.

3.3.2. Modelling of wave processes by XBeach

Numerical modelling in harbours is complex for the reason that many processes occur simultaneously and influence each other in an unknown way. Generally, in situations where short wave action cannot be neglected, it is questionable whether SB is suitable since phase information is not available. What the effects are of this limitation and how other processes are being influenced is discussed in this section. In Section 2.2, common wave processes were identified:

- Reflection.
- Infragravity motions.
- Diffraction.
- Dissipation.

Reflection

Short waves The short wave solver in SB does not contain terms that describe reflection against a sloping beach or structure. Whereas in reality reflection is expected to occur, in XBeach the short wave energy is fully absorbed (dissipated). This is because the energy is proportional to the wave height square and thus a function of water depth. To demonstrate this, we consider a bichromatic wave field that propagates obliquely towards a steep structure without wave breaking as in Figure 3.1.

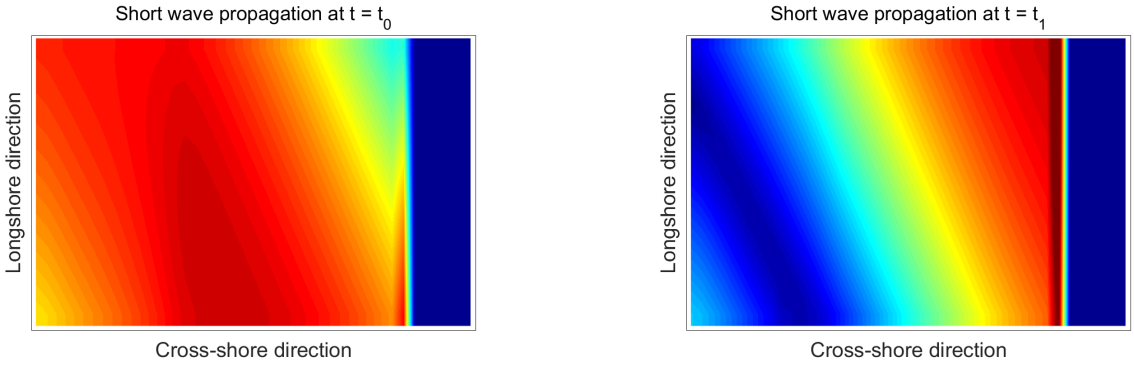

Figure 3.1: Short wave energy propagation and absorption against a steep structure. Wave energy propagation at $t = t_0$ (left plot). Some time later, $t = t_1$, energy is absorbed into the structure (right plot). Main wave propagation is to northeast.

At a certain time t_0, energy propagates towards the steep structure. Some time later, t_1, wave energy is fully absorbed into the structure. Typical diamond patterns that are characterising for reflection are not observed and hence, no short wave energy travel back offshore. The absence of reflection is a drawback since it is considered as indispensable for energy propagation further into the harbour.

The limitation does not hold for the NH model, because the *total* water surface elevation is computed and water is going up and down, similar to run-up and run-down on a beach.

Long waves The absence of reflection of the short waves affects the long waves in the SB mode, especially when the long waves are still bounded to the wave groups. The consequence of the absorbed energy, is that the bound long waves are released which will behave as free waves. This immediately indicates the model limitation, because in reality short wave does reflect off the wall and the long waves are still associated with the wave group. A study carried out by *Daly (2009)* shows that the reflection of the long waves on a sloping beach is well reproduced.

For the NH mode, 1D-tests were carried out *(Deltares (2015b))* to investigate the reflection of non-breaking long wave against a sloping (1:25) steep beach and results were compared with the analytical solution of *Carrier and Greenspan (1958)*. Results of XBeach in the mentioned literatures showed indeed good agreement with the analytical solutions. Theoretically, there is no ground to expect significant differences as both XBeach and *Carrier and Greenspan (1958)* are based on the NLSW equations.

Diffraction

Short waves Essentially, no wave action model, such as SB and SWAN, is able to reproduce diffraction, because it cannot compute the amplitude variation over a small spatial scale due to the lack of phase information. Consequently, short wave energy cannot propagate into the shadow area of a harbour. Energy is even absent if diffraction is the main mechanism of energy penetration. To confirm the lack of diffraction in the model, runs are carried out to check to what extend wave energy diffracts around a breakwater.

Result are compared with the analytical solutions of *Goda et al. (1978)*[1], which provides diffraction coefficients for random waves. It should be noted that the analytical solution is based on an ideal situation with a flat bottom, where refraction and wave energy dissipation are not present. Therefore, these processes are excluded from the model.

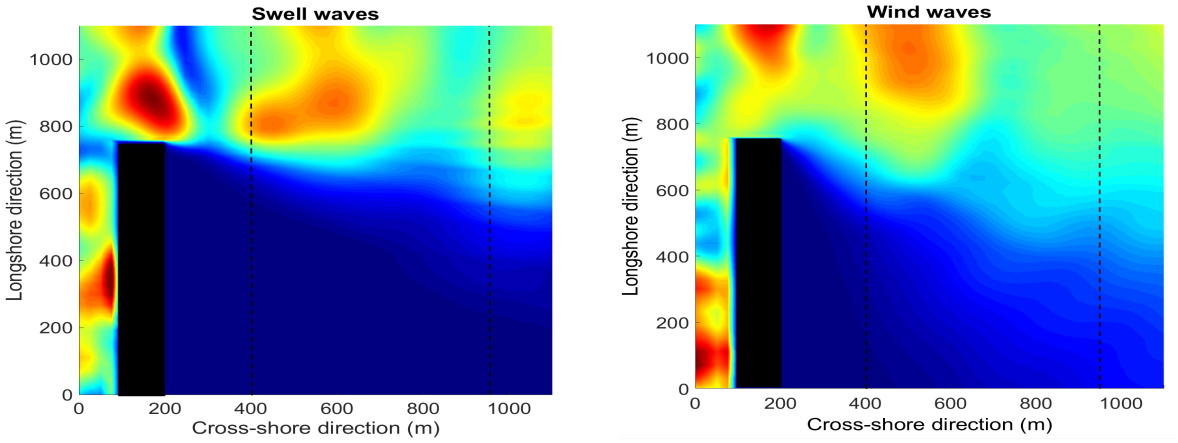

(a) Irregular wave field: swell

(b) Irregular wave field: wind

Figure 3.2: A snapshot of random short waves with characteristics of swell (left) and sea states (right), computed with XBeach surfbeat. Left dashed line is $x/L = 2$ and right dashed line is $x/L = 8$

The models with a frictionless semi-infinite breakwater are forced with a parametrised JONSWAP spectrum with directional spreading that characterises both sea (lot of spreading) and swell (hardly spreading) conditions. The hydrodynamic settings were as follows: significant wave height H_{m0} was 2.5 m, wave period T_p 10 s, water depth h of 100 m and directional spreading of 10 and 30 degrees were used for swell and sea conditions, respectively. The directional grid is discretised into 50 energy bins such that energy can propagate in all direction.

Visually, Figure 3.2a shows almost zero wave energy immediately behind the breakwater. Limited amount of energy is found behind the breakwater in Figure 3.2b, but this effect is solely due to the natural spreading of the incident waves. The diffraction coefficient is determined by the significant wave height at each location on the line $y/L = 2$ and $y/L = 8$ divided by the incident wave height next to the breakwater. The significant wave height is calculated from the root-mean-square wave height and time-

[1] It is not really correct to apply *Goda et al. (1978)* for the SB mode, as the analytical solution is derived for a directional and frequency spectrum, based on linear super position of the Sommerfeld solution for individual waves.

averaged over 1 hour. Figure 3.3 indicates that the model is indeed not able to reproduce short wave diffraction. The wave height (or energy) diminishes rapidly behind the breakwater. Several runs have been carried out to examine the effect of the bin resolution, but the effects are minuscule for 6 bins and more. Adding sufficient (natural directional) spreading of waves, the effect of compensating diffraction remains small. If we look closer to Figure 3.3, the calculated difference with *Goda et al. (1978)* for wind waves is indeed slightly smaller than for swell waves. This is also visually observed in Figure 3.2.

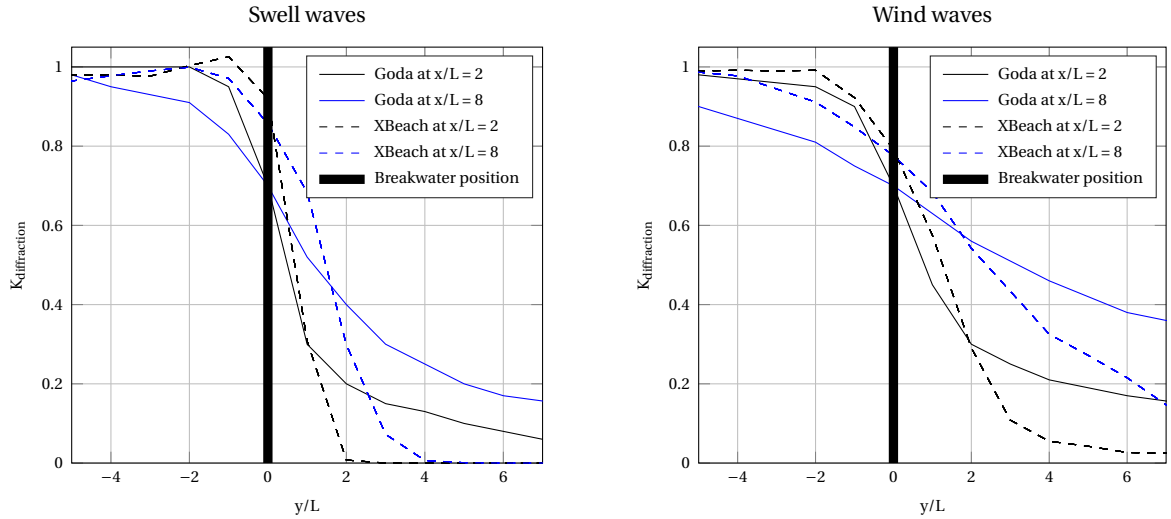

Figure 3.3: Comparison of XBeach surfbeat with analytical solution of *Goda et al. (1978)*.

The NH mode is theoretically able to compute diffraction, but the applicability is limited by the dimensionless water depth kd-value since it is depth-averaged. Accuracy is achieved for a single layer if the kd-value is ≈ 1. With the same hydraulic parameters as in SB, the corresponding value is $kd = 1.05$. The wave length is 120 m for a wave with peak period of 10 s and water depth of 20 m. The water depth is chosen such that the dimensionless water depth is ≈ 1 which is typical for harbours. The grid resolution is based on 20 grid points per wave length. Further, the simulations are run for 1 hour and 30 minutes where the first 30 minutes are regarded as spin-up time. The basic features of diffraction are again compared with the analytical solution of *Goda et al. (1978)* for both sea and swell conditions.

A snapshot is given in Figure 3.4 and the results of Figure 3.5 indicates that the phase-resolving module of XBeach is capable of reproducing diffraction. The differences between the calculation and the Goda theory are due to various reasons and cannot be retrieved ambiguously. Possible reasons are the computational grid (the grid resolution is chosen based on the peak period), short runtime or other model settings. Overall, the results are satisfactory.

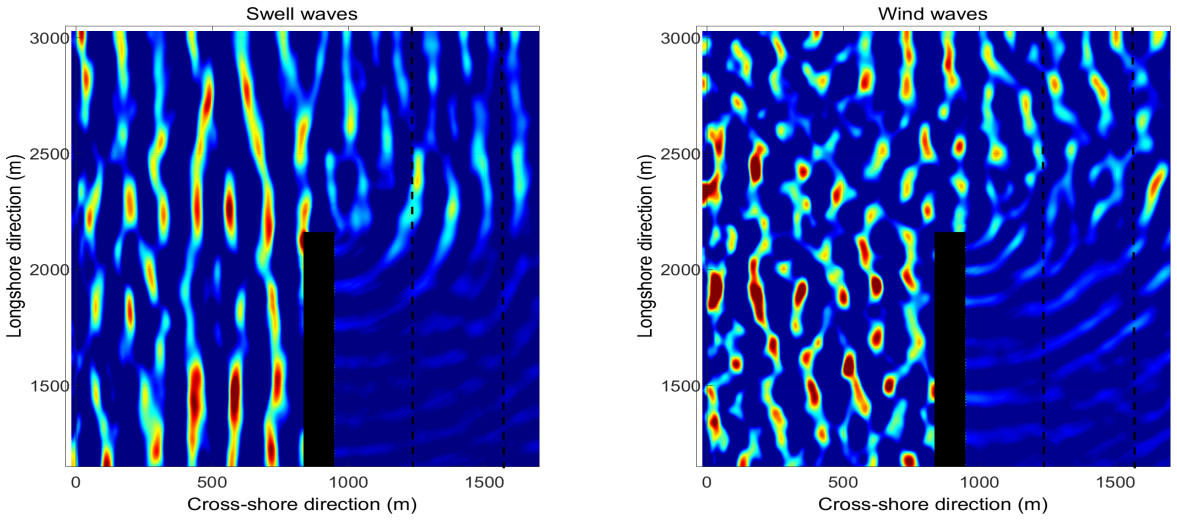

(a) Irregular wave field: swell **(b)** Irregular wave field: wind

Figure 3.4: A snapshot of total surface elevation. Left dashed line is $x/L = 2$ and right dashed line is $x/L = 5$

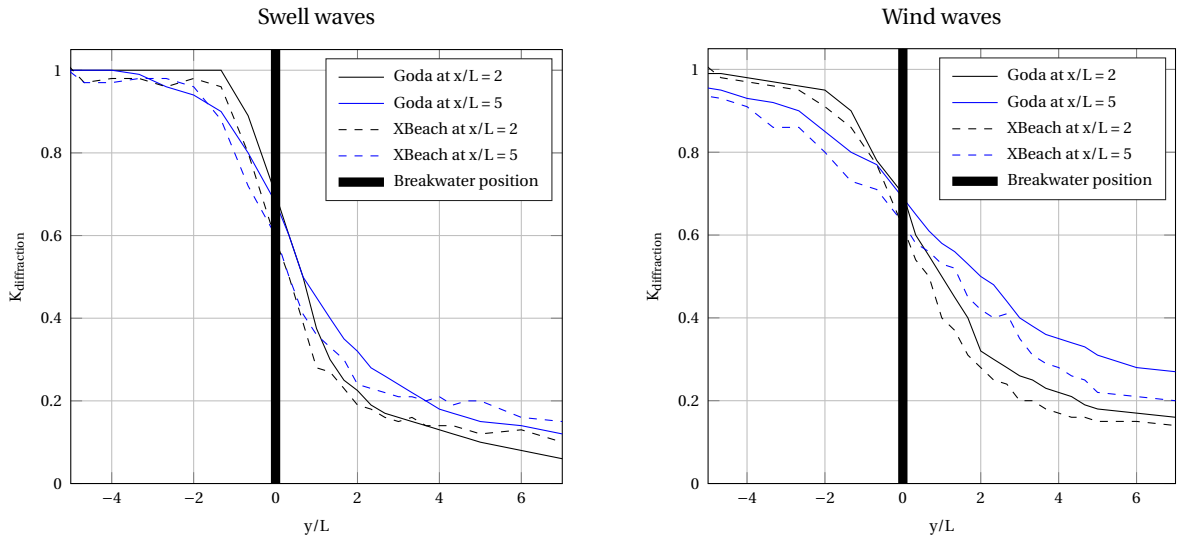

Figure 3.5: Comparison of XBeach non-hydrostatic with analytical solution of *Goda et al. (1978)*.

Some reflection pattern was observed from the lateral boundaries that propagates to the centre of the domain in the NH mode. To avoid that the diffraction coefficient is being influenced by the reflected waves, the computational domain was extended almost 3 to 4 times the length of the breakwater (not shown here). Additionally, the model domain was also enlarged in the cross-shore direction. Numerical instabilities occurred when the breakwater was situated too closely to the offshore boundary. Consequently, the computational time increased because the model domain was enlarged considerably.

Long waves Phase information is computed by solving the NLSW equations which means that long wave diffraction is solved by the model for both SB and NH. Due to the absence of diffraction of the short waves and the associated long wave, there is a water level gradient, which generates free long waves, and these long waves are flowing into the area with significant less wave energy.

Oscillations

Theoretically, SB should be able to compute the oscillations in a harbour of the long waves. The small amount of short wave energy in the harbour due to spreading carries the bound waves, but are released after the short waves are absorbed at the structures. In reality, short waves, bound waves and free waves are responsible for resonance and oscillations, whereas in SB this is predominantly the free long waves (if there is no spreading). The characteristics of these waves are mainly determined by the basin shape, dissipation mechanism and ability of energy radiating out of the harbour mouth.

Based on the governing equations the NH mode uses, harbour oscillations should also be identified by the numerical model (maybe even better than SB due to presence of short waves). Further introduction on harbour oscillations are given in Chapter 4 and examined in Chapter 6 (NH) and 7 (SB).

Dissipation

Dissipation results in the decay of wave height. In the SB mode, dissipation of short waves and long waves are treated separately but at the same time they are inseparable from each other due to the non-linear coupling. As already discussed, breaking of short waves (D_w) generates free long waves. Energy loss due to interaction between the wave motions and the bed (D_f) results in less energy transfer to the long waves (see Equation 3.1). Additionally, long waves also experience friction. Several friction formulations exist to describe flow friction which are included in the shallow water equations. The reader is referred to the XBeach manual (*Deltares (2015a)*).

Dissipation in the NH mode is directly included in the NLSW equation, e.g. via flow friction or wave breaking. It is known that dissipation is often underestimated by wave breaking, because of its depth-averaged mode where the frequency dispersion is less accurately resolved. This often results in overestimation of the wave heights. The influence of energy dissipation in a harbour is further examined in Chapter 6 (NH) and 7 (SB).

3.4. Discussion and conclusion

The physics of XBeach have been discussed and the capabilities as well as limitations are identified. Also, the basic features of the common hydrodynamic processes in general harbour applications and its relation with XBeach have been presented. It is shown that XBeach has limitations when employing it for harbour applications, as some crucial processes are not included in the model. The user should be

aware how the model limitations and assumptions affect the results. Table 3.1 summarises the opportunities and challenges of the two XBeach modes with regard to hydrodynamics in harbour applications.

Table 3.1: Opportunities and challenges of the XBeach modes in harbour applications.

XBeach mode	Pros	Cons
Surfbeat	+ Harbour oscillations resolved + Short runtime + Stable + Straightforward model set-up	– Absence of short wave diffraction & reflection – Reflection coefficient not tunable (long wave) – No structure properties
Non-hydrostatic	+ Long and short waves included + Reflection, oscillations and diffraction resolved + Straightforward model set-up + Frequency dispersion included (accurate if kd ≤ 1)	– Long runtime – Accuracy limited by *kd*-value – Depth-averaged – Reflection coefficient not tunable – No structure properties – Boundary effects

The SB mode has a big disadvantage that many short wave processes are parametrised or not even included. Only energy propagation, shoaling, refraction, wave spreading and some dissipation terms are calculated. Diffraction and reflection are considered crucial in harbour modelling which are lacking. Diffraction cannot be compensated by emphasizing on other processes (e.g. wave spreading), but there are opportunities for this model when diffraction is not dominant - whether or not with reflection. Finally, long waves are resolved, indicating that SB is able to identify resonant frequencies.

The NH mode is much more complete for the reason that both the short and long waves (high and low frequency motions) are resolved. The application limit of NH mode is mainly determined by the dimensionless *kd*-value, as well as the importance of processes that are not tunable by the user such as reflection coefficient and structure properties. The effect of porous coastal structures such as breakwater is therefore not further considered in this study.

Recall Figure 2.2, XBeach SB can be classified as wave-averaged model in the category of *wave group energy forcing SWE models*. XBeach NH is categorised as a wave-resolving model. Both modes are further examined in this study.

Finally, in this research XBeach NH mode is preferred over any phase-resolving model, because inter-model comparison can be done. In addition, once a SB model is already set-up, a switch can be made easily to the NH mode as it is almost identical and therefore saves time in setting up the model. This is considered as convenient for engineering purposes and a quick assessment of the design.

4

The physical model

4.1. Introduction

This chapter presents a description of the two measurement campaigns. For the remaining of this report, all dimensions are in prototype scale unless stated otherwise. The first laboratory experiments were conducted at Deltares in the Vinjè directional basin in 2004. The tests were carried out under controlled conditions for the purpose of validating new numerical models of wave forces on moored ships *(van der Molen, 2006)*. In this study, the dataset is only used to examine the computational skills of XBeach in a harbour basin by comparing the measured and calculated results of the hydrodynamics. Wave forces are not considered in this study.

The second dataset is used to check whether the findings of XBeach from Chapter 6 and 7 are generally applicable. This measurement campaign was carried out for the project *Benchmark tests for Harbour models* in the laboratory basin at Deltares in 2014. As the name already suggests, the dataset is used to validate numerical models for the purpose of wave hydrodynamics in harbours.

4.2. Case I: Vinjè directional basin

4.2.1. Description of the physical model

A detailed plan view of the physical model is given in Figure 4.1. The basin with a water depth of 20 m has dimensions of approximately 4 km x 4 km with a gravel slope at the back of the laboratory basin in order to prevent excess reflection of waves. The ship is positioned at the centre of the basin at a scale of 1:100, and tests were performed on a Panamax container vessel (255 m x 32.3 m x 12 m $LxWxH$).

Furthermore, the wave board has a large number of independent piston type paddles so that waves can be generated obliquely and with directional spreading. Second order long waves are included in the wave board signals in order to produce the correct wave motions. Moreover, it is equipped with an Active Reflection Compensation (ARC) to prevent re-reflection at the wave board and avoiding potential oscillations in the test basin. The coordinate system is defined as a left-handed Cartesian coordinate system with the origin at the wave board. The x-axis is defined as perpendicular to the wave board and the y-axis is parallel to the wave board. The governing hydrodynamic processes are diffraction, reflection and harbour oscillations.

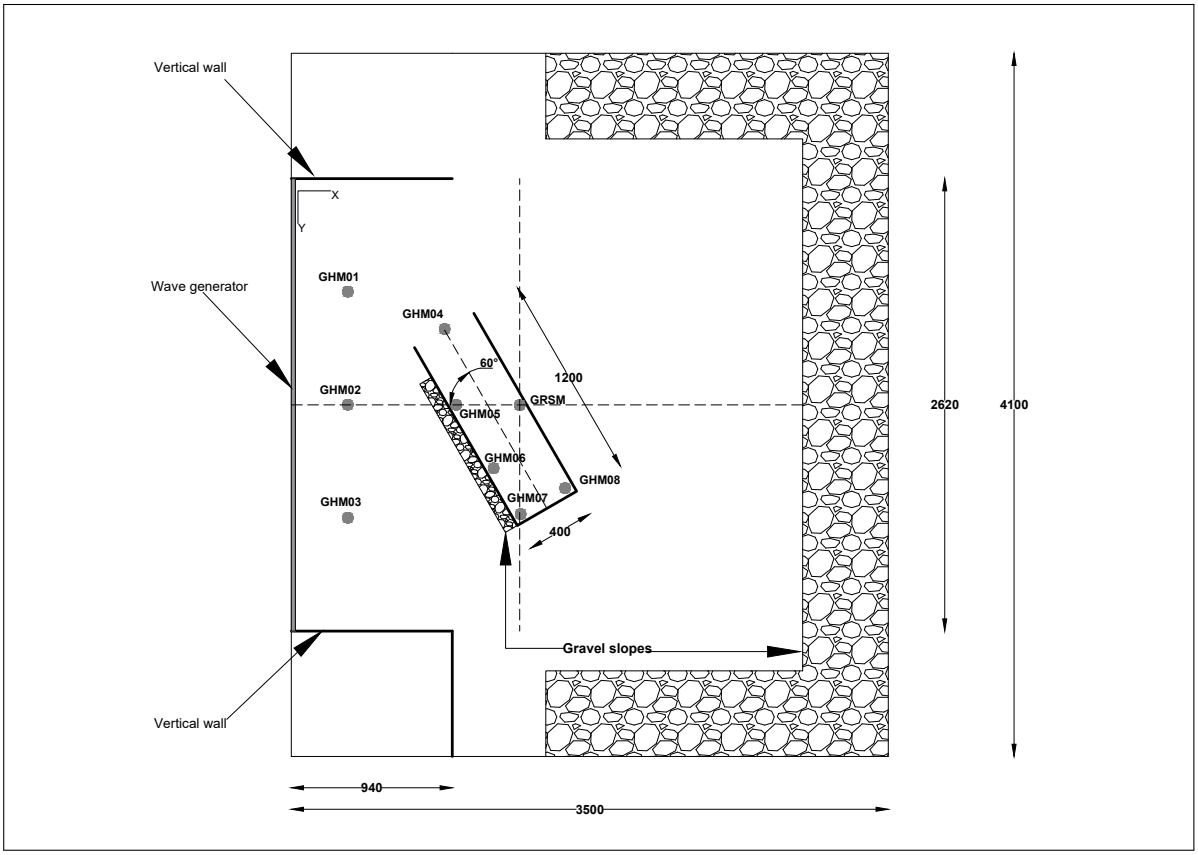

Figure 4.1: Plan view of the physical model. Adapted from *Bijleveld (2004)*.

The following schematised basin situations were set-up for the tests:
Vessel in a schematic harbour basin (Figure 4.1)

- Harbour basin has a dimension of 1200 m x 400 m (internally) and is rotated 120° degrees in the left-handed Cartesian coordinate system.
- Walls are made with B2-blocks with a width of 30 m and wrapped up with foil to ensure that it is fully impermeable for water.
- The vessel is placed at the centre of the basin along the longest wall with a spacing of 4m between wall and ship.
- A gravel slope is constructed at the outer wall facing the wave board to minimise reflection.

4.2.2. Description of the hydrodynamic data

The case considered in this study has in total 9 wave gauges. Complete time series of the water surface elevation are obtained with a time interval of 0.4 seconds and a total duration of 7 hours and 30 minutes. 3 out of 9 wave gauges (GHM01, GHM02, GHM03) are placed offshore, at a distance of 300 m from the wave board and with an equidistant spacing of 660 m. Other measurement points are located at the entrance (GHM04) and several strategic locations in the harbour (GHM05 to GHM08). Measurement point GRSM is positioned at the midpoint of the vessel. Hereafter, this measurement sensor is named GHM09.

The experiments consisted of series of regular waves, random long-crested waves and random short-crested waves. Different main wave directions, peak frequency and wave heights were used for each test case. For the random waves the parametrized JONSWAP spectrum was imposed with various hydraulic parameters. The main wave directions are defined with respect to the wave generator in the Cartesian coordinate system, i.e., direction of 270 degrees is perpendicular to the wave board.

We shall only consider the irregular waves, mimicking typical real-life wave conditions. The JONSWAP wave conditions are recorded in Table 4.1. Wave conditions A are chosen because the waves inside the harbour are dominated by long waves in SB, for which the calculation was initially developed for. Wave conditions B are picked in order to examine the presence of short waves.

Table 4.1: Wave conditions of the test series. Peak enhancement factor γ is 3.3.

Test	H_{m0} (m)	f_p (Hz)	Directional spreading (cos^{2s})	Main wave direction (°)
A1	3	0.1	$\propto$ - unidirectional	270
A2	6	0.1	$\propto$ - unidirectional	240
B1	3	0.1	s=5	270
B2	6	0.1	s=5	240

Oscillations in the harbour basin are expected in two directions: longitudinal and transversal. The longitudinal direction is a schematised 1D basin with an open boundary (harbour mouth) and closed boundary (harbour wall). The node is located at the open end of the basin whilst the anti-node can be found at the closed side. In the transversal direction, the basin is assumed to be a 1D fully closed basin with anti-nodes for the water level at both ends. The harbour frequencies are calculated with:

$$T_0 = \frac{4L}{(2m+1)\sqrt{gh}} \qquad (4.1) \qquad\qquad T_0 = \frac{2l}{n\sqrt{gh}} \qquad (4.2)$$

Where L is the longitudinal basin length, l the transversal basin length and h the water depth. Equation 4.1 calculates the eigenperiods in the longitudinal direction for $m = 0,1,2,3,\ldots,m$. For $m = 0$ the equation reduces to the fundamental mode and represents the energetic Helmholtz mode. The corresponding wave length equals four times the length of the basin (quarter-wave oscillator). The eigenperiods of the closed basin $n = 1,2,3,\ldots,n$ is represented by Equation 4.2 where the first mode has a length of two times the basin length. An overview of the possible harbour oscillations is recorded in Table 4.2.

Table 4.2: Eigenfrequencies in longitudinal and transversal directions. m and n indicate the longitudinal and transversal direction, respectively.

Longitudinal		**Transversal**	
Mode	Calculated [Hz]	Mode	Calculated [Hz]
m = 0 (Helmholtz)	0.0028	n = 0	N/A
m = 1	0.008	n = 1	0.018
m = 2	0.013	n = 2	0.035
m = 3	0.020	n = 3	0.053
m = 4	0.025	n = 4	0.070

The above given resonant frequencies are valid for an idealised 1D (rectangular) basin. By changing the harbour geometry, 2D effects might play a role if the basin is not long and narrow (width $\ll$ length), inducing coupled eigenperiods. In such cases, both the length and the width becomes important and a factor should correct for the 2D effects. The eigenperiods in a 2D basin are approximated with:

$$T_0 = \frac{2\alpha}{\sqrt{gh}}, \quad \text{where } \alpha = \frac{1}{\sqrt{\left(\frac{n}{l}\right)^2 + \left(\frac{m}{L}\right)^2}} \tag{4.3}$$

Theoretically, infinite numbers of oscillation modes are possible, but they are not always present as higher modes are often dampened out by friction or not even excited. The possible 2D resonant frequencies are listed in Table 4.3. In the measurements, resonant modes were identified by looking at the

Table 4.3: Coupled eigenfreqiencies due to 2D-effects.

Modes m	Modes n	Coupled eigenfrequencies [Hz]
1	0	0.006
2	0	0.018
1	1	0.019
2	1	0.021
2	2	0.036
0	1	0.017
0	2	0.036
1	2	0.037

peaks in the wave spectrum. In almost all cases, the first Helmholtz mode was always present as calculated in Table 4.2. Some of the coupled eigenperiods in Table 4.3 did also show up. Analysis of harbour oscillations are further elaborated in Chapter 6 and 7 along with the XBeach results.

4.2.3. Discussion of the measurement campaign

Physical modelling is a very efficient tool to obtain the wave climate in a harbour. Even though the tests were carried out in a controlled laboratory environment, it remains difficult to obtain the right accuracy especially when physical modelling is involved in shallow water with focus on the long waves. Processes that affect the measurement accuracy are discussed in this section.

The ARC in the wave board should absorb the backward travelling waves from the basin, but it is hardly possible to eliminate ***all*** reflected waves due to directional spreading and obliquity of waves. The influence of reflected short waves in this case is not significant as most of the energy is dissipated against the outer slope of the harbour basin. This however does not hold for the long waves: dissipation is not very pronounced. Additionally, the harbour basin is relatively large compared to the laboratory basin so that large part of the energy reflects and propagates back to the wave board. They are responsible for spurious and secondary effects such as (possible) oscillations in the laboratory basin. Thus, the measured time series of the total water surface elevation are contaminated with the re-reflected long waves.

Further, attempts have been made to absorb as much energy as possible at the boundaries by using gravel slopes. Standing wave pattern is possibly present in the laboratory basin, because not all long waves are absorbed at the wave board. However, oscillations are not observed in the wave spectra, but nevertheless care should be taken when interpreting the results in the harbour. A small deviation can cause a different harbour response. Due to the complexity of the laboratory basin, resonant modes are hard to determine.

A scaling method needs to be chosen to convert from physical model to prototype dimensions. Regardless the method, scaling effects always occur. The Froude scaling method was used aiming for correct scaling between the inertial and gravity forces with the dimensionless Froude number $F = U/\sqrt{gd}$ since we are dealing with free surface flow. In typical hydraulic engineering applications, gravitational forces and frictional effects (viscosity) are important. By applying the Froude scaling law it is assumed that gravitational effects are dominant over the viscous effects. The downside of this method is that viscous effects are not properly scaled, because the Reynolds parameter in model tests and prototype differs. For various reasons, Froude and Reynolds number cannot be satisfied simultaneously. The Reynolds parameter is smaller in the model tests than in prototype which means that the flow characteristic is more of a laminar-nature. Consequently, the frictional effects are larger in the experiments than in prototype (low Reynolds number, higher friction factor).

4.3. Case II: Benchmark tests for harbour models

This section presents a summary of the laboratory experiments under the project name *Benchmark Test for Harbour Models*, carried out at Deltares. For more and detailed information, the reader is referred to the report of *van der Ven (2016)*.

The goal of these laboratory experiments is to produce a dataset to validate numerical models for the purpose of wave agitation in harbours. The tests are carried out under controlled environment mimicking typical wave conditions. The laboratory experiments are scaled with the Froude scaling law on a scale of 1:20. The physical model is presented in prototype scale, because first test runs in physical model scale, numerical instabilities occurred.

A plan view of the harbour basin is shown in Figure 4.2. The usable laboratory basin with a water depth of 8.8 m has a width of 800 m and length of 600 m. The waves are imposed at the offshore boundary with

a wave generator that consists of 100 individual paddles which are able to force spread waves into the test basin. The paddles at the side of the wave generator were not always fully used in order to prevent excess reflection against the side gravel slopes. Moreover, it is equipped with an ARC to prevent re-reflection at the wave board and avoiding potential oscillations. The governing hydrodynamic processes are diffraction, reflection and harbour oscillations. Relevant structure properties are listed in Table 4.4.

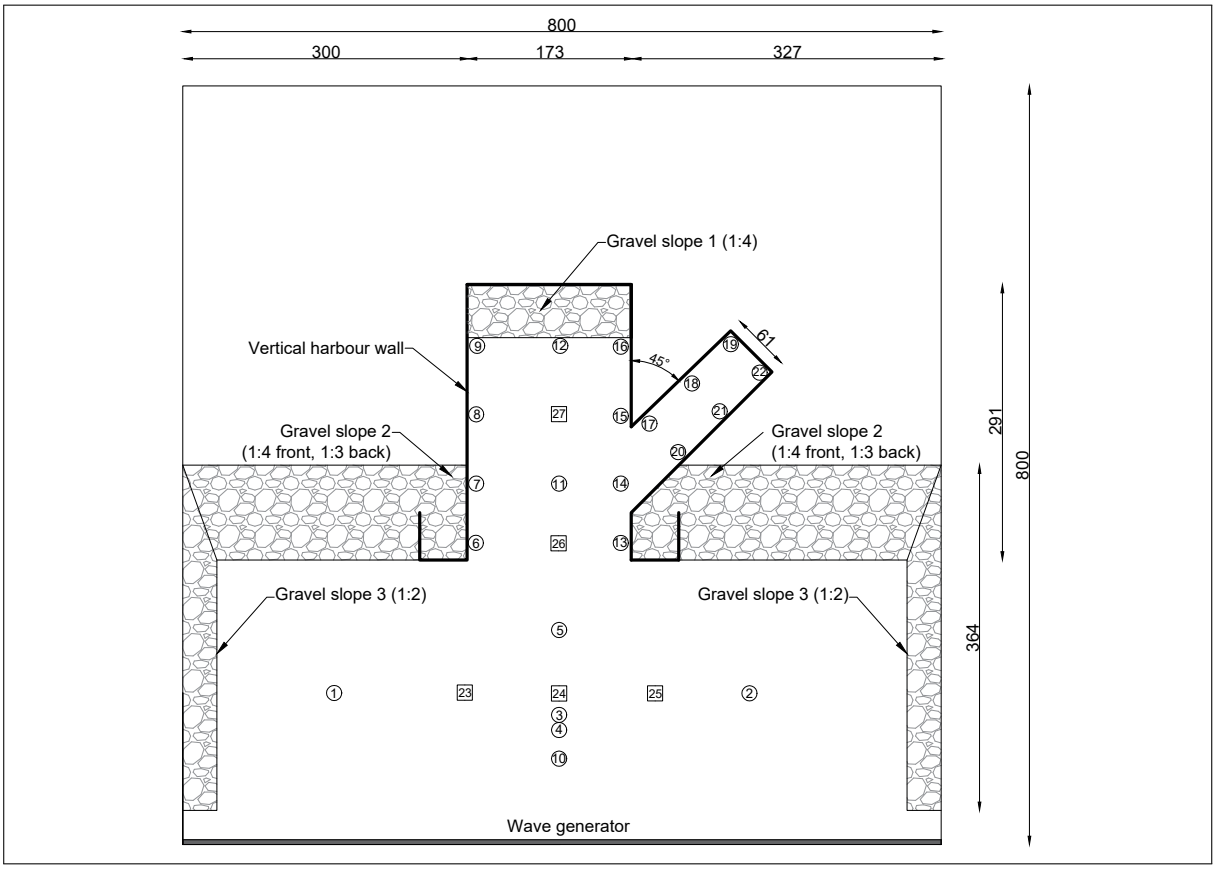

Figure 4.2: Plan view of the harbour case considered. Circles denote the wave height meters, boxes measure both wave heights and directions. Adapted from *van der Ven (2016)*.

Dimensions of the harbour basin are:

- The main harbour basin is 173 m wide and 291 m long.
- The side basin is 61 m wide and 210 m long.
- The gravel slopes are placed in order to minimise reflection of the short waves.

Table 4.4: Structure properties.

	Length (m)	Width (m)	Height (m)	Slope	Material
Harbour wall	4	6	26	Vertical	Concrete
Gravel slope 1	–	56	14	1:4	Gravel
Gravel slope 2	–	100	14	1:4	Gravel
Gravel slope 3	–	36	18	1:2	Gravel

4.3.1. Description of the hydrodynamic data

The case considered in the validation study has in total 27 wave gauges. Complete time series of the water surface elevation are obtained with a time interval of 0.11 seconds and with a total duration of 2 hours and 15 minutes. The wave gauges are positioned close to the harbour walls, because at this location vessels (un)load their cargo and thus encounter the most nuisance at that place.

Various wave conditions were imposed on the physical model: monochromatic waves, bichromatic waves, spectral waves (JONSWAP) and combination of sea and swell waves. The main wave directions are defined with respect to the wave board in the Cartesian coordinate system, i.e., direction of 90 degrees is perpendicular to the wave board. The x-axis is defined along the wave board, the y-axis defined positive at 90 degrees counter-clockwise to the wave board with the origin at the leftmost point of the wave board.

The considered wave conditions in this study are irregular waves, described with a JONSWAP spectrum. The JONSWAP wave conditions are recorded in Table 4.5. The main differences between the two selected wave conditions are the significant wave height H_{m0} and the directional spreading.

Table 4.5: Wave conditions of the test series. Peak enhancement factor γ is 3.3.

Test	H_{m0} (m)	f_p (Hz)	Directional spreading (cos^{2s})	Main wave direction (°)
T038	0.98	0.15	s = 4	90
T046	1.04	0.15	$\propto$ - unidirectional	90

Harbour oscillations are expected in two directions: longitudinal and transversal for both the main and side basin. The theoretical resonant frequencies are calculated from Equations 4.1 and 4.2 and are listed in Table 4.6. The expected resonant frequencies are based on a simple rectangular basin.

Table 4.6: Eigenfrequencies in longitudinal (m) and transversal n directions.

Main basin		**Side basin**	
Mode	Calculated [Hz]	Mode	Calculated [Hz]
m = 0 (Helmholtz)	0.0081	m = 0 (Helmholtz)	0.011
m = 1	0.024	m = 1	0.030
n = 1	0.027	n = 1	0.077

4.3.2. Discussion of the measurement campaign

Measurement errors are inevitable and can cause the discrepancies between the measurements and the modelling results. Some issues regarding physical modelling have already been addressed in Subsection 4.2.3 and also apply here.

The measurement accuracies of the equipment are available and are as follow. The wave height meters have an accuracy of 0.5%. This allow us to say that the measurements are accurate and that any differences between the model results and measurements are mainly due to discretisation, schematisation and/or lack of relevant processes in the numerical model.

4.4. Assumption for numerical modelling with XBeach

Assumptions are made with regard to the measurements in order to set-up the XBeach model. When analysing the model results and the measurements, it is necessary to keep in mind the following:

- The long waves are assumed to be long enough such that it fully reflects off the structures. This is not a bad assumption because in XBeach long waves are also fully reflective. Short wave energies are assumed to be absorbed (SB) or nearly dissipated (NH) when they approach the sloping gravel structure.
- The measured time series of the surface elevation is considered to be correct, although it could be contaminated with re-reflected waves from the wave generator (see Subsection 4.2.3). Both the physical model and XBeach show limitations with regard to energy absorption at the offshore boundary, although different in nature (numerical versus mechanical). The wave fields for both the model tests and numerical modelling could therefore differ slightly, but the effect is not very clear.
- At first, bottom friction of the short waves for the SB mode is assumed to be of minor importance because of the smooth flat bed in the basin. Additionally, the laboratory experiments were carried out in intermediate waterdepth where friction is less pronounced.
- The measurements are presented in prototype scale which means that the physical model has already been scaled. Due to the laminar-nature of the flow in the model tests (lower Reynolds number) and thus higher frictional effects, the model results are expected to be (slightly) overestimated.
- Wave breaking is not significant, because the characteristic wave height over wave length is below the steepness-induced breaking criteria, see Section 2.2 of Chapter 2.

4.5. Conclusion

This chapter has given an overview of the physical model tests conducted at Deltares in 2004 and 2014. Case 1, as presented in Section 4.2, is used to examine the calculation abilities of XBeach in a fairly simple, rectangular harbour basin. The second case, discussed in Section 4.3, is used to check whether the findings of the test case are generally applicable. For both cases, the governing wave processes are reflection, diffraction and harbour oscillations. Only these will be further considered in this study. Further, the wave conditions imposed in the model are shown, along with the expected harbour oscillations. Also, some crucial aspects regarding the measurement campaign are pointed out such as the inability of absorbing extremely spread waves and scaling effects. These findings need also be taken into account when setting up the numerical model and comparing the results.

Methodology & Numerical Modelling

5

Methodology and Terminology

5.1. Methodology

Two cases (Chapter 4) are considered in this study to assess the model performance. For both cases, the measured results are simply compared with the results as calculated by XBeach SB and NH. An extensive analysis is carried out for the first case (Chapter 6 and 7), while for the second case (Chapter 8), it serves as a confirmation or refutation of the findings of Case I.

A common method is introduced to assess the model accuracy in a more objective way: the bias and the Mean Average Error index (MAE) (see for example *Sutherland et al. (2004)* and *Roelvink et al. (2009)*). The bias of an individual wave gauge is calculated as:

$$bias = \frac{\left(X^i_{XB} - X^i_{Lab}\right)}{X^i_{Lab}} \tag{5.1}$$

and the MAE index is computed with:

$$MAE = \frac{1}{N}\sum_{i=1}^{N}\left|\frac{\left(X^i_{XB} - X^i_{Lab}\right)}{X^i_{lab}}\right| \tag{5.2}$$

where N is the number of data points, X^i_{XB} and X^i_{Lab} are the calculated and measured variable, respectively. The bias in Equation 5.1 is the difference between the model parameter and measured parameter, normalised with the measured parameter. The MAE is the average of biases and an index of the model skill.

The assessment of the measurement-model and model-model agreement is as follows. A MAE index $\leq$ 0.20 is regarded as good, 0.20 < MAE $\leq$ 0.35 is regarded sufficient, and index of MAE > 0.35 is considered

poor. The same holds for the bias of the individual wave gauges. The range is based on the uncertainties in the calculation model, absence of various processes and measurement errors. Additionally, the values (long wave heights) are small and thus the MAE index is more sensitive for a deviation.

5.2. Terminology

For the remaining of the thesis, the results are presented separately for the short and long waves. The terminology throughout the report is consistent and is defined as follows. The long waves are defined as 0 Hz ≤ Hz ≤ 0.04 Hz and the short waves as f > 0.04 Hz. Because above this limit, a clear distinction is observed in the wave spectra between the short and long waves, see also Appendix A. The wave heights calculated from the wave energy in the SB mode (short wave module) are also classified as short waves.

The focus in this study is on the resonant frequencies, wave heights and wave periods. These resonant frequencies are the frequencies when the wave periods corresponds to the eigenmodes of the harbour basin. They are determined by analysing the wave spectrum and calculating the largest energy peaks. Further, the significant wave heights and wave periods are estimated with $H_{m0} \simeq 4\sqrt{m_0}$ and $T_{m01} \simeq \frac{m_0}{m_1}$, respectively. m_0 is the water level variance of the energy spectrum and m_1 is the first-order moment of the spectrum.

6

Case I: Non-hydrostatic

6.1. Introduction

This chapter discusses the ability of XBeach NH by reproducing Case I as discussed in Section 4.2 of Chapter 4. It was concluded that diffraction, reflection and harbour oscillations are the governing wave processes with this harbour layout. Based on the literature review in Chapters 2 and 3, the NH mode should capture these processes. The model performance with this increased complexity where various wave processes can interact is further examined here. The goals of discussing NH mode of XBeach are as follow:

- Examine the predictive skill in harbours with the NH mode for both the short and long waves by comparing the model results with the measurements.
- Discuss the shortcomings of SB in Chapter 7 using the results of NH.

Additionally, in Chapter 7 the results of NH are compared with SB for the long waves.

The outline of this chapter is as follows. Firstly, a brief introduction about the model set-up is given in Section 6.2. Secondly, the results are compared with the measurements in Section 6.3. The chapter is concluded in Section 6.4.

6.2. Model set-up

A brief overview of the general model parameters are discussed below. The chosen model parameters are set according to the imposed conditions of the measurements. Hydraulic/model parameters that

are not trivial are kept default. For a more detailed description, the reader is referred to Appendix A. The NH model settings are as follows:

- Non-uniform grid resolution of 4 m based on 30 grid points per wavelength (rule of thumb) in and near the harbour basin. At the lateral boundaries the grid resolution are 10 m to reduce the simulation time as well as dampening out the reflected waves due to boundary effects (for the latter, see also Subsection 3.3.2 of Chapter 3.
- Bottom friction C = 55 $m^{1/2}/s$ (XBeach default).
- Harbour walls C = 55 $m^{1/2}/s$ (XBeach default).
- Gravel slope between wave maker and harbour wall C = 20 $m^{1/2}/s$, to compensate for the higher friction of the gravel slope. This value is chosen based on several trial - and error runs.
- Model is forced at the offshore boundary with a parametrised JONSWAP spectrum, see Table 4.1.
- Gravel slope at the rear of the domain was excluded, otherwise the computations takes too long.
- Weakly-reflective offshore boundary condition is imposed where reflected long waves can pass through the boundary with minimal reflection if they are travelling nearly perpendicular.
- Advective boundaries are imposed at the lateral sides of the domain. Using the default Neumann boundary condition resulted in a gradual drop of the water level. The use of this boundary condition, second-best after Neumann, induces the reflection problem as described in Subsection 3.3.2.
- A CFL - condition of 0.5 is used to ensure numerical stability due to the high and steep waves.

6.3. Results

This section compares the results of NH with the measurements as presented in Section 4.2 of Chapter 4. Firstly, a general remark is made on the required simulation time to obtain reliable spectral results. The reproduced short waves are presented first, followed by the long waves.

6.3.1. General

The time required to obtain reliable spectral parameters is determined with Figure 6.1. The wave heights at each burst half hour are normalised with the wave height at the end of the simulation. The upper plot of Figure 6.1 shows to be steady-state after 3.5 hours (spin-up time excluded). As a rule of thumb, approximately 500 to 1000 waves are needed to obtain spectral wave parameters, which corresponds to $\approx$ 3 hours.

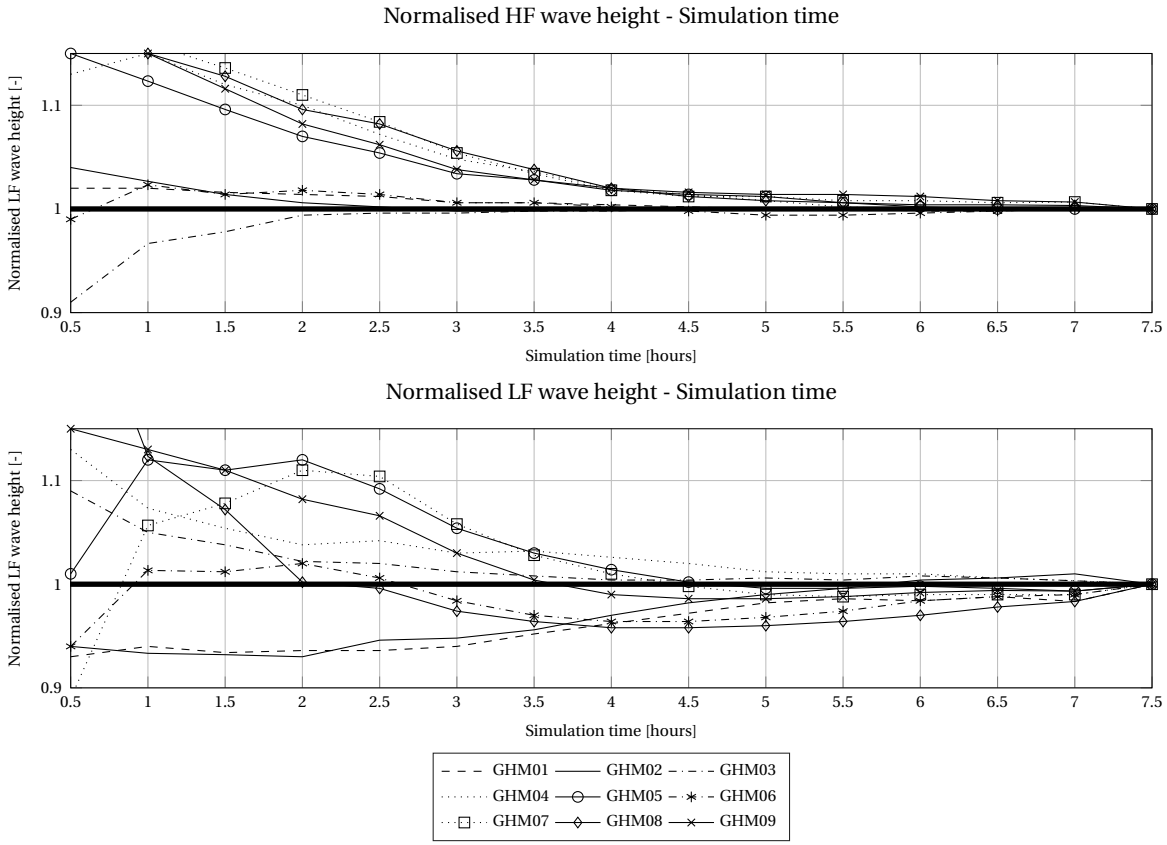

Figure 6.1: Required simulation duration of XBeach in Test A1.

The required simulation duration for the long waves is determined based on lower plot of Figure 6.1. Although it shows the same trend as for the short waves, the long waves never reach a steady-state during the simulation. The determination of the wave heights with a duration of 4.5 hours should be sufficient.

6.3.2. Short waves

This subsection compares the results of NH with the measurements as discussed in Section 4.2 of Chapter 4 for both the short-crested and long-crested short waves. The directional spreading parameter in the JONSWAP is set to $s = 1000$ for the long-crested wave conditions, as recommended by the XBeach manual, corresponding to $\approx 2.5°$. The short-crested waves has a spreading parameter of $s = 5$ which is $\approx 35°$.

In a semi-confined system such as a harbour, the wave field may be dominated by the standing wave pattern which is observed in the calculations (for example Figure 6.2). The spectral wave heights at some locations are consistently higher (node of the water level) than other locations (anti-node of the water level). Furthermore, the one-to-one comparison is not advised for the reason that the location of the wave gauges in the laboratory tests also plays an important role. An example is the measurement

location GHM06. Here, the measured wave height is slightly lower than at other locations inside the harbour. Possibly, the wave gauge is situated on the transition between the node and anti-node and consequently a lower wave height is measured. This trend is also observed for the other test cases. Therefore, this wave height obtained at this location is therefore less reliable.

By plotting the measured wave heights (circles) on the overview map, it gives a better view whether the point output is situated on the node, anti-node or in between. The choice for the output location can differ with a factor two in the significant wave height for the short waves. This point output problem can be avoided by requesting the water levels with a distance from the exact output location, for instance with a circle with a diameter of a typical vessel size. The diameter of the circle equals 120 m, half the vessel size considered in Case I. A smaller circle diameter may result in a smaller range (i.e. $H_{m0,max}$ and $H_{m0,min}$) of the significant wave heights, while a larger circle results in a larger standard deviation. Additionally, the circle covers an area where both the nodes and anti-nodes are found.

The averaged significant wave heights from the circle and spectral wave periods with the uni-directional wave conditions are recorded in Table 6.1 and visualised along with the measurements in Figures 6.2 and 6.5. It should be noted that, due to the averaging of the wave heights, some information is lost and that the possible differences between the measurements and model results cannot be retrieved unambiguously.

Table 6.1: Significant wave heights in metres and spectral wave periods in seconds of Tests A1 and A2. MAE A1 H_{m0} = 0.06, MAE A1 T_{m01} = 0.14, MAE A2 H_{m0} = 0.15 and MAE A2 T_{m01} = 0.12.

	Test A1						**Test A2**					
GHM	H_{m0} Lab	H_{m0} XBeach	Bias	T_{m01} Lab	T_{m01} XBeach	Bias	H_{m0} Lab	H_{m0} XBeach	Bias	T_{m01} Lab	T_{m01} XBeach	Bias
1	3.01	3.00	-0.05	8.17	9.31	+0.14	6.08	5.64	-0.07	8.46	9.33	+0.10
2	2.96	2.90	-0.02	8.16	9.32	+0.14	6.65	6.95	+0.05	8.43	9.21	+0.09
3	3.12	2.95	-0.06	8.09	9.33	+0.16	6.01	6.23	+0.04	8.16	9.46	+0.16
4	3.65	3.75	+0.03	8.50	9.69	+0.14	3.87	3.95	+0.02	8.57	9.63	+0.12
5	2.91	2.92	+0.05	8.55	10.3	+0.20	2.84	3.39	+0.20	9.06	10.3	+0.13
6	2.27	2.65	+0.16	8.64	10.3	+0.19	2.47	3.14	+0.27	8.99	10.2	+0.13
7	2.80	2.74	-0.02	9.66	10.5	+0.09	2.67	3.15	+0.18	9.68	10.5	+0.09
8	2.63	2.68	+0.02	9.64	10.2	+0.06	2.59	3.10	+0.19	9.69	10.2	+0.06
9	2.65	2.81	+0.06	8.98	10.0	+0.11	2.60	3.08	+0.19	8.88	10.1	+0.13

In Test A1, the governing calculated wave height corresponds quite well with the measurement. Despite the absence of the side walls, structure properties and the reflection at the lateral boundaries, the overall relative error is less than 10% which is very reasonable.

Figure 6.3 shows some statistical information of the calculated wave heights. The midpoint of the circle, which is the 'exact' location of the point output, deviates quite a bit. This demonstrates the consequence of comparing a point output directly with the measurements. Therefore, it is recommended to

use the averaged wave height from the 'circle output' and taking into account the standard deviation.

The energy spectra are also compared with the measurements in Figure 6.4. The offshore spectrum (upper left plot) is the averaged spectrum of the three offshore measurement locations (GHM01 to GHM03). Despite the fact that the structure properties and side walls are not included in the calculation model, the spectrum show good correspondence with the measurements, indicating that physics are well modelled. Inside the harbour basin, the averaged spectra derived from the circle agree reasonably with the measurements: the energy distribution along the frequency domain is well captured by XBeach. The irregular pattern in the energy spectrum is due to the reflected waves against the harbour walls (standing waves).

In Test A2, the calculated wave heights are slightly overestimated, see Table 6.1 and Figure 6.5. The overestimation is confirmed by the statistical analysis of Figure 6.6, where most of the point outputs on the circle lie above the measured wave heights. Figure 6.7 present the energy spectrum of Test A2 at various locations. Similar trend is also observed in Test B2. The spectra show indeed the overestimations. However, the physics are still well reproduced as in Test A1 with these extreme wave height. The overestimation with similar wave condition was also demonstrated by *Dobrochinski (2014)*, where the author used the 2-layer SWASH model.

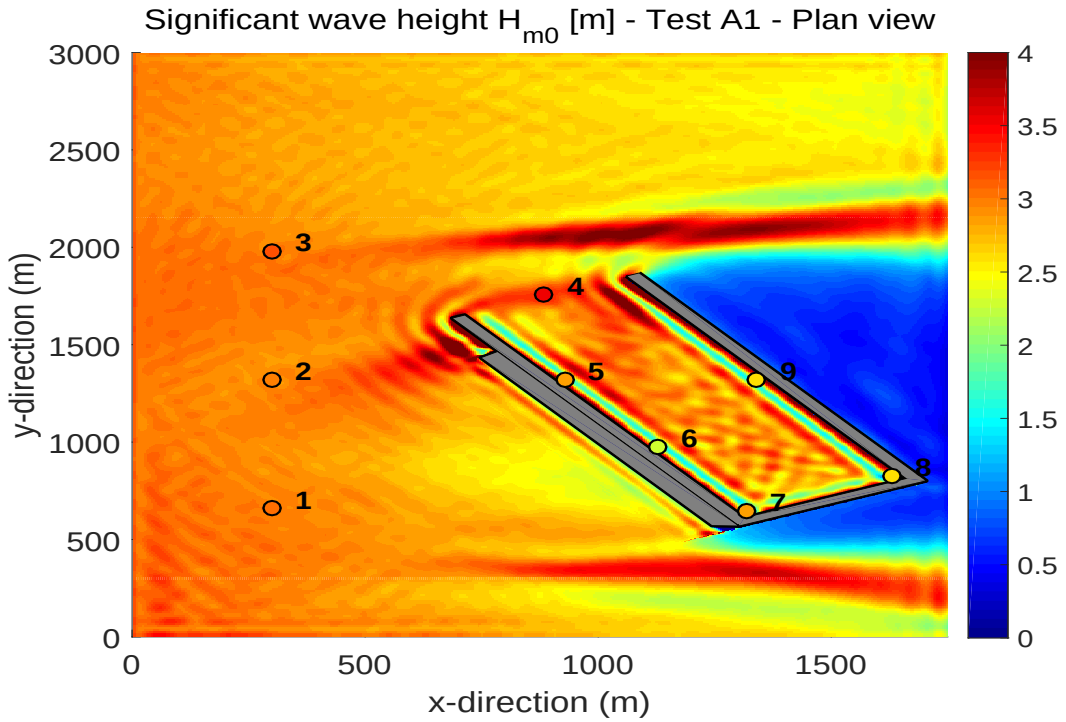

(a) Test A1: plan view of H_{m0}. The circles indicate the measured wave heights.

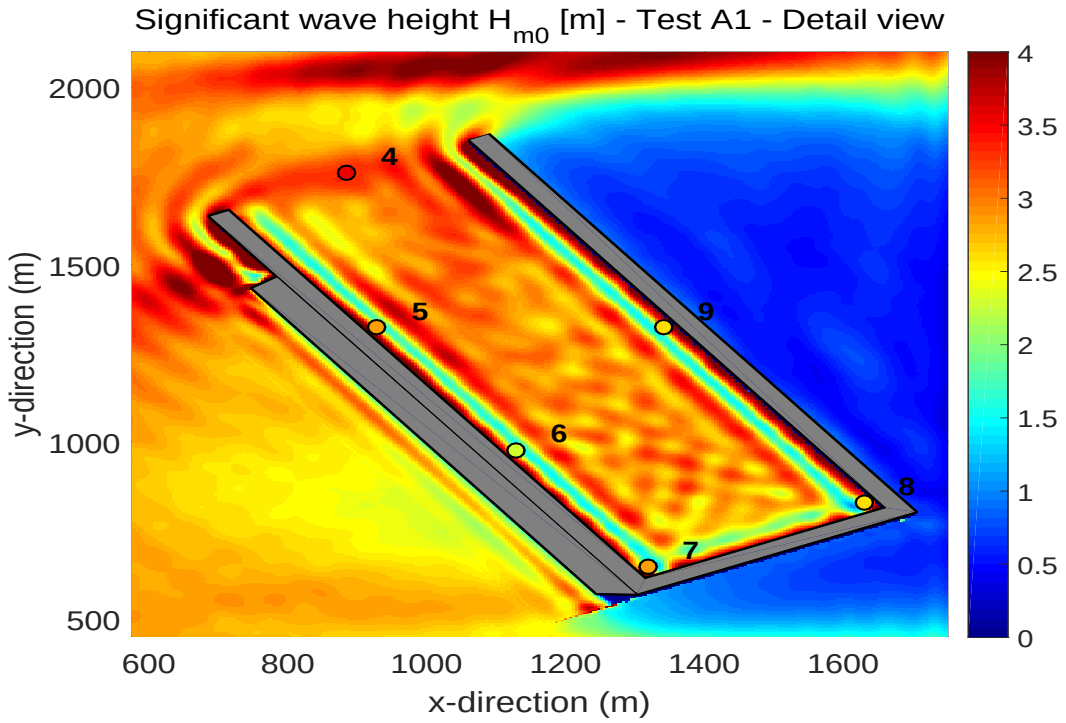

(b) Test A1: detailed view of H_{m0}. The circles indicate the measured wave heights.

Figure 6.2: Overview plot of Test A1.

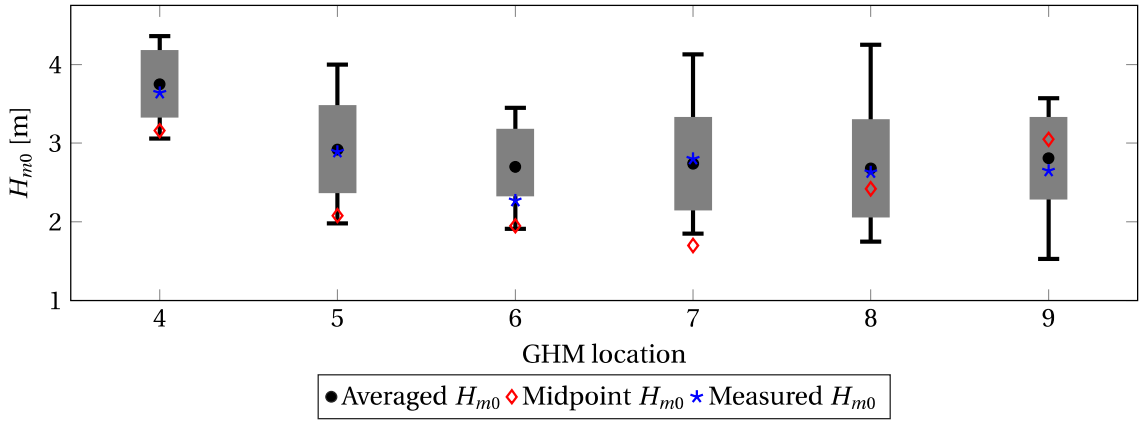

Figure 6.3: Test A1: comparison with measurement. Gray box is standard deviation and vertical line the range of the wave heights calculated by XBeach.

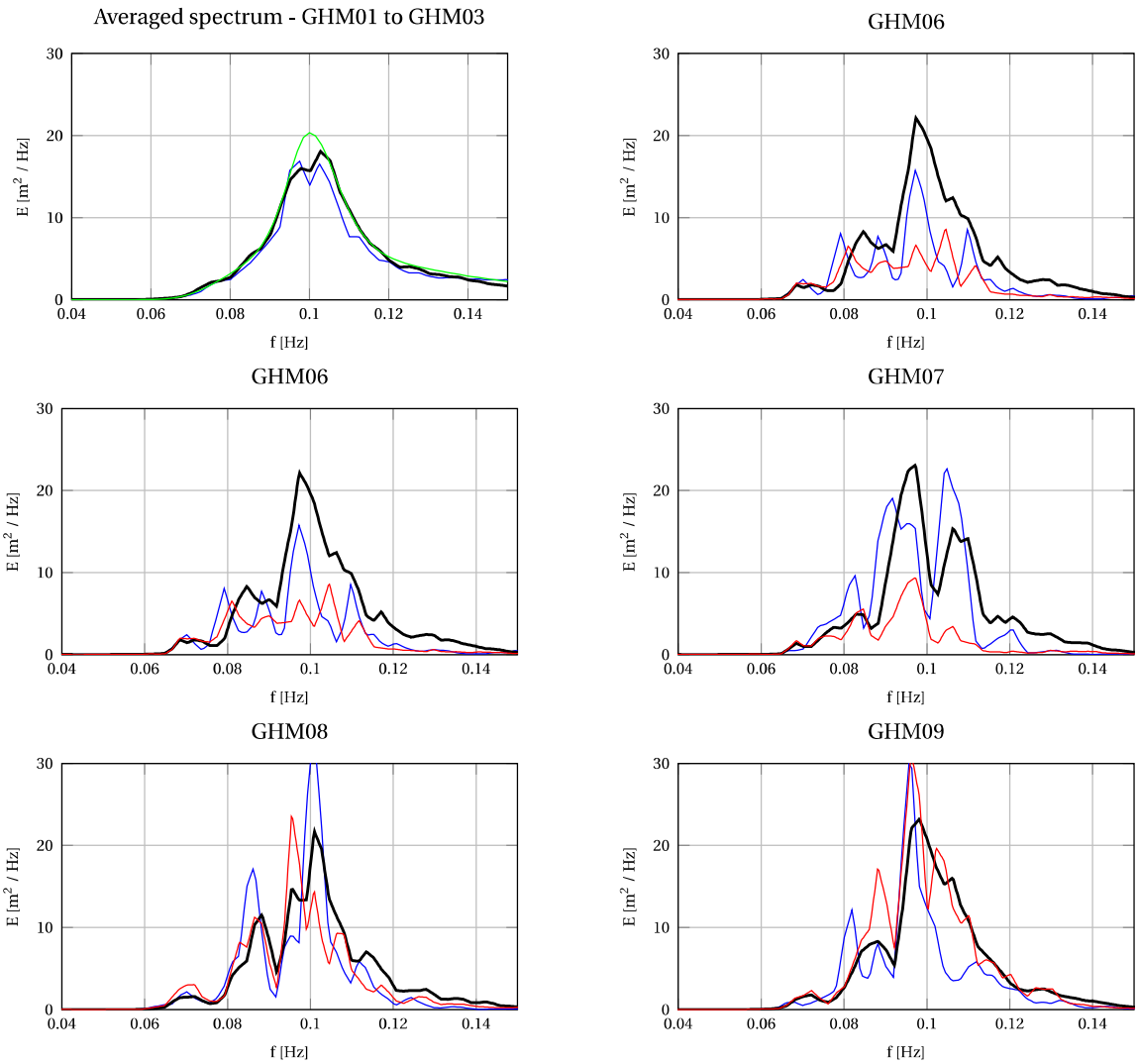

Figure 6.4: Spectra of Test A1. Measured (–), averaged from circle (–), point output (–) and target spectrum (–).

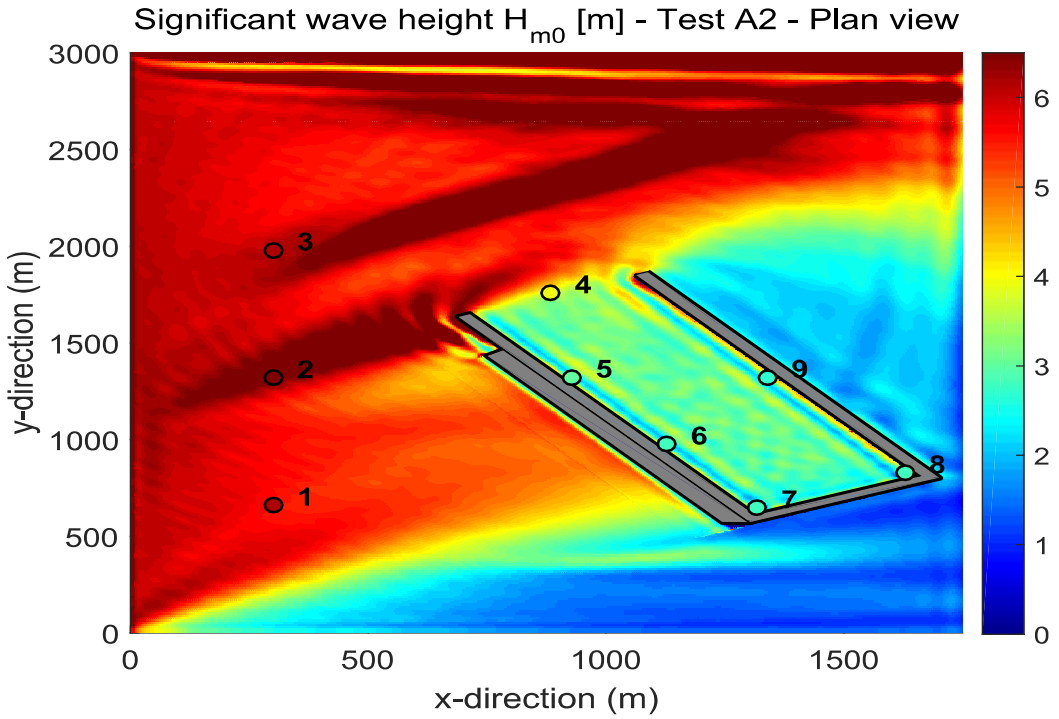

(a) Test A2: plan view of H_{m0}. The circles indicate the measured wave heights.

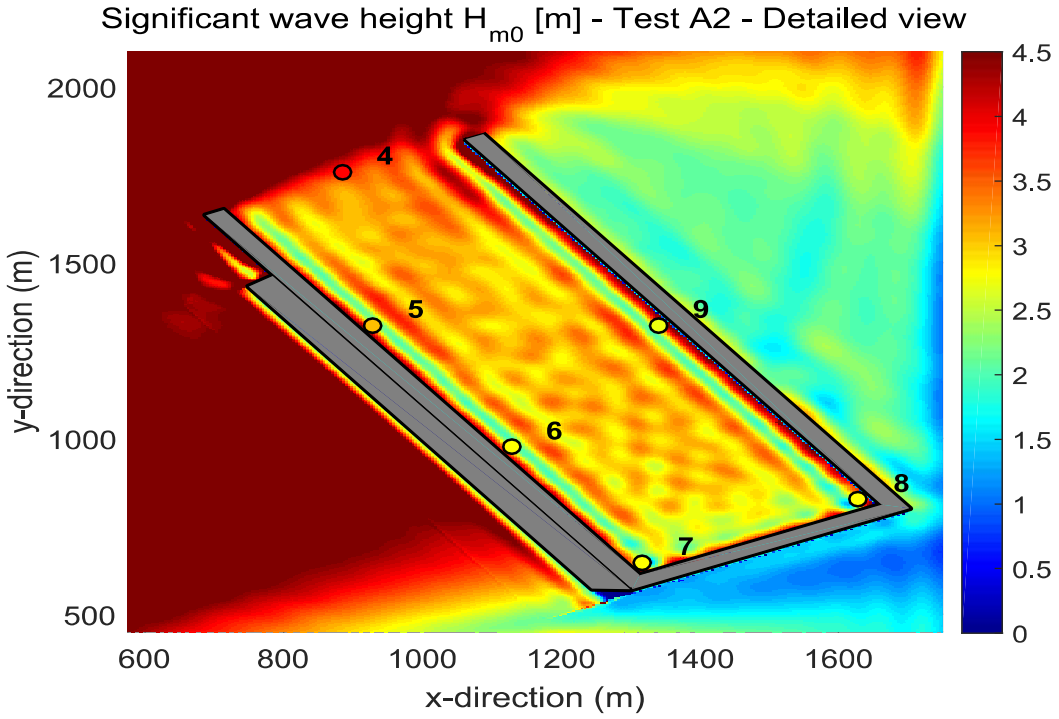

(b) Test A2: detailed view of H_{m0}. The circles indicate the measured wave heights.

Figure 6.5: Overview plot of Test A2.

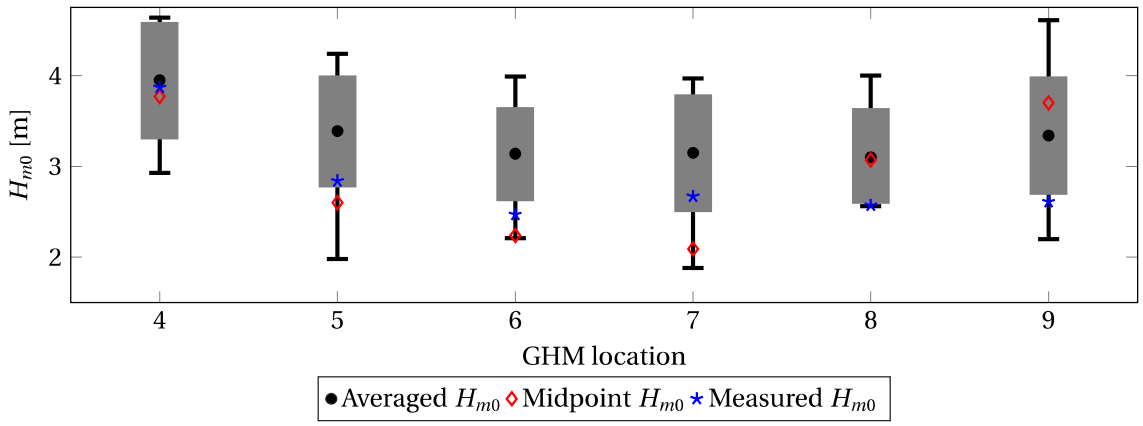

Figure 6.6: Test A2: comparison with measurement. Gray box is standard deviation and vertical line the range of XBeach wave heights.

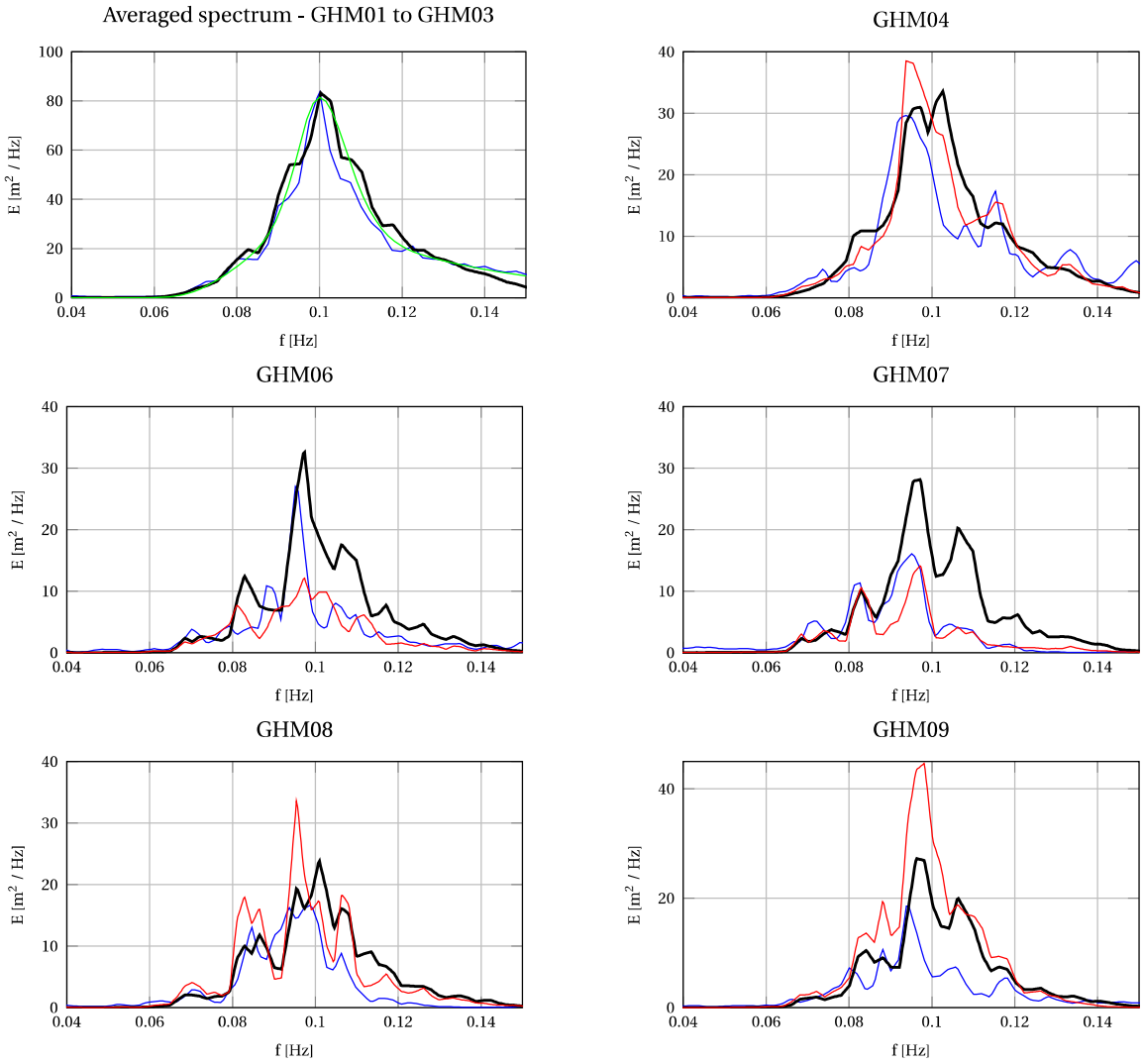

Figure 6.7: Spectra of Test A2. Measured (–), averaged from circle (–), point output (–) and target spectrum (–).

The significant wave heights and spectral wave periods with the short-crested wave conditions are listed in Table 6.2 and visualised along with the measurements in Figures 6.8 and 6.11. The short-crested wave conditions impose an additional difficulty for the calculation model at the offshore boundary. It requires a nearly perpendicular backward travelling (long) wave, which is in reality not a bad assumption because the short waves dissipate in the nearshore area. In Tests B, the imposed wave conditions consist of significant wave spreading which may reflect back towards the offshore boundary. The requirement cannot be met and consequently it is unable to eliminate all the oblique backward travelling waves. The drawback is more pronounced for waves with significant spreading.

Both Test B1 and B2, despite the offshore boundary limitation of both the NH and physical model, the offshore wave heights are in good correspondence. By looking at the offshore spectra in Figures 6.10 and 6.13 (upper left plot), the physics are well reproduced, indicating that the use of this boundary condition does not impose a big error on the calculations.

The calculated wave heights in the harbour basin are quite accurate wherein the difference is generally less than 10%. Statistical analysis in Figures 6.9 and 6.12 demonstrate (again) the inaccuracy of the use of a point output due to the standing wave pattern. Finally, the energy spectra in Figures 6.10 and 6.13 show that the energy distribution along the frequency range is well calculated.

The spectral wave periods are in all tests slightly overestimated with approximately 10%. This is because the numerical model introduces some damping due to the chosen grid resolution. The energy level of the high-frequency tail of the high-frequency part is underestimated, resulting in a small overestimation.

Table 6.2: Significant wave heights in metres and spectral wave periods in seconds of Tests B1 and B2. MAE B1 H_{m0} = 0.07, MAE B1 T_{m01} = 0.09, MAE B2 H_{m0} = 0.08 and MAE B2 T_{m01} = 0.07.

	Test B1						**Test B2**					
GHM	H_{m0} Lab	H_{m0} XBeach	Bias	T_{m01} Lab	T_{m01} XBeach	Bias	H_{m0} Lab	H_{m0} XBeach	Bias	T_{m01} Lab	T_{m01} XBeach	Bias
1	3.15	3.11	-0.01	8.52	9.29	+0.09	5.81	5.35	-0.08	8.29	9.23	+0.11
2	3.10	3.18	+0.03	8.53	9.30	+0.09	6.10	5.98	-0.02	8.24	8.74	+0.06
3	3.14	3.21	+0.02	8.45	9.43	+0.12	6.28	6.78	+0.08	8.24	8.82	+0.07
4	3.10	2.84	-0.09	8.56	9.68	+0.13	5.33	4.65	-0.13	8.44	8.98	+0.06
5	2.55	2.75	+0.08	8.91	10.1	+0.14	4.14	4.44	+0.07	8.75	9.30	+0.06
6	2.34	2.76	+0.18	9.15	10.1	+0.10	3.81	4.27	+0.12	8.92	9.33	+0.05
7	2.67	2.80	+0.06	9.83	9.91	+0.01	3.98	4.25	+0.07	9.53	10.3	+0.08
8	2.39	2.61	+0.09	9.83	9.67	-0.02	3.93	4.20	+0.07	9.50	9.83	+0.03
9	3.16	2.88	-0.09	9.13	9.93	+0.09	4.48	4.47	-0.05	9.10	10.0	+0.11

In Figures 6.2a, 6.5a and to lesser extend Figure 6.11a, there is a strong wave height gradient between the lateral boundary and the harbour mouth. The current boundary condition is an intermediate form between Neumann (no gradient) and zero-velocity (full reflection), for which the latter is responsible

for the reflection pattern. To demonstrate this, an additional simulation is carried with a lateral boundary condition that fully reflects the waves. The use of zero-velocity boundary condition shows similar pattern (the wave heights in the harbour are overestimated as well), which indicates that the strange pattern outside the harbour is due to the chosen boundary conditions (in combination with the harbour).

Finally, the studies of *Dobrochinski (2014)* and *Rijnsdorp and Zijlema (2016)* showed with SWASH that two vertical layers are required to capture the wave dynamics accurately. The kd-value is 1.04, which is slightly above the recommended value of 1 for the depth-averaged mode. Nevertheless, here it was found that with a single layer the offshore wave characteristics are well reproduced. Inside the harbour, this is difficult to determine because the wave heights are averaged over a certain area.

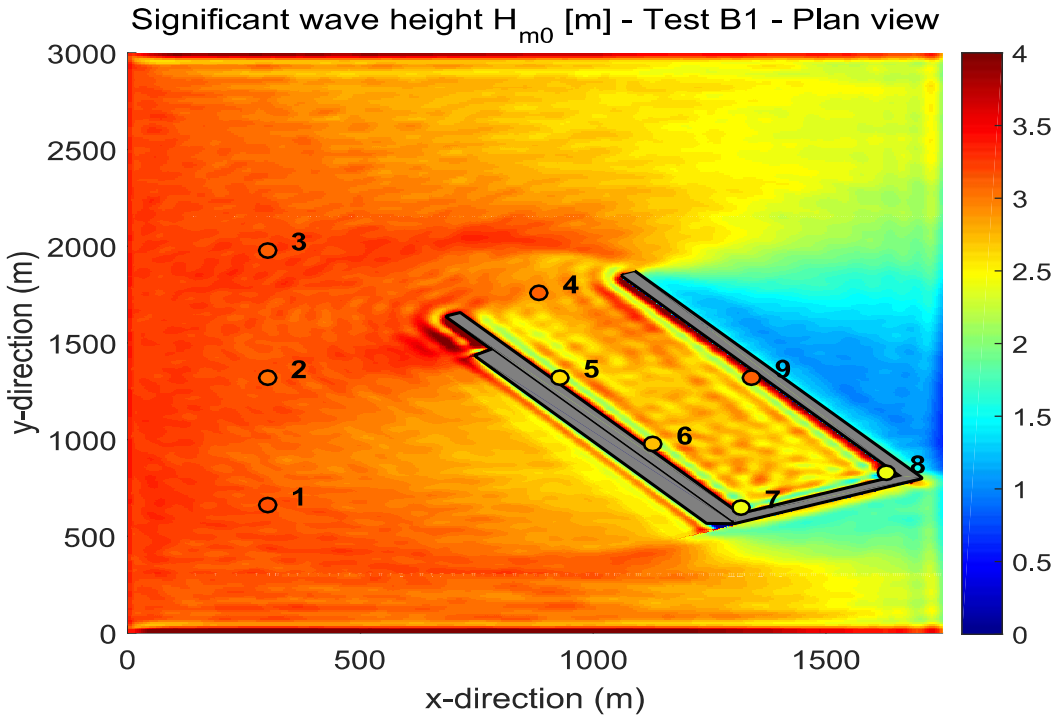

(a) Test B1: plan view of H_{m0}. The circles indicate the measured wave heights.

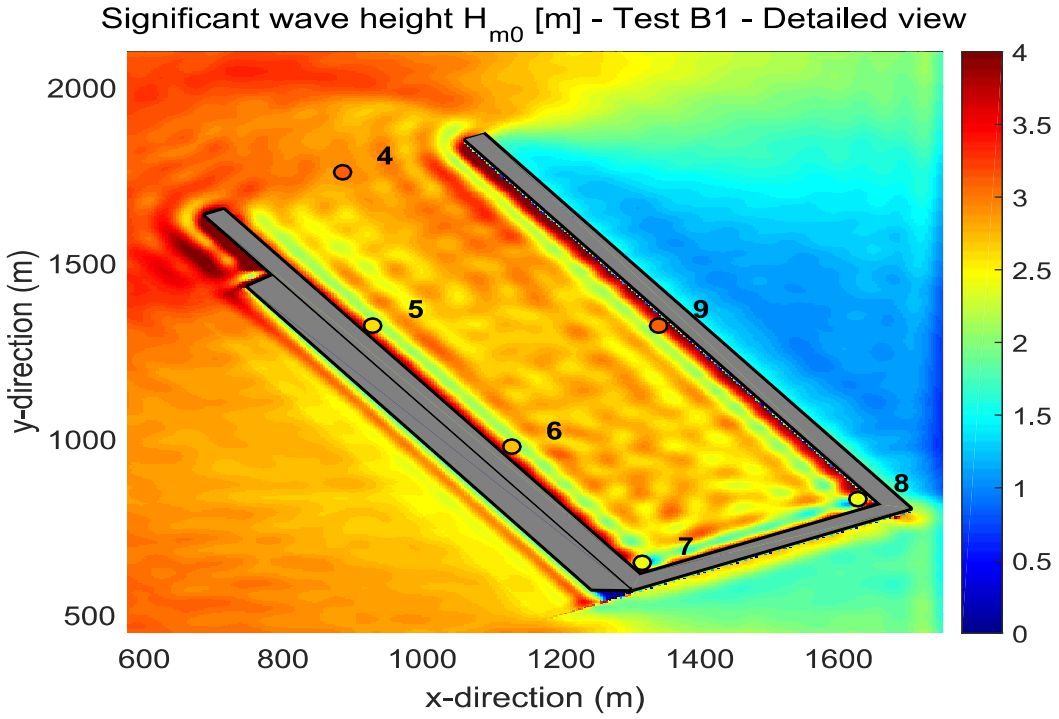

(b) Test B1: detailed view of H_{m0}. The circles indicate the measured wave heights.

Figure 6.8: Overview plot of Test B1.

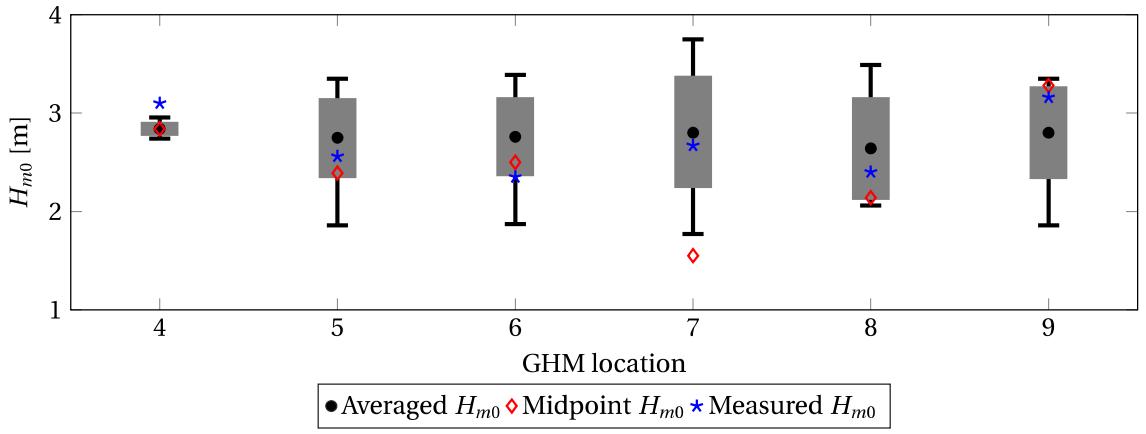

Figure 6.9: Test B1: comparison with measurement. Gray box is standard deviation and vertical line the range of XBeach wave heights.

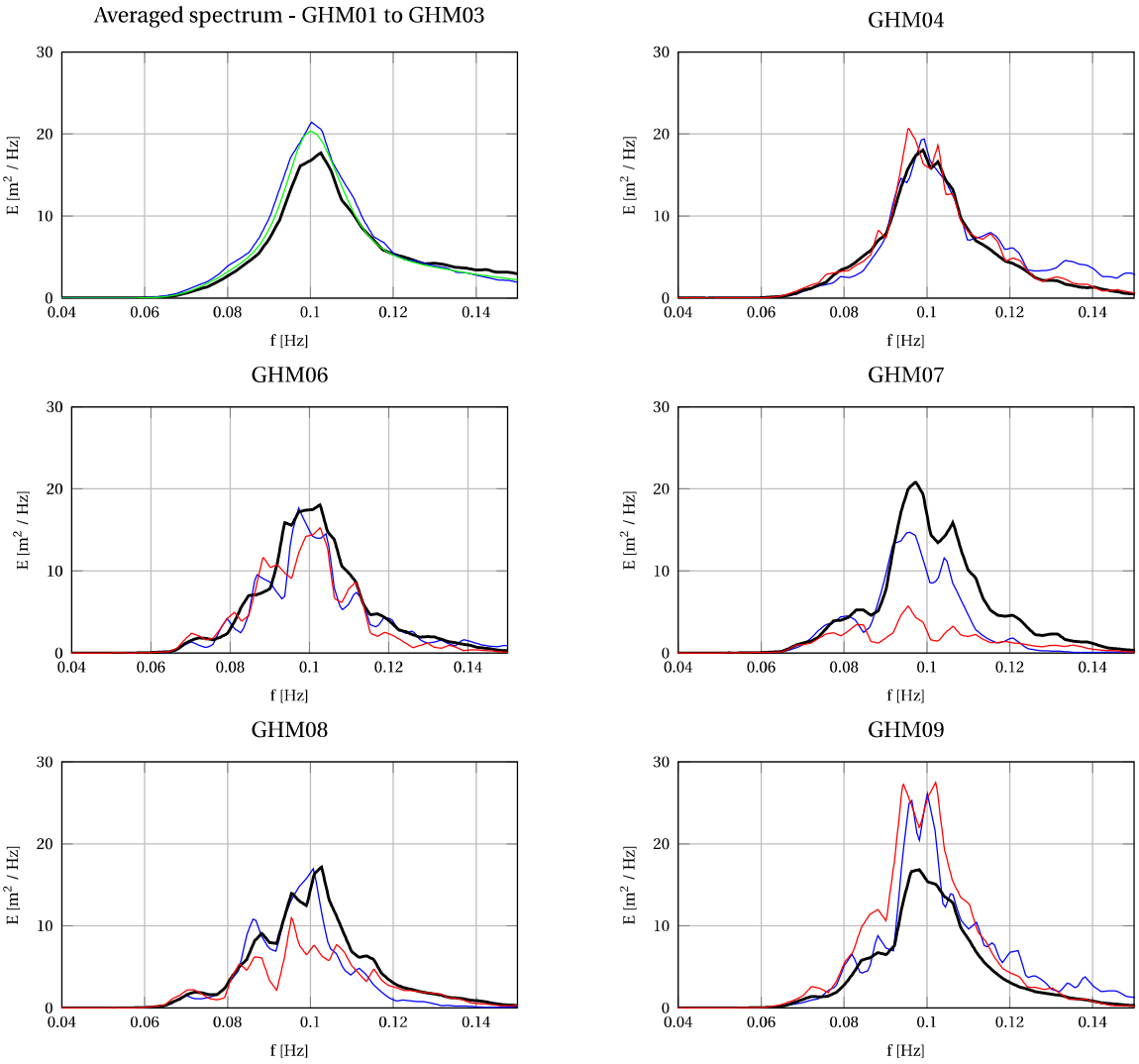

Figure 6.10: Spectra of Test B1. Measured (–), averaged from circle (–), point output (–) and target spectrum (–).

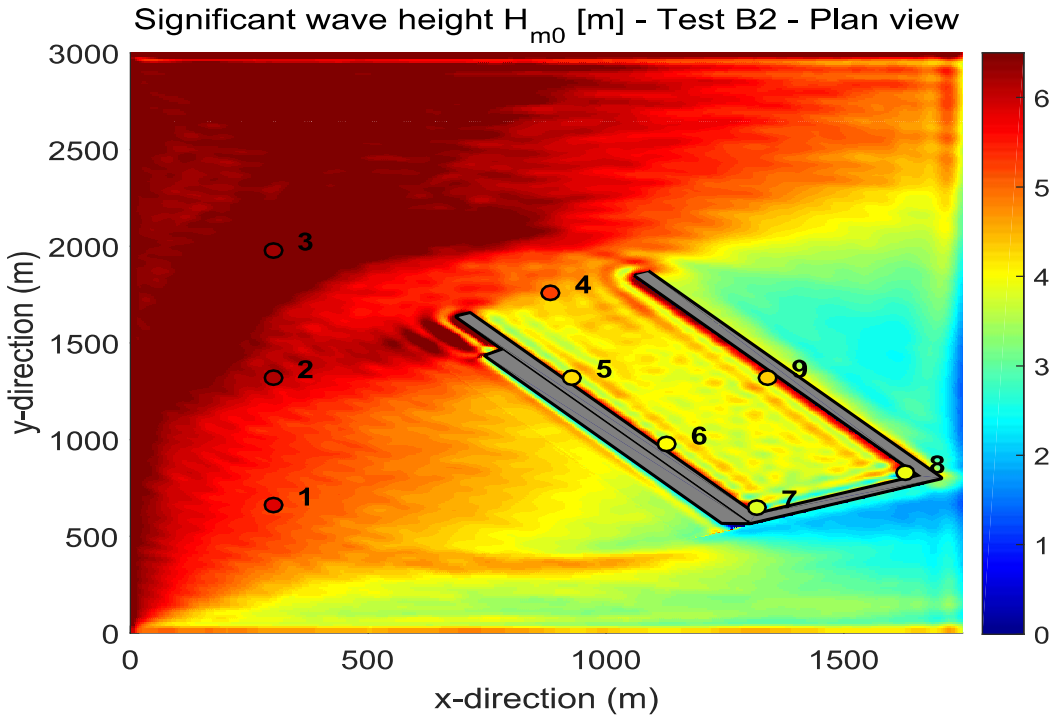

(a) Test B2 plan view of H_{m0}. The circles indicate the measured wave heights.

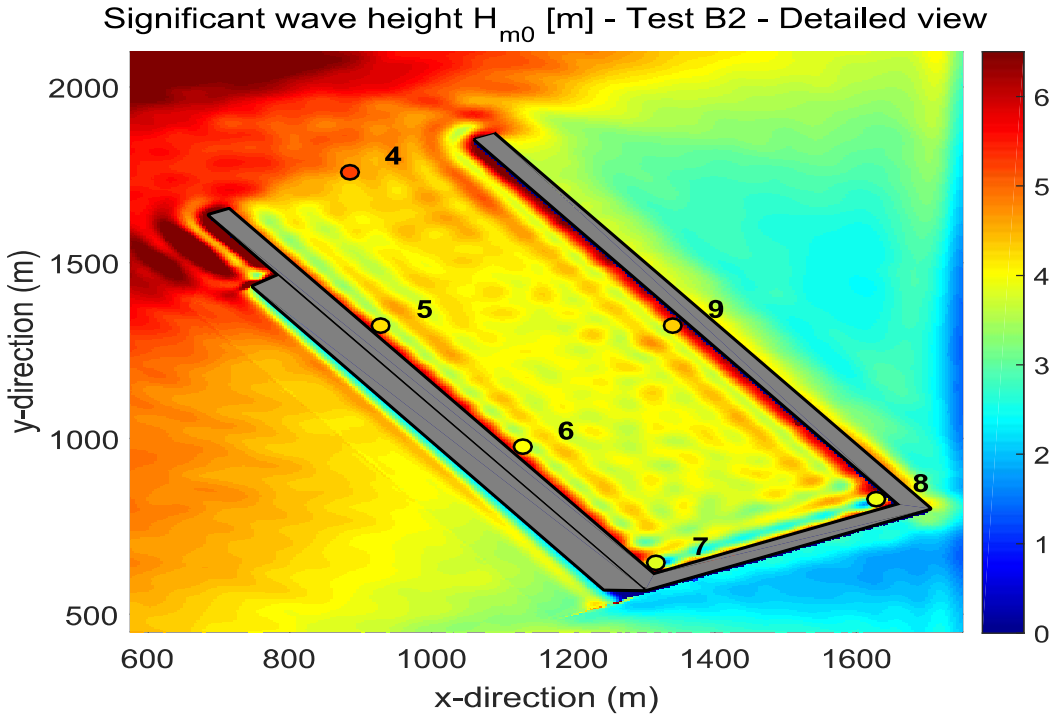

(b) Test B2: detailed view of H_{m0}. The circles indicate the measured wave heights.

Figure 6.11: Overview plot of Test B2.

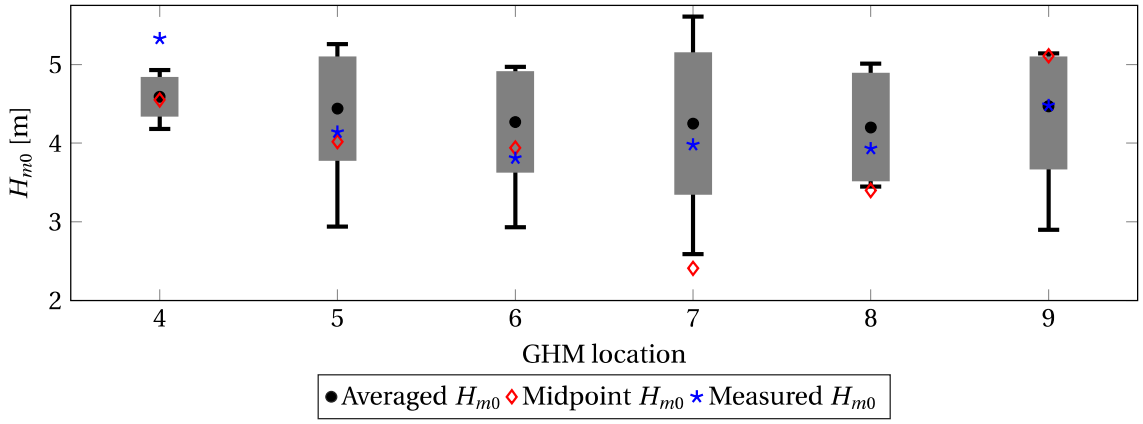

Figure 6.12: Test B2: comparison with measurement. Gray box is standard deviation and vertical line the range of XBeach wave heights.

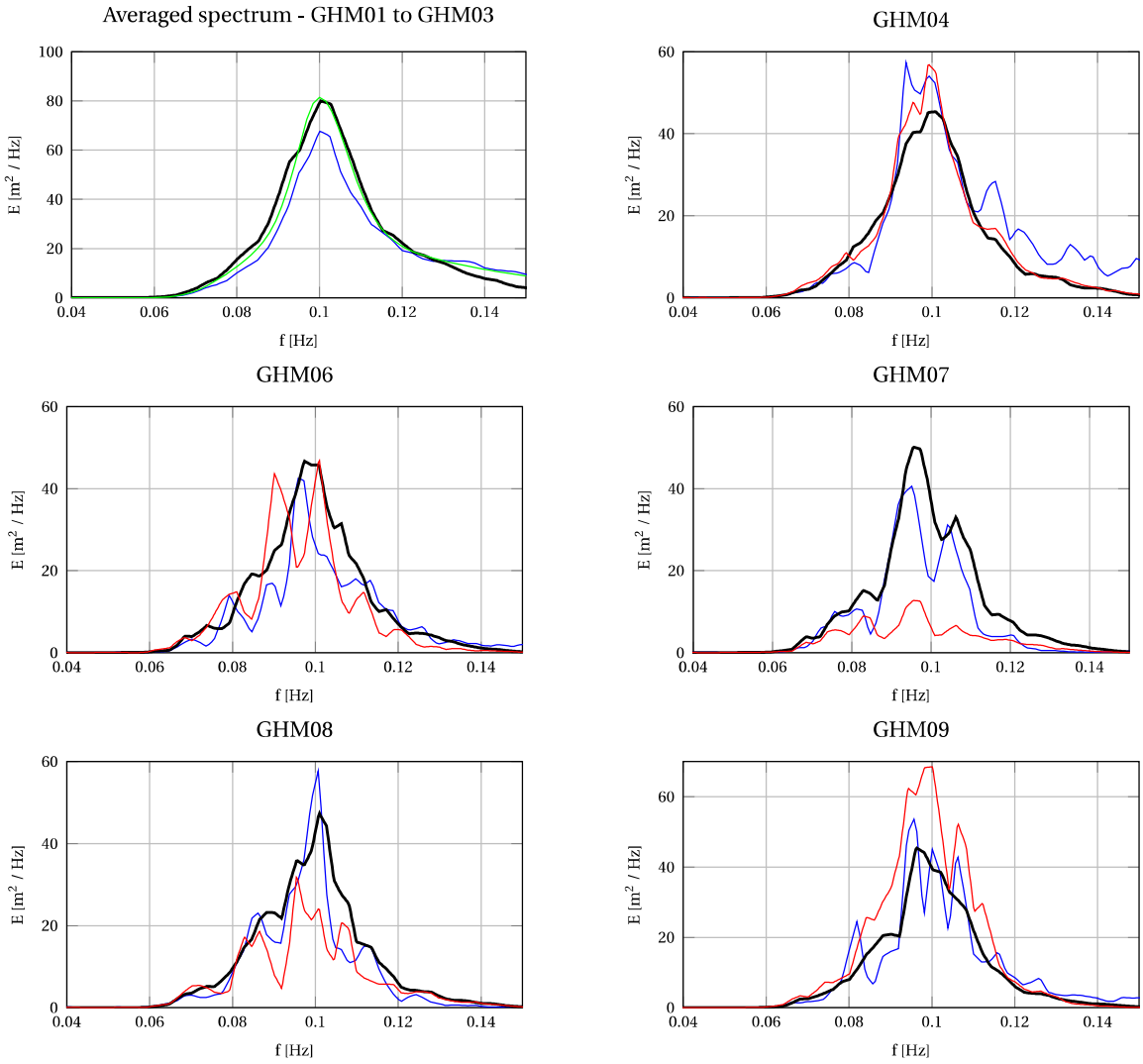

Figure 6.13: Spectra of Test B2. Measured (–), averaged from circle (–), point output (–) and target spectrum (–).

6.3.3. Long waves

This section compares the results of the long waves with the measurements for both the long-crested and short-crested wave conditions, Test A1 and B1, respectively. Test A2 is underestimated (further discussed in Chapter 7) by XBeach NH, but the resonant modes are well identified. Test B2 shows similar results as A1 and B1 and the reader is referred to Appendix A for the results. The focus of this subsection is on the spectral wave heights, wave periods and the resonant frequencies.

The results of the spectral wave heights H_{m0} are shown in Figure 6.14. The significant wave heights are well calculated by XBeach with MAE indices smaller than 0.20. Looking at the spectrum might be more convenient to examine whether the physics are correctly modelled. Table 6.3 and Figure 6.15 give the calculated resonant frequencies and spectra, respectively. With a MAE index of 0.05 for the first mode, the difference is acceptable. The spectra in the corner of the harbour show a correct representation of the energy distribution along the infragravity band. All the resonant modes, longitudinal, transversal and 2D-effects are identified.

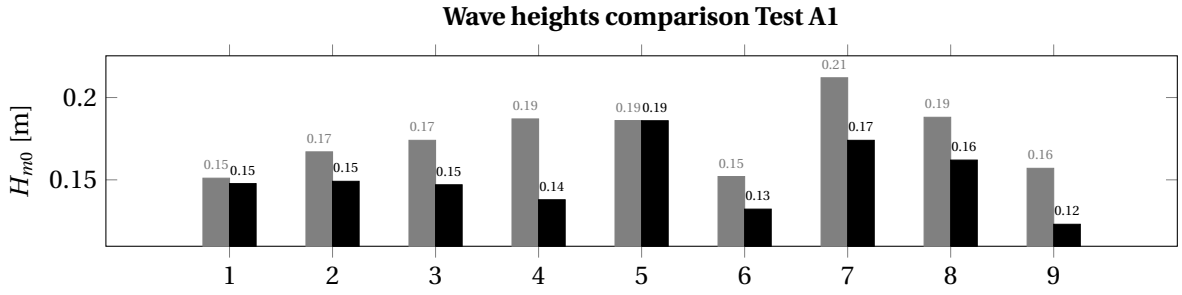

(a) Test A1. MAE total = 0.17, MAE offshore = 0.12 and MAE harbour = 0.20.

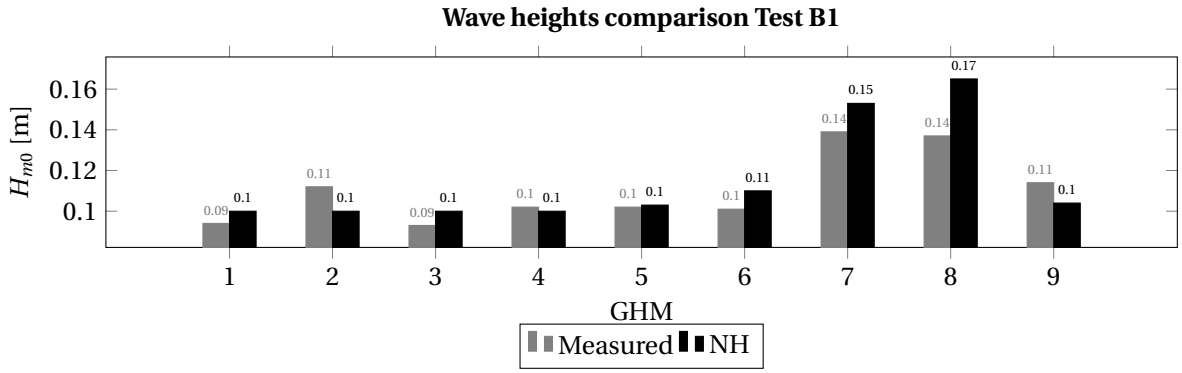

(b) Test B1. MAE total = 0.10, MAE offshore = 0.12 and MAE harbour = 0.08.

Figure 6.14: Comparison of the long wave heights.

The wave periods are summarised in Figure 6.16. The MAE indices are in the order of 0.10 which is quite good. The spectral periods slightly overestimated because T_{m01} is more sensitive for the low-frequency energy than high-frequency tail of the spectrum, see Chapter 5.

Table 6.3: Longitudinal resonant frequencies at GHM08, Test A1. Bias (NH - lab) of Helmholtz mode is 0.05.

Mode	XBeach (Hz)	Measured (Hz)	Theoretical (Hz)
01	0.0024	0.0023	0.0028
02	0.0068	0.008	0.008
03	0.013	0.013	0.013

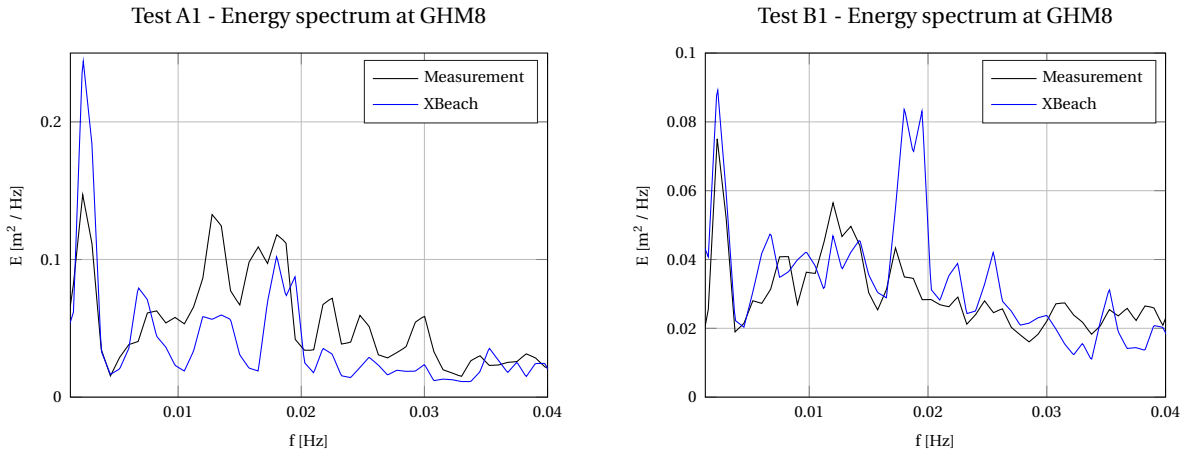

Figure 6.15: Energy spectrum of Tests A1 and B1.

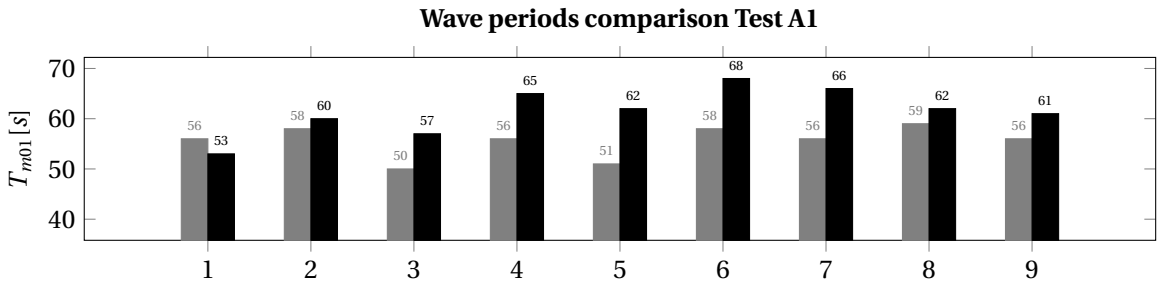

(a) Test A1. MAE total = 0.11, MAE offshore = 0.07 and MAE harbour = 0.13.

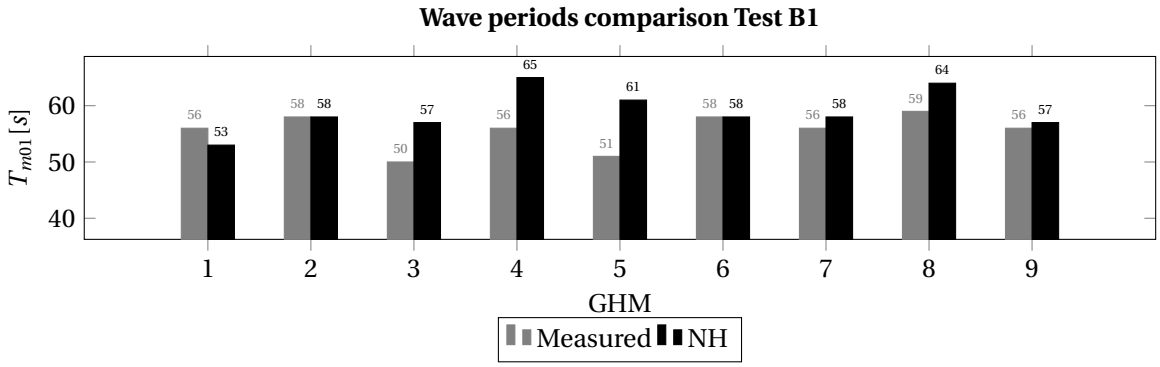

(b) Test B1. MAE total = 0.09, MAE offshore = 0.06 and MAE harbour = 0.09.

Figure 6.16: Comparison of the significant wave periods.

6.4. Conclusion

The capabilities of XBeach NH have been investigated in simple rectangular harbour basin by comparing the XBeach results with the measurements. Based on the MAE indices, the NH mode performs quite well for both the short and long waves. Regarding the analysis, the following conclusions can be drawn:

Short waves

- The short wave heights and periods are well calculated in the harbour, even with very steep waves. *Rijnsdorp and Zijlema (2016)* showed that two layers are required to capture the dispersion characteristics of the primary waves. However, it is shown in this study that single layer is sufficient to capture the offshore wave characteristics. The MAE index is in the order of 0.10 (MAE $\leq$ 0.20 is regarded as good, and MAE $>$ 0.35 is poor).
- When deriving hydraulic parameters from the wave spectrum, the choice of the location output in the calculation model is very important due to the standing wave pattern in the harbour basin. It is advised to take the area of interest into account to determine the wave height if the standing wave pattern is pronounced, e.g. length of a ship.

Long waves

- The theoretical and measured resonant frequencies are identified in XBeach. Also, the energy at the resonant frequencies is well predicted.
- The significant wave heights are well predicted with all the imposed wave conditions. The MAE index is below 0.15.
- The significant wave periods are well reproduced. The MAE index is generally in the order of 0.15 or lower, which is considered to be good.

In the next chapter, Chapter 7, the SB mode is further examined. A relation is made with the NH mode, because it is proved that the results of the NH are quite acceptable.

7

Case I: Surfbeat

7.1. Introduction

This chapter presents the results of SB and the comparison with the measurements. The model set-up is briefly discussed in Section 7.2. Section 7.3 shows the results of the numerical model and are directly compared with the measurements. An extensive sensitivity analysis is carried out on the relevant parameters in Section 7.4. The comparison with the NH mode is done in Section 7.5 and the chapter is concluded in Section 7.6.

7.2. Model set-up

The calculation model uses the default settings if the hydraulic/model parameters are unknown. Other values are the same as in the NH mode (where possible), such that a fair comparison can be made. For a detailed model set-up description, the reader is referred to Appendix A. The SB model settings in a nutshell are as follows:

- Non-uniform grid resolution of 10 m in and near the harbour. At the boundary of the domain the grid cells are 20 m. Grid resolution is based on 30 grid points per long wavelength.
- Directional grid from 180 degrees to 360 degrees w.r.t. the north for the perpendicular travelling waves. Directional grid from 150 degrees to 360 degrees w.r.t. the north for oblique waves. 4 energy bins are used for short wave propagation. Using more energy bins did not improve the long waves much.
- Bottom friction C = 55 $m^{1/2}/s$ (XBeach default).

- Harbour walls C = 55 $m^{1/2}/s$ (XBeach default).
- Gravel slopes C = 20 $m^{1/2}/s$, similar to that of the NH mode.
- Model is forced at the offshore boundary by imposing a JONSWAP spectrum (Table 4.1).
- For the flow, a weakly-reflective offshore boundary condition is imposed where reflected long waves can pass through the boundary with minimal reflection.
- Neumann boundary condition at the lateral boundaries, for both waves and flow. By doing so, there is no lateral gradient.
- CFL - condition of 0.7 is used (XBeach default).

The side walls (see Chapter 4) near the wave generator were not included due to instabilities of the model. The absence of the side walls is fairly justified as the results show similar trend as *van der Molen (2006)*, where the author did include the side walls.

7.3. Results

Simulations are carried out based on the model settings as discussed in Section 7.2. This section compares the calculated results with measurements as described in Chapter 4. Further, the results are presented separately for the short and long waves. In Subsection 7.3.2, the short waves are discussed. Subsequently, the long waves are reproduced and compared with the measurements in Subsection 7.3.3.

7.3.1. General

It is expected that the duration of the simulation affects the calculated wave heights in the long wave band. Figure 7.1 shows the time required to obtain a steady-state solution.

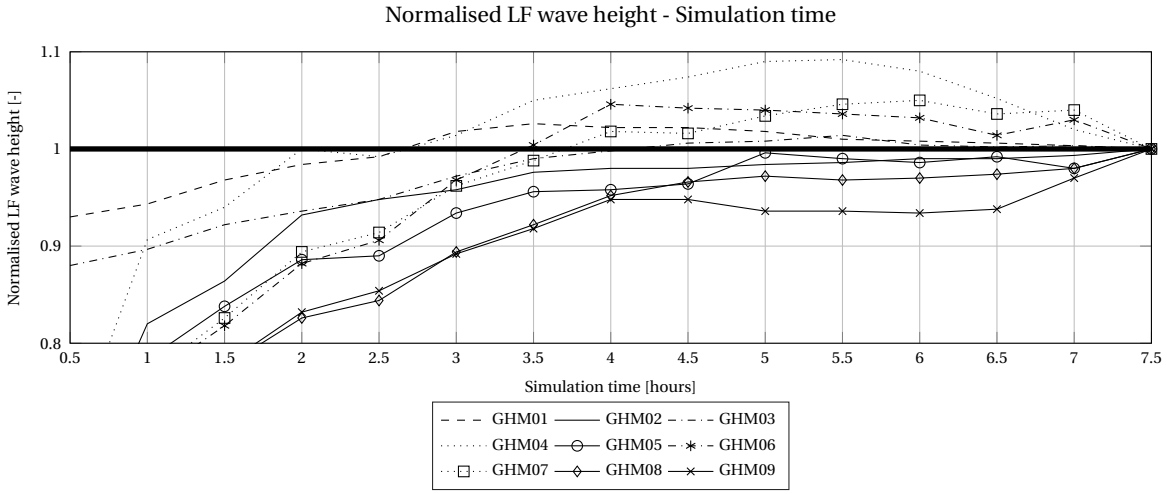

Figure 7.1: Required simulation duration of XBeach in Test A1.

The long wave heights at each burst half hour are normalised with the wave height at the end of the simulation. The offshore wave heights (GHM01 to GHM03) require approximately 2 to 3 hours to be stable. This rather long realisation time could be explained by the reflection characteristics and inability to fully absorb the reflected waves. Inside the harbour, it appears that the wave height never really converged to a certain value, but it shows to be steady-state after ≈ 5 hours. The offshore forcing are of random nature, so it is possible that oscillations and resonance may occur at an arbitrary time during the simulation: the random sloshing in the harbour may cause this 'never-converging' pattern. As a rule of thumb it is recommended to have 500 - 1000 incoming waves in order to obtain reliable results from the wave spectrum . For these reasons, the remaining simulations are run for 7 hours and 30 minutes, same duration as the measurements, in order to eliminate all the uncertainties.

The realisation time for the short wave energies are much smaller than for the long waves where the wave energies need to be averaged over a certain period (say 1 hour). The wave heights of the short waves (H_{rms}) in SB are calculated from the averaged time series of the energies and multiplied with $\sqrt{2}$ to obtain the significant wave height H_{m0}.

7.3.2. Short waves

Figure 7.2 gives an overview of the wave heights for the short waves H_{m0} for long-crested (upper plot) and short-crested (lower plots) wave conditions. The calculated wave heights can be found in Appendix A, Table A.4.

Inside the harbour, the wave heights differ significantly which is expected as only the energies are resolved. Thus, there is no diffraction of the short waves. This was demonstrated with the NH mode (MAE index ≈ 0.10 - 0.15), where phase-information of the short waves is considered and thus diffraction. Here, the MAE indices for all wave conditions are poor and are larger than 0.35. In harbour where short waves are present, this is entirely due to wave spreading. Unfortunately, there are no other possibilities to improve short wave modelling in harbours. Using SB to predict hydrodynamics in harbours is therefore strongly discouraged. Finally, the short waves seem to play a striking role in the accuracy of the long wave heights, which is discussed in Subsection 7.3.3.

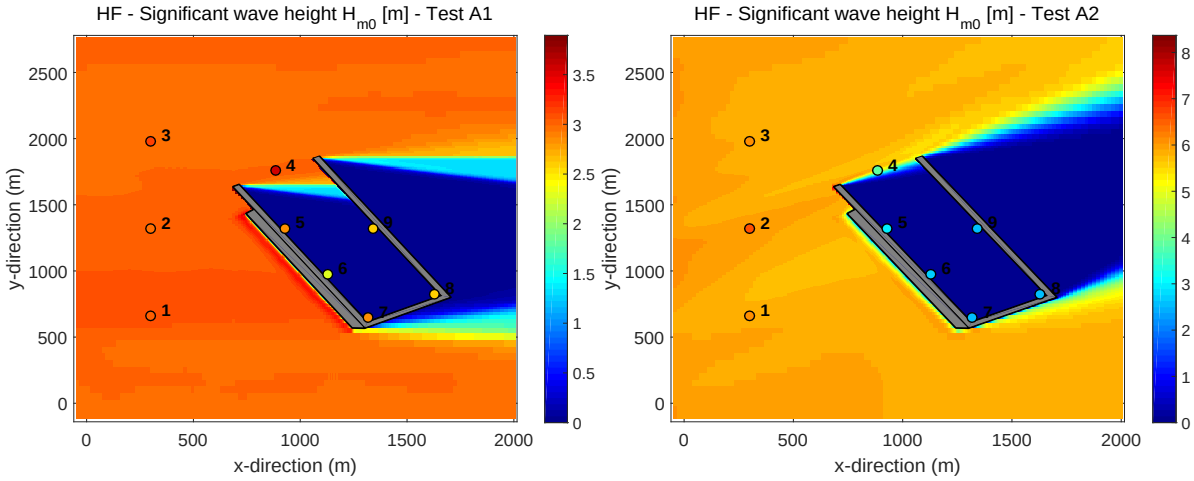

(a) Test A1

(b) Test A2

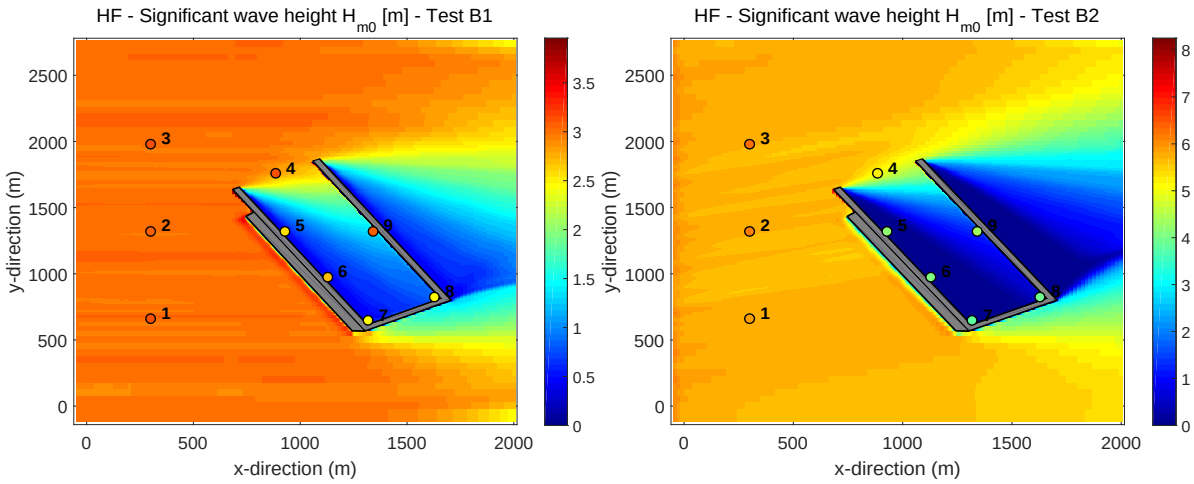

(c) Test B1

(d) Test B2

Figure 7.2: Wave height H_{m0} of long-crested (upper) and short-crested waves (lower). Circles denotes the measured wave heights.

7.3.3. Long waves

This subsection presents the results of the long waves, split into long-crested and short-crested waves. For the former, there is hardly short wave energies present in the harbour, whereas for the latter some wave energies are present in the harbour due to spreading.

Long-crested waves This part discusses the results of the long-crested long waves. In the report of the laboratory experiment *(Bijleveld, 2004)* it is not described what is meant by long-crested or uni-directional waves. Therefore, an estimation is made for the directional spreading visually from the figures of *van der Molen (2006)*. The chosen directional spreading is about 5 degrees, which corresponds to $s = 200$. The effect of wave spreading is further discussed in Subsection 7.4.1.

Because of the uni-directional nature of the waves, the wave action is predominantly due to the free long waves in the harbour, as short wave energy is almost absent, see upper plots of Figure 7.2. SB should be able to predict the wave heights for the long waves, as XBeach is developed to perform calculations in situations where long waves are dominant. The results of the long wave heights are summarised in Figures 7.3 and 7.4. The wave heights inside the harbour follows the trend of the measurements: locations with higher waves are also calculated and vice versa.

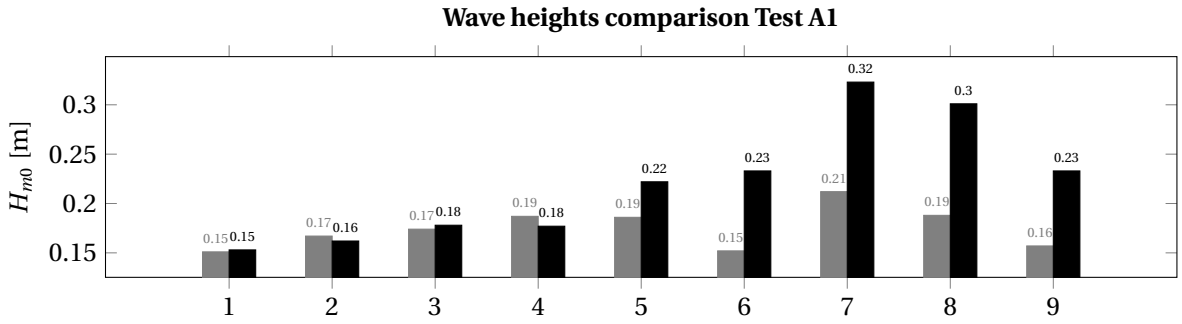

(a) Test A1. MAE total = 0.27, MAE offshore = 0.04 and MAE harbour = 0.38.

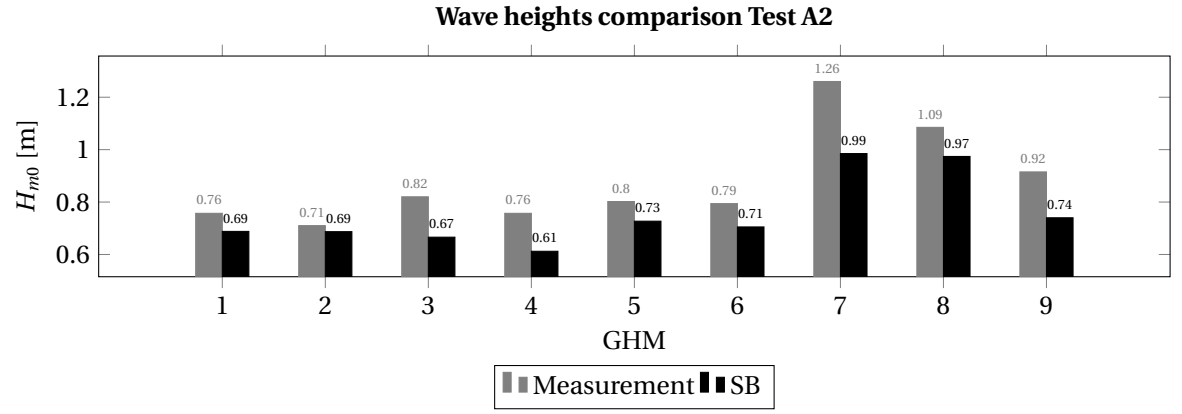

(b) Test A2. MAE total = 0.13, MAE offshore = 0.10 and MAE harbour = 0.14.

Figure 7.3: Significant wave heights in metres with long-crested wave conditions.

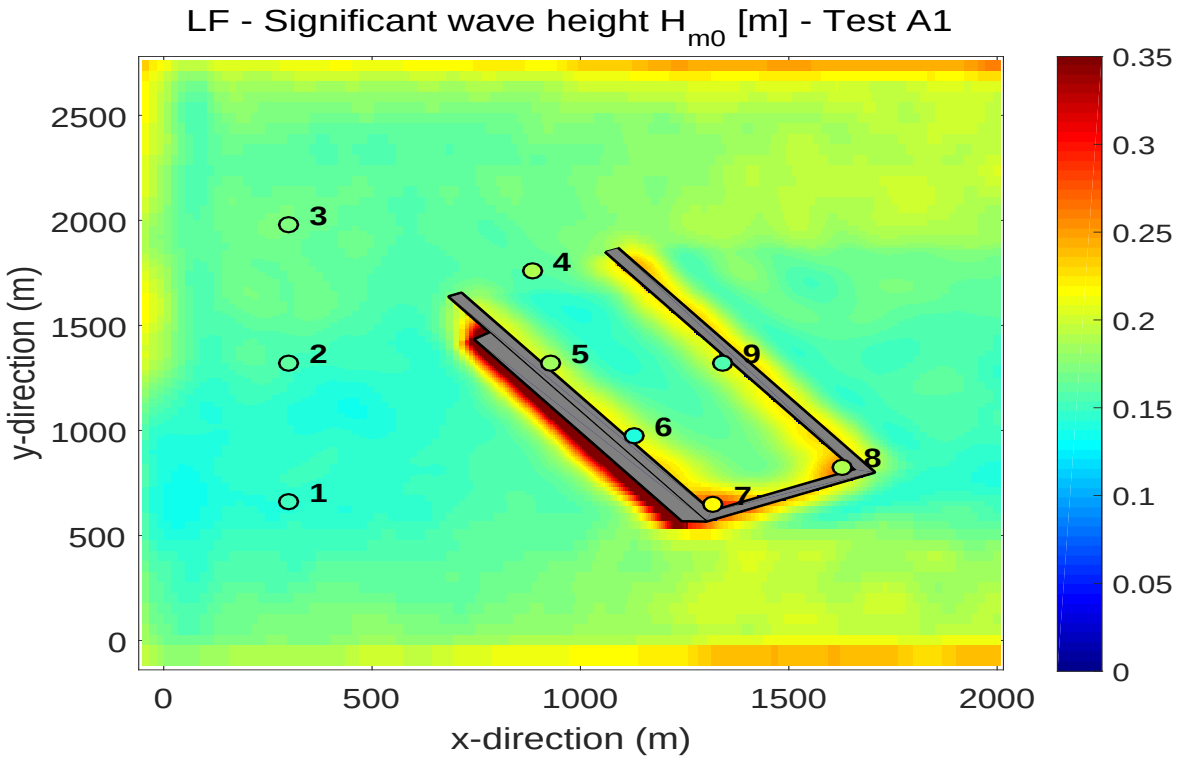

(a) Test A1

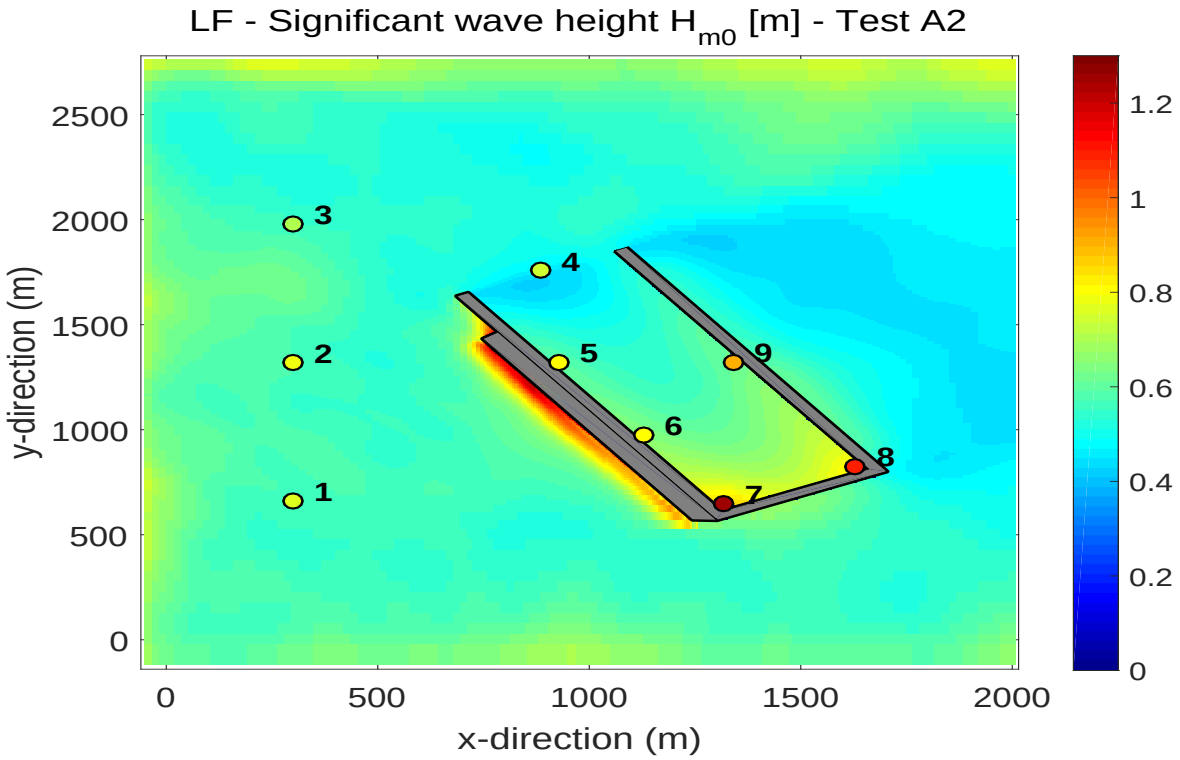

(b) Test A2

Figure 7.4: Significant wave height H_{m0} of long-crested waves with $s = 200$. The circles denote the measured wave heights.

In Test A1 the wave heights are overestimated and the greatest differences are to be found at the corners of the harbour. The MAE index of 0.38 in the harbour is relatively poor. Plausible explanations for the overestimations are:

- Scaling effects / insufficient damping in the calculation model. The influence of the scaling effects is examined and documented in Appendix A. It is shown that simulations carried out in physical model scale, the wave heights are still overestimated.
- The absent of short waves in the harbour. The long waves in the harbour are free, because short waves are not present (and thus not bounded to the wave groups). With the presence of short waves, the long waves are more 'controlled', which have already been demonstrated with the NH mode resulting to more accurate wave heights. The long waves in the NH mode are bounded resulting in a higher accuracy. The role of the short waves is further examined in Subsection 7.3.3 where the waves are short-crested and with a sensitivity analysis in Section 7.4.

Test A2, however, is underestimated with a MAE index of 0.14 inside the harbour. The main differences here are the mean wave direction of the propagating energy and the significant wave height. Wave energy is travelling entirely past the harbour mouth (Figure 7.4b) and there is no direct interaction with the short waves.

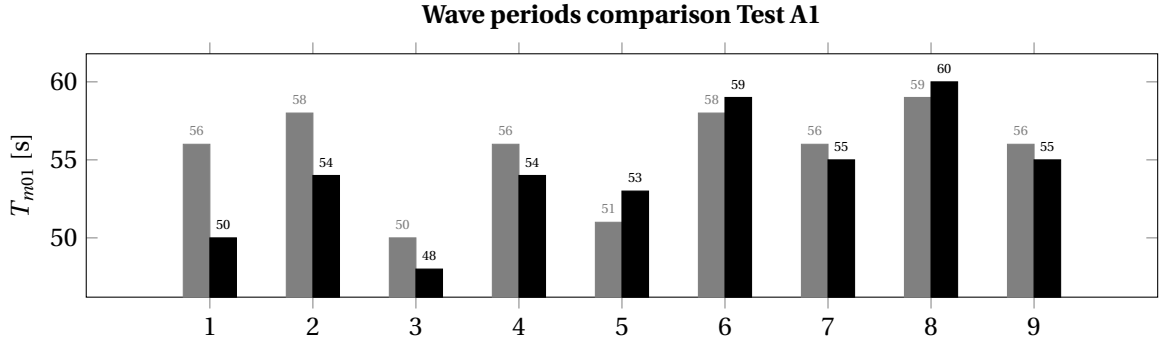

(a) Test A1. MAE total = 0.04, MAE offshore = 0.07 and MAE harbour = 0.04.

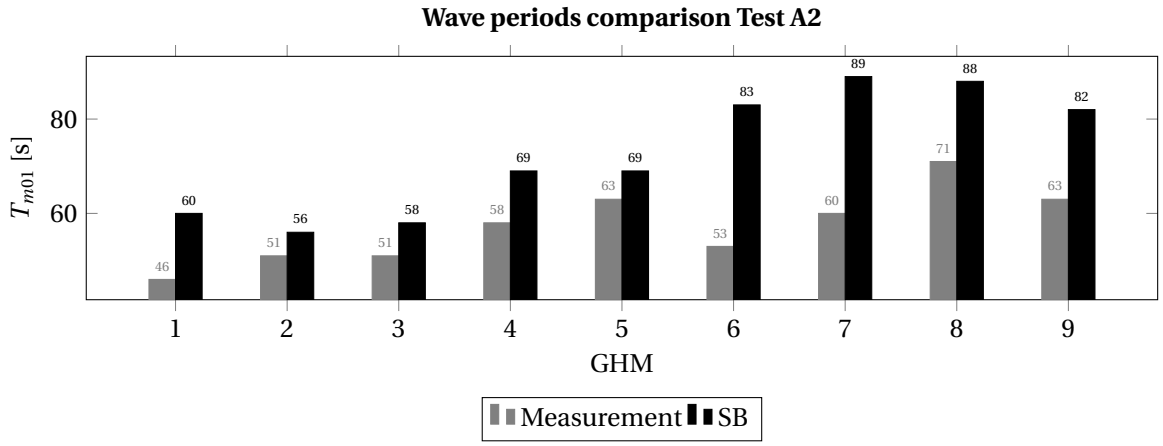

(b) Test A2. MAE total = 0.26, MAE offshore = 0.18 and MAE harbour = 0.32.

Figure 7.5: Spectral wave periods in seconds.

Figure 7.5 shows the measured and the calculated wave periods of the long waves at each location. The calculated and the measured wave periods are in great agreement for Test A1, indicating that the physical processes are well reproduced. Test A2 however, the differences are quite large. The T_{m02} of Test A2 was also calculated. The wave periods did decrease, because the 'centre of gravity' of the energy spectrum is situated more on the higher frequency part than T_{m01} and thus less sensitive for the lower frequency noise. Nevertheless, similar trend as T_{m01} is observed and the wave periods are overestimated.

A closer inspection on the wave spectra can give an explanation whether the physics are correctly modelled. Figure 7.6 gives the measured and calculated spectrum of the low-frequency part of Tests A1 and A2 at the corner of the harbour. The calculated and measured spectra are in reasonable agreement in the sense that measured peaks are also calculated by XBeach. Moreover, the resonant frequencies in the calculations corresponds well with the measured and theoretical values as listed in Table 7.1. The Helmholtz resonant frequency is well calculated with a MAE index of 0.09. Other sharp peaks in the energy spectrum are related to transversal or 2D effects.

Table 7.1: Longitudinal resonant frequencies at GHM08, Test A1. Bias (SB - lab) of Helmholtz mode is 0.09.

Mode	XBeach (Hz)	Measured (Hz)	Theoretical (Hz)
01	0.0025	0.0023	0.0028
02	0.0074	0.008	0.008
03	0.013	0.013	0.013

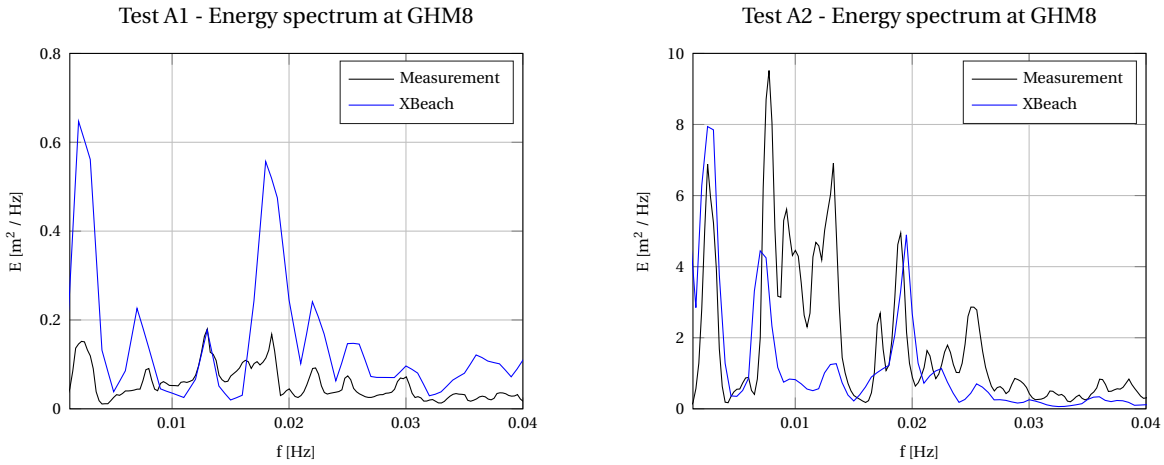

Figure 7.6: Energy spectrum of Tests A1 and A2 at location GHM08.

A peculiar observation is the peaks in the wave spectrum around the frequencies of Hz = 0.009 – 0.012 of Test A2 (Figure 7.6, right plot), which are not associated with the resonant modes. *van der Molen (2006)* argued that these are standing waves in the laboratory basin, which are not well dampened out and being amplified in the harbour. The result of NH mode shows similar trend which indicates that the discrepancy is related to the measurements, rather than a model limitation. Nevertheless, the physics are still well reproduced and the corresponding resonant frequencies are identified.

The main findings of the long-crested long waves are:

- SB overestimates the wave heights, which is due to the absent of short waves in the harbour (NH further supports this theory). The effect of short waves on the long waves is further examined in Test B1 and B2 as well as in Subsection 7.4.1 with a sensitivity analysis. SB performs poor with a MAE index of 0.38.
- The XBeach model is able to calculate the right energy distribution along the infragravity band. The calculated spectra follow the trend of the measured spectra.
- The wave periods seem to increase with increasing obliquity of the mean wave direction.
- The theoretical resonant frequencies are well calculated by XBeach, though not always visible in the measurements. Nevertheless, the Bias (0.09) of the Helmholtz mode is quite good.

Short-crested waves This part discusses the results of the short-crested long waves. A significant difference with the uni-directional waves is the ability of energy penetration into the harbour due to directional spreading, see the lower plots of Figure 7.2. Now the energy field inside the harbour consists of short wave (energy), bound long waves and free long waves. The wave heights in both tests are summarised in Figures 7.7 and 7.8.

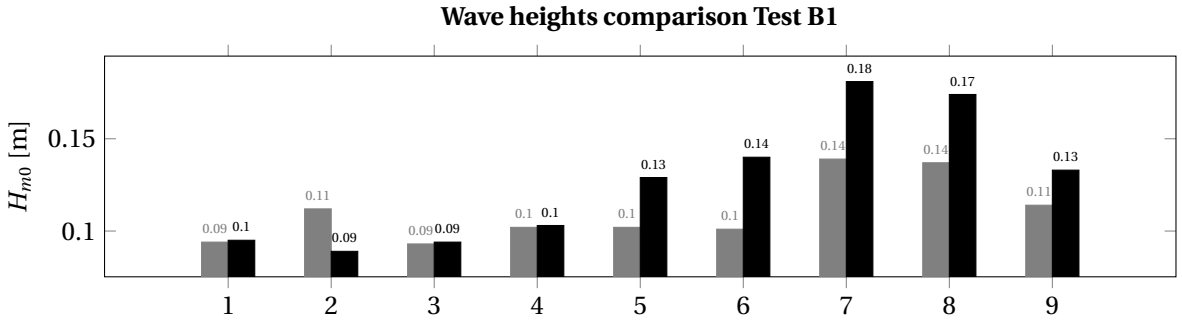

(a) Test B1. MAE total = 0.15, MAE offshore = 0.10 and MAE harbour = 0.17.

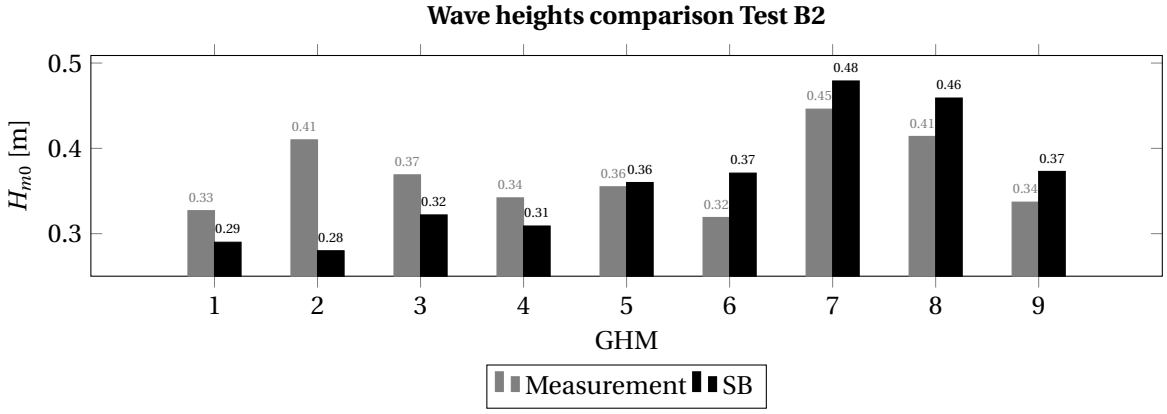

(b) Test B2. MAE total = 0.13, MAE offshore = 0.19 and MAE harbour = 0.10.

Figure 7.7: Significant wave heights in metres with short-crested wave conditions.

Generally, the calculated wave heights are in reasonable agreement, although slightly overestimated at all location inside the harbour. For both tests, the total MAE index is quite good. As already argued in Subsection 7.3.3, the presence of the short waves might play an important role on the calculation of the spectral wave heights. With these short-crested wave conditions, there is significant more short wave energies in the harbour, resulting in better correspondence of the long waves with the measurements. This is because the long waves are bounded to the short wave groups, and thus cannot 'freely' amplify in the harbour. The NH mode in Chapter 6 showed that in presence of short waves, the wave heights for the long waves are quite accurate. Additionally, an extensive sensitivity analysis is carried out in Section 7.4 to identify the crucial parameters.

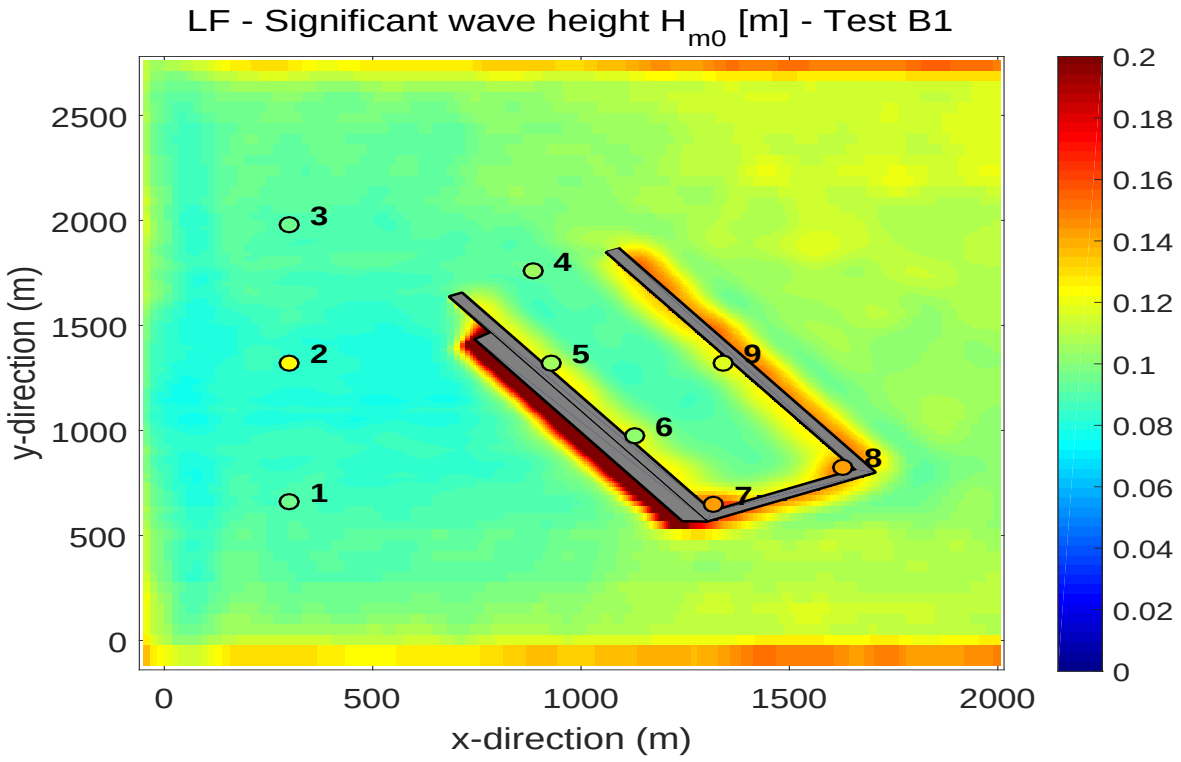

(a) Test B1

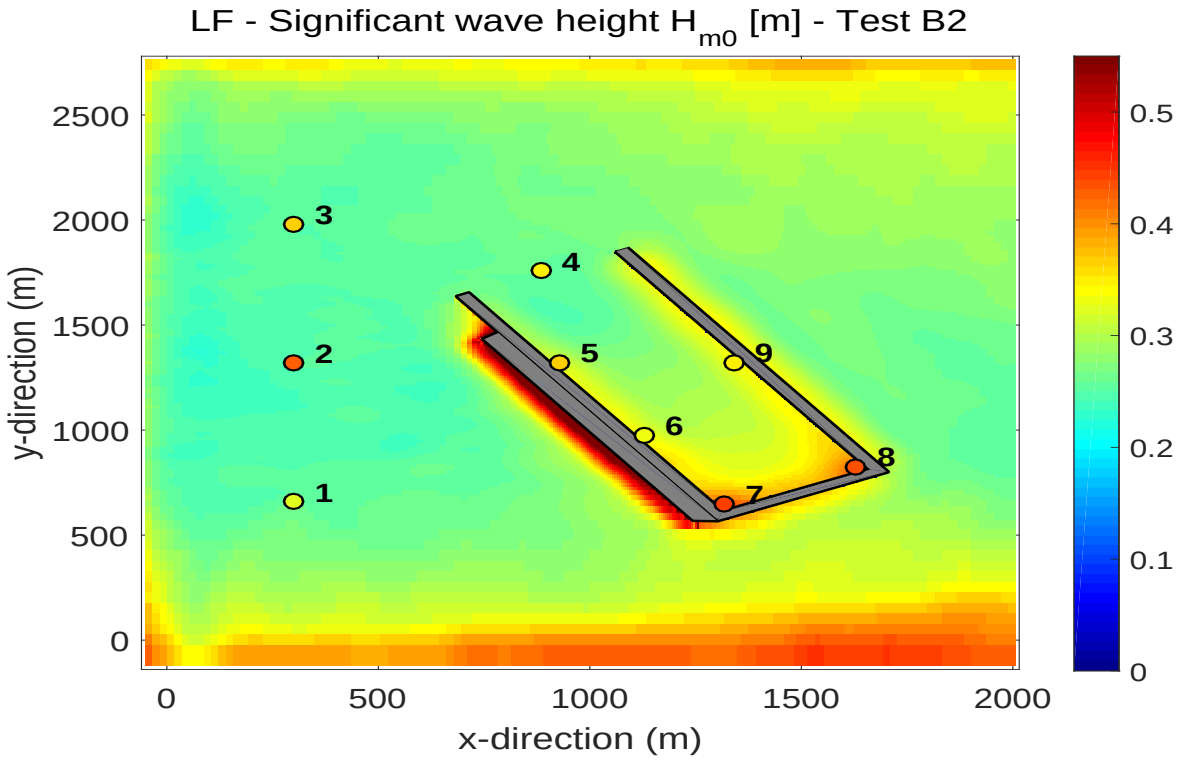

(b) Test B2

Figure 7.8: Significant wave height H_{m0} of short-crested waves with $s = 5$. The circles denote the measured wave heights.

The calculated and measured wave periods are shown in Figure 7.9. Test B1 is in good agreement, whereas Test B2 shows a bigger difference with the measurements.

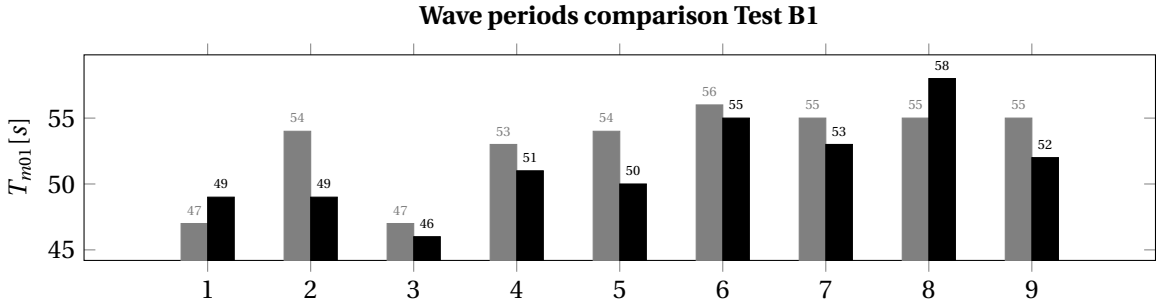

(a) Test B1. MAE total = 0.05, MAE offshore = 0.06 and MAE harbour = 0.05.

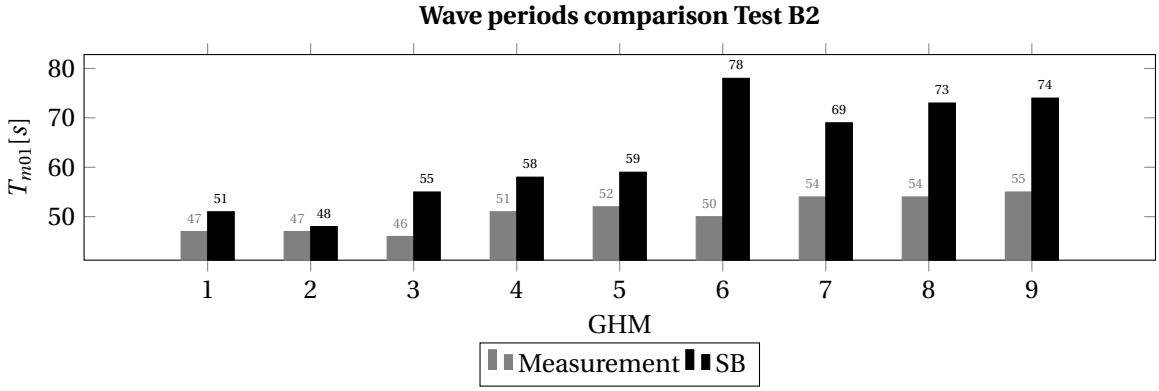

(b) Test B2. MAE total = 0.23, MAE offshore = 0.10 and MAE harbour = 0.30.

Figure 7.9: Mean wave periods in seconds.

Until here, it is observed that for very oblique incoming waves (< 270°) the wave periods increase in the calculation model for both Test A2 (long-crested) and B2. Therefore, an additional analysis is carried out by varying with the mean wave direction. By increasing the obliquity with respect to the harbour mouth, it is expected that the calculated wave periods also increase. This is also modelled, see Figure A.14 in Appendix A and similar trend is also observed when calculating T_{m02}, though the overestimation was slightly less for the latter (in the order of 5 seconds). However, a sound physical relation could not be found in this study.

Figure 7.10 shows the measured and the calculated spectra at the corner of the harbour for Test B1 and B2. Except for the first natural Helmholtz mode, other resonant peaks are not very pronounced in the measurements or not even excited. The spectrum calculated by XBeach and the measured spectrum show large differences in the energy distribution along the frequencies. The spectral peaks calculated by XBeach corresponds to the theoretical resonant frequencies as listed in Table 7.2, but are not visible in the measurements. The resonance frequencies are more pronounced with the more energetic wave condition in Test B2 ($H_{m0} = 6m$), right plot of Figure 7.10.

Table 7.2: Longitudinal resonant frequencies at location GHM08, Test B1. Bias (SB - lab) of Helmholtz mode is 0.09.

Mode	XBeach (Hz)	Measured (Hz)	Theoretical (Hz)
01	0.0025	0.0023	0.0028
02	0.0069	0.008	0.008
03	0.013	0.012/0.014	0.013

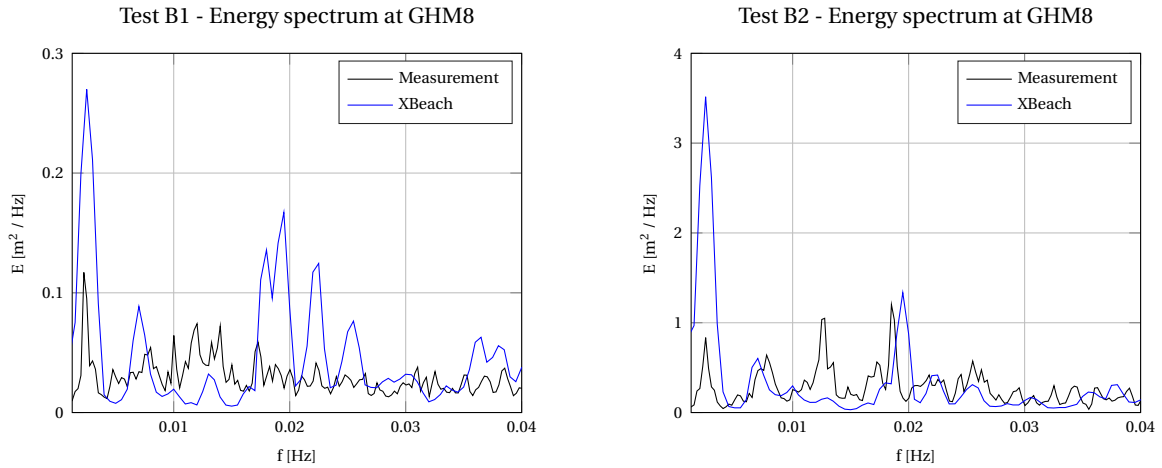

Figure 7.10: Energy spectrum of Tests B1 and B2 at location GHM08.

The main findings with regard to the short-crested waves in this section are as follows:

- The wave heights for the long waves are well predicted with a MAE index in the order of 0.10 - 0.15.
- The calculated and measured wave heights are in better agreement compared to the tests with the long-crested conditions. The overestimation is smaller (both in absolute and relative terms). The role of the short wave energies in the harbour is demonstrated here and with the NH mode in Chapter 6. Additional analysis is carried out in Section 7.4.
- The wave periods are well predicted in Test B1. A high measured wave period is also calculated by XBeach and vice versa. However, large deviations are found for the very oblique wave (with respect to the harbour mouth). Same results were also found for the long-crested waves.
- The theoretical resonant frequencies are well calculated by XBeach, though not always visible in the measurements.

7.4. Sensitivity analysis

This section presents the results of the sensitivity analysis on the hydrodynamic module of SB for harbour applications. The analysis is carried for the parameters that affect the long waves only, because it is demonstrated that short wave action in the harbour is too inaccurate due to the absence of diffraction. From the results in Section 7.3, the role of short waves in the harbour and the possible dissipation mechanisms were identified as the sources that cause the differences between the calculation and measurements. To this end, we shall discuss the effects of directional spreading and friction. First, the expected influence of the parameter is first elaborated after which the results are presented. Test A1 and B1 are further analysed in this section.

7.4.1. Directional spreading

Long-crested waves have typically spreading of less than 10° which shows swell wave characteristics. The directional spreading is specified with cos^{2s} in the JONSWAP spectrum and values of $s > 100$ corresponds to (long-crested) swell waves. Short-crested waves, typically wind waves, have spreading in the order of 20 ° or more and thus parameters of $s < 20$. We shall examine the spreading parameter of s =1 to s =10000, corresponding to 57 degrees and 0.8 degrees respectively. The energy propagation into the harbour is entirely due to wave spreading.

Figure 7.11 shows the influence of directional spreading on the wave heights for high s-values at two locations inside the harbour. It appears that the chosen wave spreading is important because it has significant influence on the wave heights. A slight deviation in the parameter, especially near $s = 400 - 500$, leads to a different harbour response. The lower two plots in Figure 7.11 show the wave heights as function of the spreading parameter for various frequency bands. It appears that the lowest frequency band, containing the Helmholtz mode, is the most sensitive for wave spreading for s-values larger than 500 while the others remain unaffected. This trend is also observed in the spectra of the upper plots of Figure 7.11. The energetic Helmholtz mode, first natural mode and around f = 0.02 Hz the response is the greatest.

So far, the increase in wave height for $s > 500$ is remarkable, since the difference between $s = 500$ and $s = 10000$ is less than three degrees and the wave height is twice as high. The harbour response due to this little difference in spreading is highly unlikely realistic and therefore not reliable. Additional runs were done with Test A2, and similar trend was observed. The wave heights differ too much from the measurements and the crude overestimation is purely numerical. An additional run was carried out with a more realistic s-value of 70. The harbour response is very similar to the results of $s = 100$.

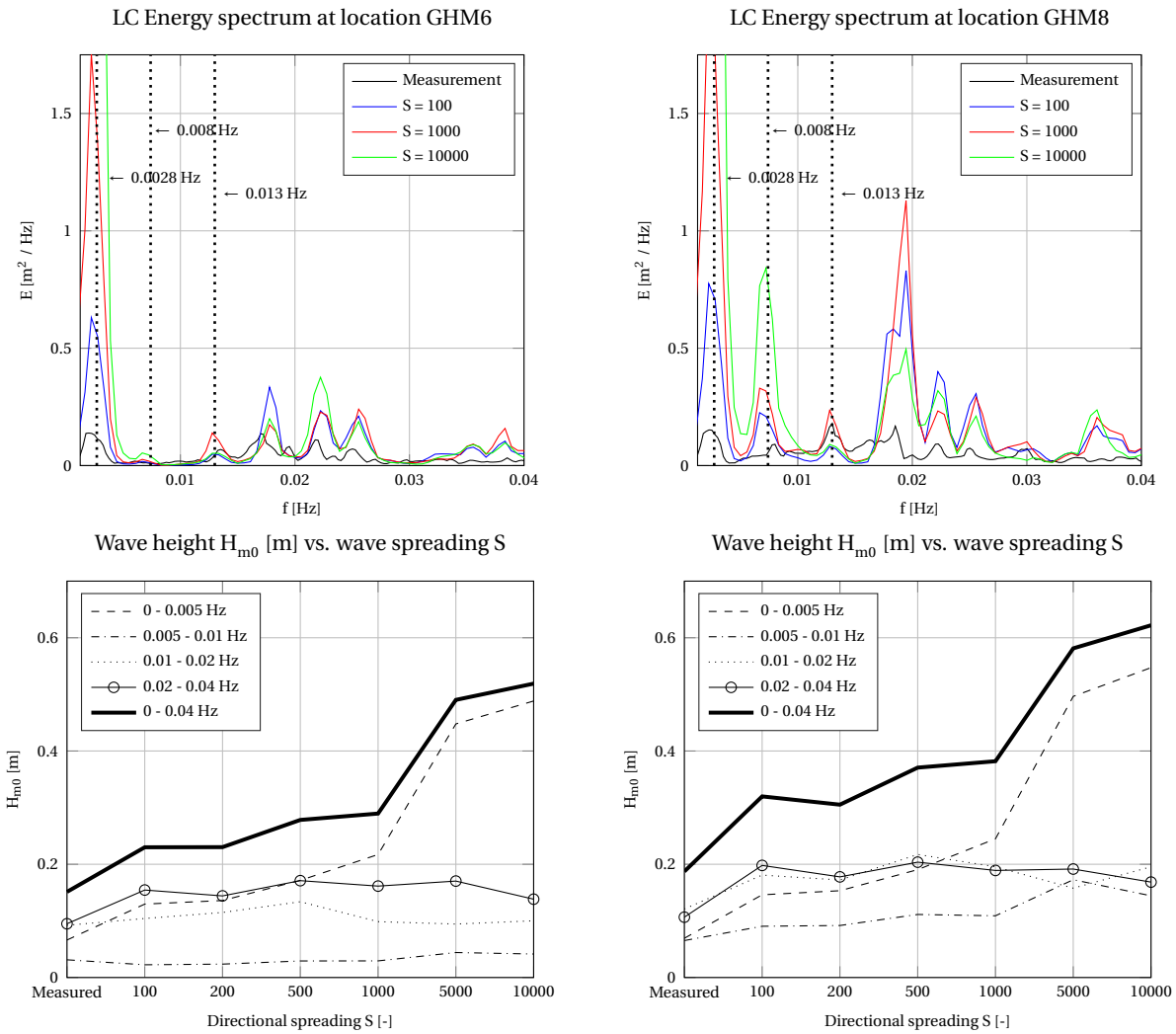

Figure 7.11: Long-crested: spectra for various spreading (upper) and wave height as function of spreading (lower). The vertical lines indicate the first three longitudinal resonant frequencies.

Figure 7.12 gives the wave heights for various directional spreading in the short-crested wave range. Now, the frequency band with the Helmholtz mode seems not to be very sensitive to the varying spreading parameter but an increasing trend in wave heights is still observed with decreasing spreading. The higher order frequencies are more affected by spreading, especially around the frequency Hz = 0.02.

Around this frequency the influence of 2D-induced resonance is to be observed in both Figures 7.11 and 7.12. The 2D resonant frequencies (Table 4.3 in Section 4.2.2) the wave heights are amplifying (quite arbitrary with spreading), indicating that 2D effects are not to be neglected whereas in laboratory experiments these modes are not always measured or dampened out. It is not clear why the Helmholtz mode in the long-crested wave conditions are sensitive for spreading, whereas the 2D resonant frequencies are affected the most by the short-crested waves.

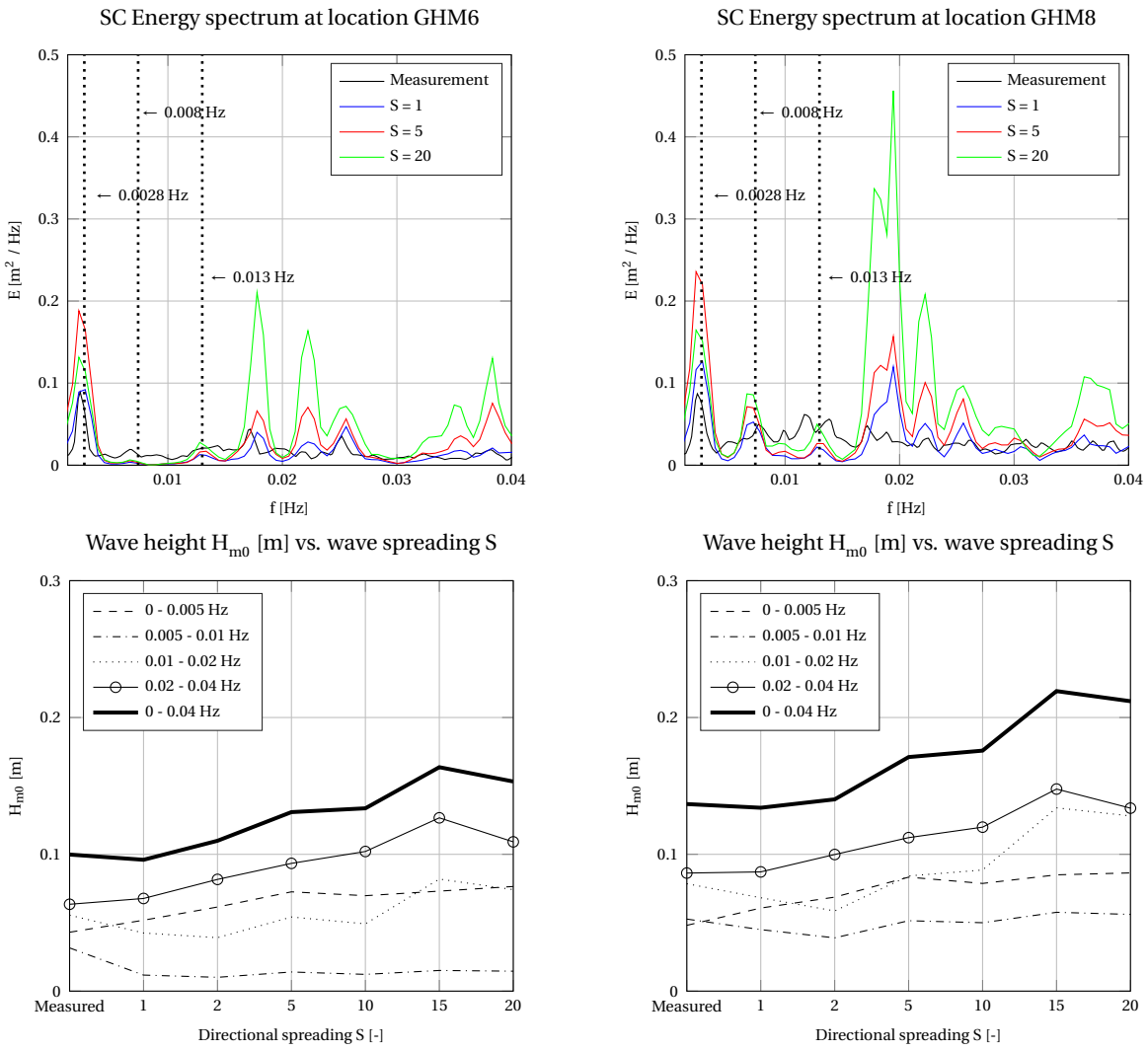

Figure 7.12: Short-crested: spectra for various spreading (upper) and wave height as function of spreading (lower).

Sand (1982) showed in his research that both the wave heights and periods for the long waves are also affected by the amount of wave spreading. Significant wave heights and periods increases with decreasing spreading. Table 7.3 shows the wave period as a function of wave spreading calculated by XBeach. XBeach shows good agreement with the measured wave period, except for $s > 500$. The sudden increase in wave period for a high s-value was also observed in the wave heights. Overall, the trend is well computed in the sense that less spreading leads to larger wave period. This also indicates that the physical processes are well modelled.

Table 7.3: Mean wave period for varying spreading parameter at location GHM08.

	Short-crested						**Long-crested**					
Spreading s	1	2	5	10	20	Lab	100	200	500	1000	10000	Lab
T_{m01} (s)	55	55	54	56	53	55	56	61	66	80	165	60

The model is relatively insensitive for varying spreading parameter in the short-crested waves range, but wave height starts to grow for uni-directional waves. There is no direct explanation for this behaviour, but it is possible that the SB mode is not really suitable with long-crested waves in harbours. This is not regarded as a big disadvantage, because it is questionable whether an extreme spreading parameter is realistic in coastal and port engineering practices.

7.4.2. Friction

The friction is referred to both the short waves and long waves. The short wave friction is related to the dissipation of short wave energies in SB. The results is that less energy is transferred to the long waves. In this case, at intermediate water depth, short wave friction is not very pronounced. A high friction coefficient has to be used to reduce the wave height. The analysis is documented in Appendix A. It is theoretical more sound to look at the friction for the long wave.

Generally, increasing flow friction reduces the long wave energy and thus the wave heights. We examine two types of friction formulation: Manning[1] n and Chézy C. Manning is depth-dependence:

$$n = \sqrt{\frac{c_f h^{\frac{1}{3}}}{g}} = \frac{h^{\frac{1}{6}}}{C} \tag{7.1}$$

where C is the Chézy coefficient, c_f the dimensionless friction coefficient and h the local water depth. As long waves are sloshing in the basin, with water motions that move up and down, energy dissipates more due to the local smaller water depth. The ideas of increasing friction are to:

- Examine the effect of flow friction on the wave heights.
- Compensate for the scaling effect as discussed in section 4.4.

The friction coefficients are adapted from *G.J. Arcement and Schneider (1989)*. The results for both friction coefficients are very similar. In this subsection, only the results of Chézy are presented. The results of Manning friction are documented in Appendix A.

Figure 7.13 presents the wave spectra and wave heights as function of the Chézy of Test A1 with long-crested wave condition at two locations inside the harbour (GHM06 and GHM08). The runs are carried out with values varying from C = 10 – 110. Realistic values are in the range of $C \approx 30-90$, representing sandy to rocky bed. If we look carefully to the lower plots of Figure 7.13 in the range of $C \approx 30-90$, the wave heights does not change much. The increase (decrease) in wave heights are only in the order of 2 - 3 cm with increasing (decreasing) Chézy coefficient. Only the extreme values show some significant change in the wave heights, which is in this particular case (laboratory settings) quite unrealistic. High friction in XBeach cannot dissipate the overestimated energy sufficiently in the harbour.

[1] Manning can be seen as the depth-dependent formulation of Chézy.

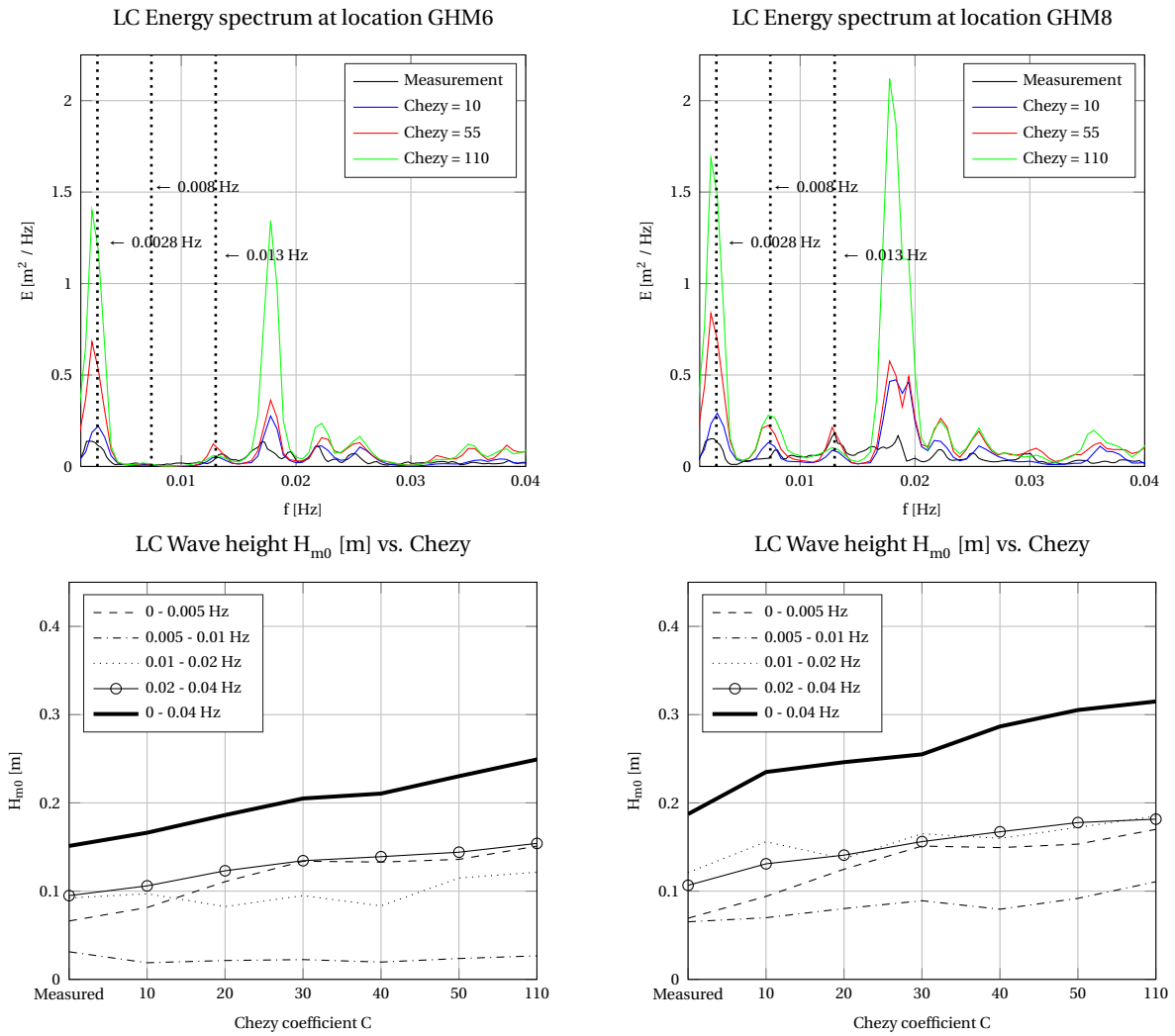

Figure 7.13: Test A1: spectra for various Chézy coefficient (upper) and wave height as function of Chézy coefficient (lower) for long-crested waves.

The overestimated wave heights in Test A1 as discussed in Section 7.3 is not due to insufficient friction in the computational domain, but are more related to the presence of short waves in the harbour. However, increasing friction **does** have influence on the calculated wave heights. This is in particular interesting for Tests B where both the absolute and relative differences of the wave heights are smaller. Therefore it is anticipated that better results are obtained for the short-crested wave conditions.

Figure 7.14 shows the spectra and wave heights for various Chézy coefficient. The lower plots of Figure 7.14 display the wave heights as function of Chézy coefficient. At both two locations inside the harbour, a value of $C \approx 30$ - 35 show good correspondence with the measurements. This trend is also observed in the spectra (upper plots of Figure 7.14), but there is a overestimation of the wave energy around the frequency of Hz = 0.02.

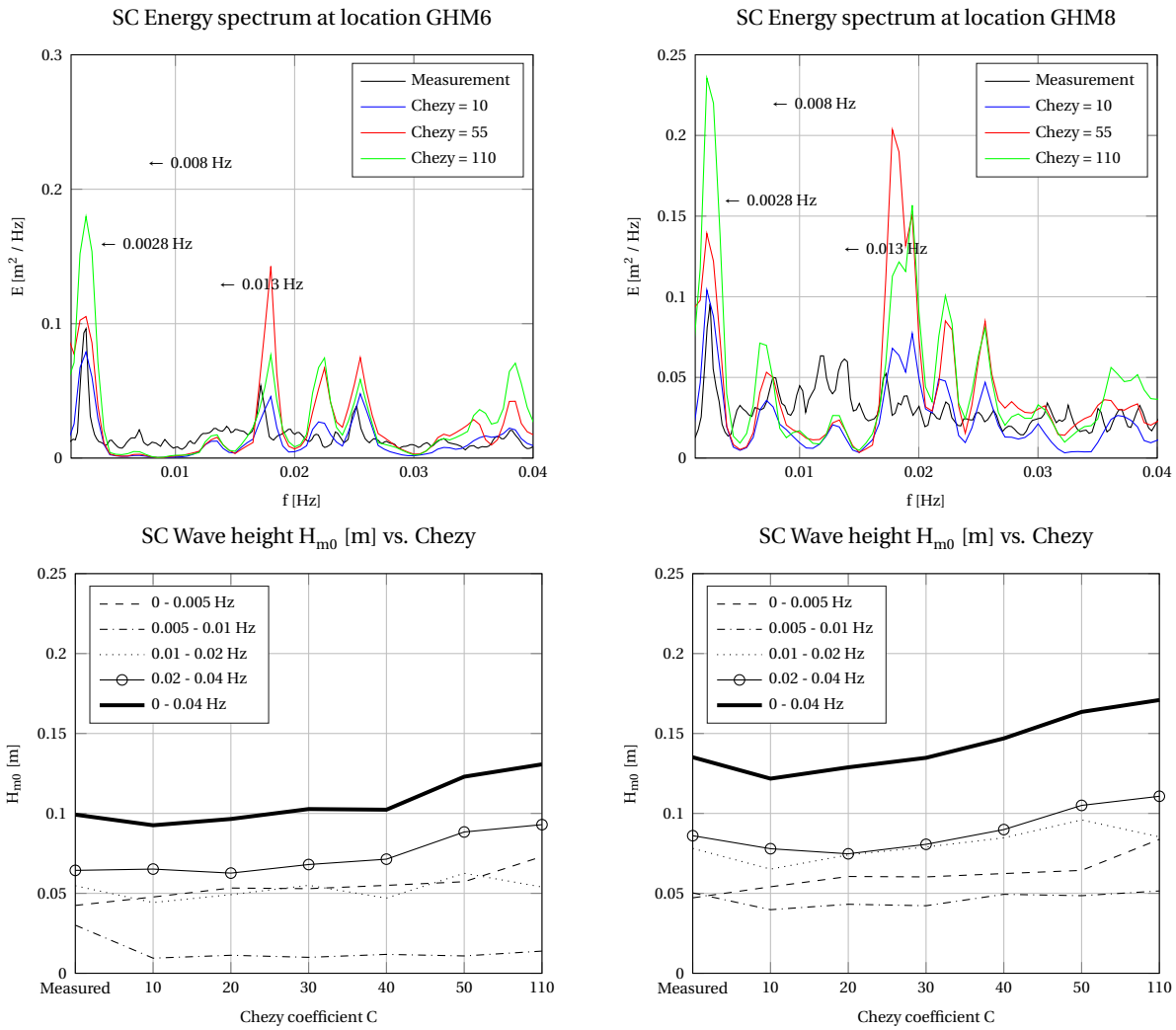

Figure 7.14: Spectra for various Chézy coefficient (upper) and wave height as function of friction (lower) for short-crested waves.

The main points of this sensitivity analysis are elaborated hereafter:

- The wave heights increase with decreasing spreading. By decreasing the spreading of the waves, their energy level in the harbour decreases as well. The waves are not controlled by the short waves and thus resulting in strong amplification of the long waves.
- The considered long-crested wave conditions in this sensitivity analysis is quite unrealistic: up to $s = 10000$. From $s > 500$, a strong growth in the wave height is observed. Fortunately, in coastal engineering the long-crested wave is a rare phenomenon.
- Insufficient friction is not the main mechanism that causes the difference between the calculated and measured wave heights. Only extreme friction factors can dissipate the long-crested long wave energy significantly, but this result in unrealistic friction values to achieve good compliance with measurements. The short-crested wave conditions show better correspondence with measurements. The role of the short waves is striking.

7.5. Model comparison: surfbeat vs. non-hydrostatic

This section compares the predictive skills of the two modes within XBeach. Firstly, the Helmholtz mode is compared in Subsection 7.5.1. Secondly, in Subsection 7.5.2 the wave heights and wave periods are further analysed. The section is concluded in Subsection 7.5.3 with a general discussion.

Model comparison and evaluation for the short waves are not done, simply because SB underestimates the wave heights in the harbour and there are no model parameters to improve short wave modelling. Where short waves need to be calculated, the phase-resolving mode is preferred.

7.5.1. Helmholtz mode

The most energetic natural mode of a harbour is the Helmholtz mode in the longitudinal direction. In this subsection, the spectral wave heights of the Helmholtz mode are compared by integrating over a narrow frequency band ($0.0015 \leq$ Hz ≤ 0.0035). Figure 7.15 shows the spectral wave heights of this mode.

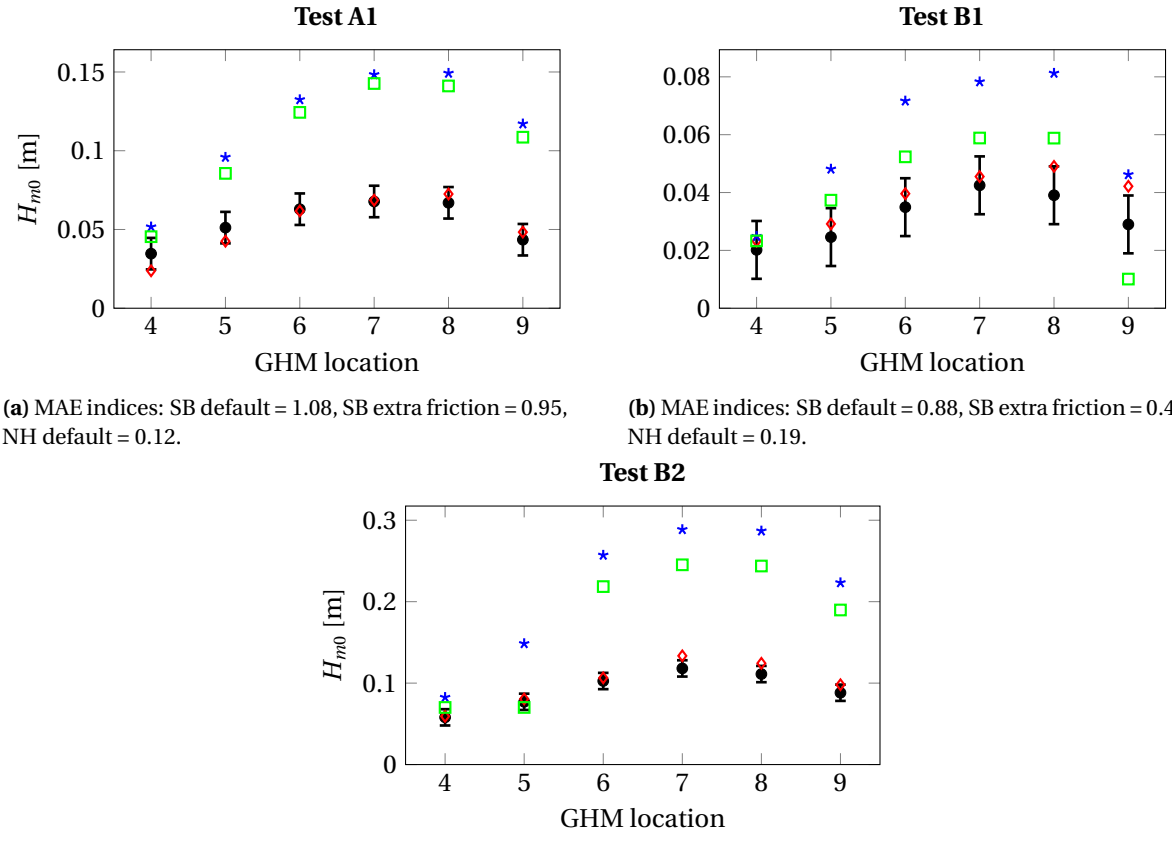

(a) MAE indices: SB default = 1.08, SB extra friction = 0.95, NH default = 0.12.

(b) MAE indices: SB default = 0.88, SB extra friction = 0.44, NH default = 0.19.

(c) MAE indices: SB default = 1.29, SB extra friction = 0.95, NH default = 0.10.

Figure 7.15: Spectral wave heights of the Helmholtz mode. The vertical line indicates a 1 cm band.

The default mode of SB and NH (⋆ and ◊) refers to the default friction coefficient of C = 55 $m^{1/2}/s$. The 'friction' mode (□) is the model with a slightly rougher bathymetry with C = 30 $m^{1/2}/s$.

The energy in the range of the Helmholtz frequency is overestimated in SB with factor 2 to 3. In the NH mode, short waves with its bound wave diffract into the harbour. Because there is no significant wave breaking with these wave conditions, there is always an interaction between the short and long waves, where the amplification is 'controlled' by the short waves. This interaction is less pronounced or even absent in SB.

Increasing the friction does further decreases the wave heights. However, the effect is marginal and only reduces the wave height in the order of 2 - 3 cm. This is in line with the expectation that energy decay is due to energy radiating out of the harbour, rather than being dissipated by friction. The energy level is calculated well by the NH mode. In all cases, there is almost a one-to-one similarity with the measurements.

7.5.2. Significant wave heights and wave periods of the long waves

For all cases, the NH mode reproduces the short and long waves quite well. For the SB mode, the short waves were - as expected - not well reproduced, whereas the long waves were reasonably modelled. This subsection compares the spectral wave heights and period of the long waves.

Figure 7.16 shows the spreading of the wave heights for both XBeach modes.

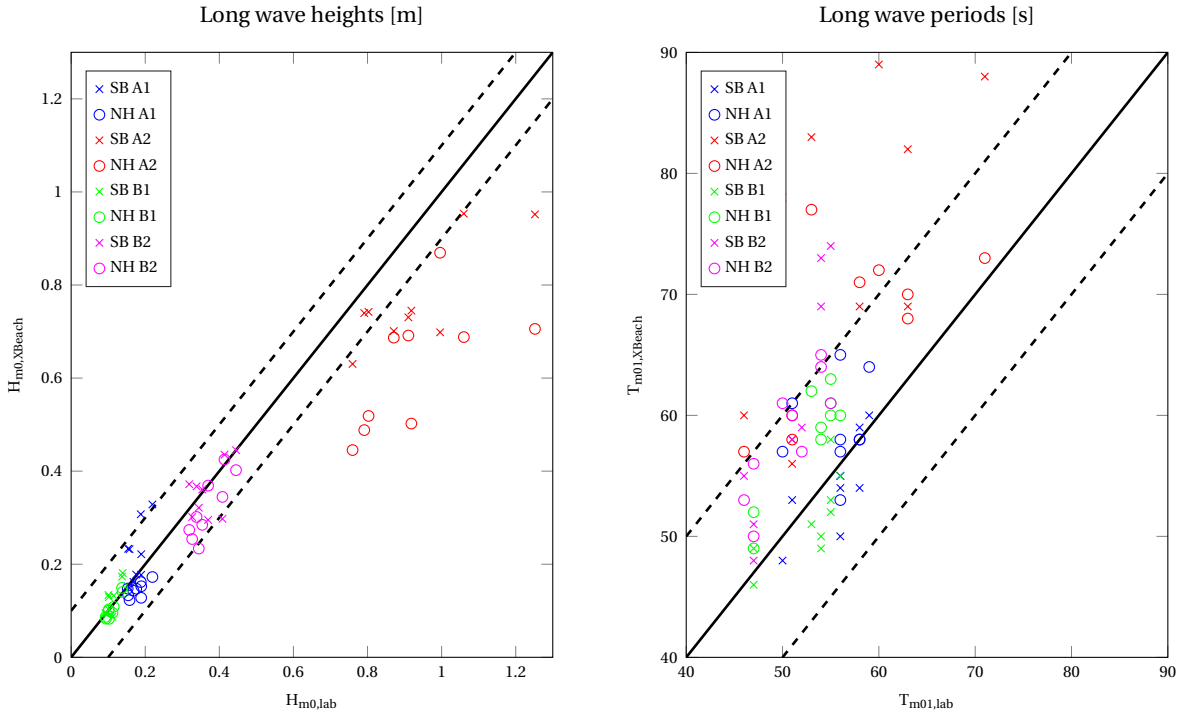

Figure 7.16: Comparison wave heights and periods. The solid line (−) denotes perfect agreement, the dashed line (−−) indicates the 10 cm and 10 s band for the wave height and period, respectively.

Generally, the calculated wave heights lie in between the 10 cm deviation band, except Test A2. This was related to the amplification of the long waves once they propagated into the harbour in the laboratory experiments. The calculated wave periods show larger scatter. For the SB mode, there seem to be a relation between the obliquity of the waves with respect to the harbour mouth, but a physical explanation could not be found in this study. Same trend was found if T_{m02} is calculated instead of T_{m01}, but the overestimation was less.

A comparison with the MAE index is made for all the wave gauges together (GHM01 to GHM09), offshore (GHM01 to GHM03) and wave gauges inside the harbour (GHM04 to GHM09). The considered parameters are shown in Figure 7.17. The resonant frequencies are very well predicted by both SB and NH with almost identical MAE indices. It should be noted that the values of the resonant frequencies are in the order of (O)10^{-1} and (O)10^{-2} and a small deviation results in a high relative difference (bias). These frequencies can always be identified, regardless the wave conditions.

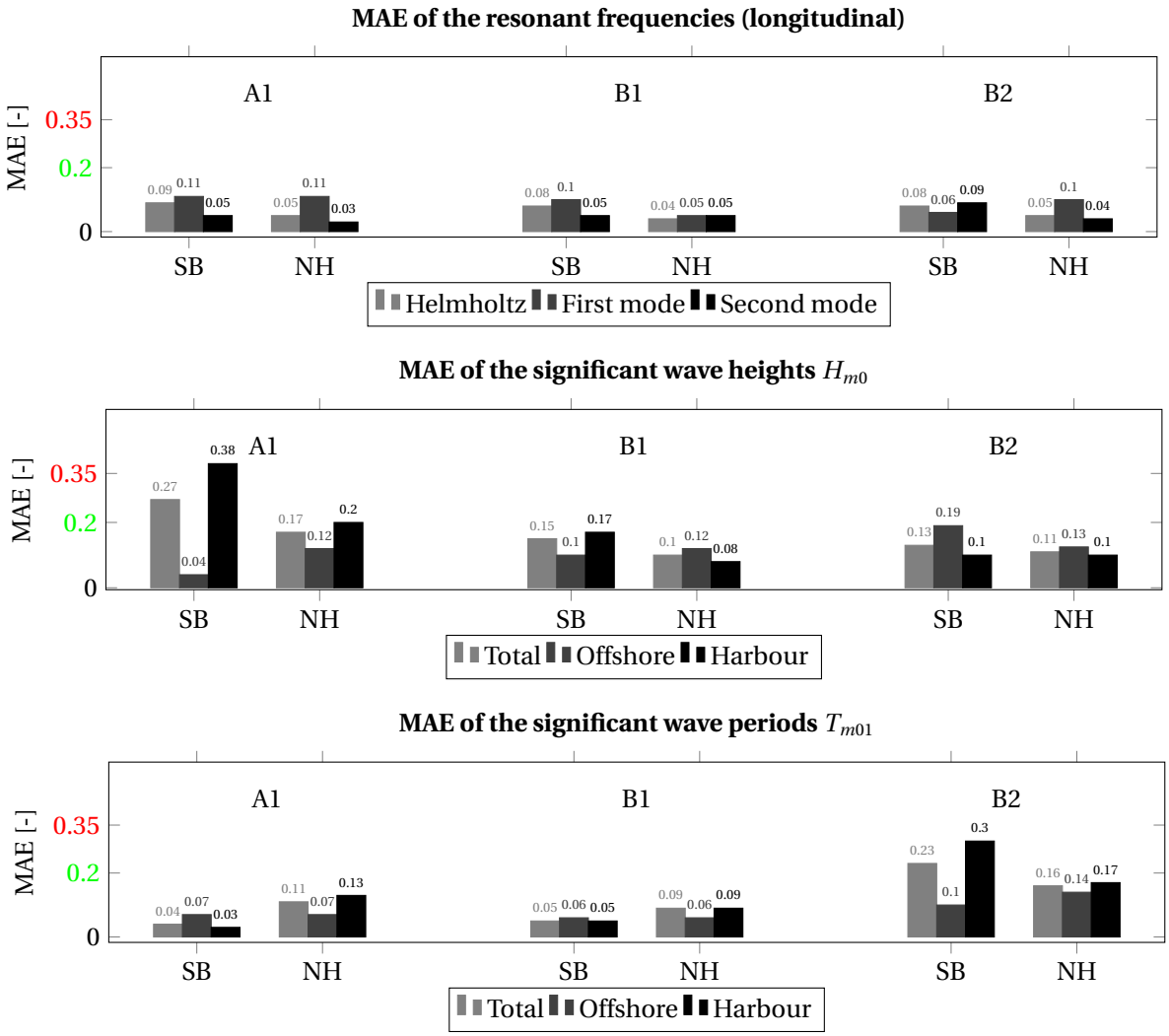

Figure 7.17: MAE indices of the resonant frequency (upper plot), wave heights (centre plot) and wave periods (lower plot).

Further, the calculation of the wave heights is in all cases slightly better for the phase-resolving mode

than the phase-averaging mode of XBeach. SB does not perform very well in Test A1 (MAE = 0.27), where the short waves are completely absent in the harbour. The predictive skills of XBeach of the long waves where short waves are able to propagate into the harbour are almost equal. For the calculation of the wave periods, more confident is placed in the NH mode.

7.5.3. Discussion: surfbeat or non-hydrostatic?

Until here, the accuracy of predicting the resonant frequencies, wave heights and wave periods has been analysed. A brief discussion of XBeach is given regarding applicability and computational efficiency.

Short waves can only be accurately predicted by NH mode. This is because in the SB mode, there is no diffraction in the model. Obviously, modelling of the short waves with harbours that are subject to direct wave attack is potential for SB but not further considered in this study.

Both modes predicted the right resonant frequencies, but SB overestimated the energies in the spectrum. Consequently, the wave heights are overestimated, whereas the NH mode predicts the wave heights much better in the considered cases. In the SB mode, the accuracy of the wave heights for the long waves depends on the presence of short wave energies in the harbour. When they are absent, the NH mode is recommended. If short wave energies are able to propagate into the harbour (e.g. spreading, mean wave direction), the SB can be used as well. However, this is very case dependent.

In engineering practises, not only accuracy of the numerical model is important. Often, a trade-off needs to be made between the accuracy and computational time. Preferably, a simulation should be finished within one night. We will indicate the computational efficiency. Table 7.4 provides an overview of the computational efficiency of XBeach. It should be noted that the total computational time for the

Table 7.4: Computational efficiency, based on Test A1.

	NH	SB
Grid resolution (m)	4 - 6	10 - 20
Number of computational grids	262 425	59 976
Simulation time (hours)	6	6
Averaged time step (s)	281 385	194 399
Amount of time step	0.07	0.11
Processors used	23	1
Comp. time (hours)	15.5	3.7
Comp. cost (processors × comp time)	356.5	3.7
Comp. cost (comp. time (s) × processors) / grid cell	4.9	0.23
Comp. cost (comp. time (s) × processors) / time step / grid cell	1.75×10^{-5}	1.20×10^{-6}

SB mode includes the calculation of the short wave energies on the directional grid. Clearly, SB is much faster and cheaper than NH. This is because of the spatial grid resolution of SB, which is an order of magnitude larger than NH.

More aspects should be considered when comparing the computational efficiency. Firstly, the SB mode does not provide the total water elevation, but only the long wave elevation. Secondly, the computa-

tions were carried out on different machines with different properties. The runs of SB were carried out on a PC with Intel i7-4700 processor, 3.1GHz with a single core. NH was carried out on a remote machine consisting of 23 Intel cores (exact type is unknown) with a GHz of 2.1. Thirdly, due to the lateral boundary issues and the exclusion of the rear slope, the computational domain is different for NH. Nevertheless, it can be concluded that SB is much faster (at least 1 order of magnitude in time) given that the short waves are not fully resolved.

In other words, when accuracy is important more confident is place in the NH mode. SB is more applicable if only an estimation of the wave height and period is sufficient.

7.6. Conclusion

The capabilities of XBeach SB to reproduce the hydrodynamics have been examined extensively in a rectangular harbour basin with very oblique incoming waves. The results have been compared with data obtained from the measurements in the Vinjè directional basin of Deltares. The following conclusions can be drawn from the analysis:

Short waves

- Wave heights for the short waves are not well calculated in the harbour with SB. MAE indices are larger than 0.35 (MAE $\leq$ 0.20 is regarded as good, and MAE $>$ 0.35 is poor). This is related to the wave-averaging mode of the short wave module in SB where there is no phase information available. Hence, diffraction is not considered which results in significant differences between the measurements and calculations.

Long waves

- The (theoretical) resonant frequencies are always identified in XBeach, though not always measured. In the measurements, these are dampened out, whereas in XBeach the energies amplify (too much). The MAE indices of the resonant frequency is less than 0.10.
- The significant wave heights are overestimated, which is related to the absence/presence of the short waves. The short waves 'control' the long waves such that it minimises the amplification in the harbour. This hypothesis is further supported in Chapter 6, with the NH mode (long waves are bounded to the wave groups), and also with an extensive sensitivity analysis with varying spreading parameter. The indices vary from 0.10, where short wave energies are present in harbour, to 0.38 where the short waves are completely absent.
- The calculation of the spectral periods for the long waves becomes problematic for very oblique incoming waves. Additional analysis shows that the wave periods increases with increasing angle with respect to the harbour mouth. A sound physical explanation could not be found in this study.

Comparison with the non-hydrostatic mode

- Generally, $MAE_{NH} \leq MAE_{SB}$ where the indices of NH are always smaller than 0.20.
- The spectral energy distribution over the frequencies in the NH mode corresponds much better with the measurements than SB. For the latter, the energies are generally overestimated. The role of the short waves, which prevents the long waves to amplify too much, is demonstrated.
- The calculated wave heights for the long waves by NH have a higher accuracy than SB. Also, more confidence is placed in the NH mode in calculating the wave periods for the long waves.
- SB is at least 1 order of magnitude in time faster. This is because the grid resolution is based on a long wavelength, whereas for the NH is based on the peak frequency of the short waves.

8

Case II: Non-hydrostatic & Surfbeat

8.1. Introduction

In the previous case with a simple rectangular basin, the model performances of both SB and NH mode have been examined, where the considered governing processes were diffraction, reflection and harbour oscillations. A slightly different harbour layout is used in this second case to make sure that the findings in the previous chapters are not case dependent. Similar governing processes are considered in order to confirm or refute the findings of Case I.

The approach and analysis are similar to that of Case I, where the focus is on the resonant frequencies of the long waves, spectral wave height H_{m0} and spectral wave periods T_{m01} for both the high-frequency (short waves) and low-frequency (long waves) part of the wave spectrum. The split-frequency between the short and long waves is again chosen at f =0.04 Hz. Further, the imposed wave conditions and the considered harbour layouts have already been discussed in Section 4.3 of Chapter 4.

The structure of this chapter is similar to that of Chapter 6 and 7 and is as follows. Firstly, the model set-up is discussed in Section 8.2. The results are presented in Section 8.3 and the chapter is concluded in Section 8.4.

8.2. Model set-up

This section presents a brief overview of the model set-up for both the NH and SB mode for the Tests T038 and T046 and are the same for both tests. The offshore and lateral boundary conditions are similar to that of Case I (see Sections 6.2 (NH) and 7.2 (SB) of Chapters 6 and 7, respectively). Other settings may vary and are described further below.

Non-hydrostatic

The NH model settings are as follows:

- Grid resolution of 1.4 m (40 grid points per wavelength, corresponding to a peak period of 6.67 s). This grid resolution is similar to the work of *Monteban (2016)*, where the author reproduced the laboratory experiments with SWASH and MIKE21 with the same harbour layout. By choosing a similar grid size, a fair comparison is possible.
- Bottom friction of n = 0.03 and gravel slope friction of n = 0.075 (Manning). These friction coefficients are chosen based on several trial-and-error runs such that the calculated offshore wave characteristics match the measurements.
- The model is forced at the offshore boundary with a parametrised JONSWAP spectrum, as listed in Table 4.5 of Chapter 4.
- Lateral advective boundaries are applied, which is an intermediate solution between Neumann and zero-velocity boundary. The Neumann boundary condition could not be applied due to discrepancy in the calculation model, see also Section 3.3.2.
- Weakly-reflective offshore boundary condition is used where reflected (long) waves can pass through the boundary with minimal reflection. This boundary is at the position of the wave generator.
- CFL - condition of 0.5 is used to ensure stability, similar to that of Case I of NH.

Surfbeat

The SB model settings are as follows:

- Grid resolution of 4 m, based on approximately 40 grid points per long wavelength. One long wavelength, approximately 200 m, is approximately 5 times the short wavelength corresponding to the peak period of 6.66 s. See also Appendix A.
- Bottom friction of n = 0.03 and gravel slope friction of n = 0.075 (Manning), similar to the friction coefficient of the NH mode, see above.
- The model is forced at the offshore boundary with a parametrised JONSWAP spectrum, as listed in Table 4.5 of Chapter 4.
- For the flow, a weakly-reflective offshore boundary condition is imposed where reflected long waves can pass through the boundary with minimal reflection. This boundary is at the position of the wave generator.
- Neumann boundary condition is applied at the lateral boundaries for both short and long waves. This boundary condition ensures that there is no gradient along the boundaries.
- CFL - condition of 0.7 is used to ensure stability, similar to that of Case I of SB.

8.3. Results

This section compares the results of XBeach with the measurements of Tests T038 and T046. The results are presented separately for the short waves (f > 0.04 Hz) and long waves (f ≤0.04 Hz). Further, only the results of the side basin are presented. The results of the main basin are quite good for both modes of XBeach, with MAE indices in the order of 0.10 - 0.20 for both tests (T038 and T046) for the wave heights and wave periods. However, in the SB mode there are some spatial variation of the wave heights. The calculations for the main basin and additional SB results are documented in Appendix B.

8.3.1. Short waves

This subsection presents the XBeach (NH and SB) results of the wave heights for the short waves in the side basin.

Figure 8.1 shows the calculated significant wave heights in the side basin. These wave heights are calculated by averaging the significant wave height over a circle with a diameter of 30 m, which has a similar order of magnitude as Case I, see also Subsection 6.3.2 of Chapter 6. The NH mode calculates the wave heights quite accurately, with a MAE index of about 0.10 and generally within the 20% deviation band. An overview plot of the wave heights is presented in Figure 8.2. The results confirm the ability of NH to predict hydrodynamics in sheltered areas with the governing wave processes as diffraction, reflection and harbour oscillations.

Further, SB underestimates the wave heights at all locations. This is because phase information is required (diffraction) for accurately resolving short wave propagation into the basin. The underestimation is in Test T038 slightly less (compared to Test T046) where wave energies are able to propagate into the basin by means of directional wave spreading.

The spectral wave periods are well predicted by NH. The MAE indices are in the order of 0.15 for both tests. The reader is referred to Appendix B for an overview of the wave periods of NH.

The findings in this subsection of the short wave are in agreement with the findings found in Case I in the previous chapters. The NH mode is able to predict the short waves in the harbour quite accurately with the method of circle. It should be noted that using this method, the averaged wave climate can be calculated quite accurately, but the exact point output information is lost and it cannot be retrieved unambiguously. By looking at the overview plot, it is possible to derive the (standing) wave pattern inside the harbour since these are modelled quite accurately. Further, the SB mode demonstrates again the inability to model short waves in harbour. In test T038, even with significant spreading, the waves penetrate easier into the harbour basin than in Case I, but SB still underestimates the wave heights crudely. Summarised, the results are consistent with the findings of Case I.

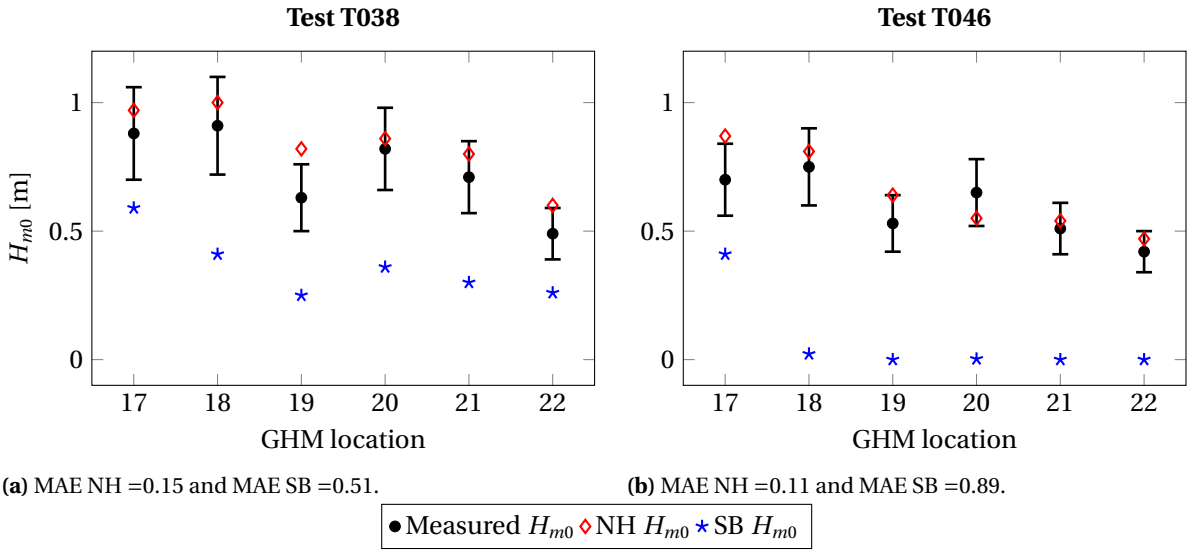

(a) MAE NH =0.15 and MAE SB =0.51.

(b) MAE NH =0.11 and MAE SB =0.89.

Figure 8.1: Significant wave heights of in the side basin with short-crested (left) and long-crested wave conditions (right). The vertical line indicates a 20% measurement deviation. Note that the wave height of NH is determined by averaging the wave height over a circle with diameter of 30 m.

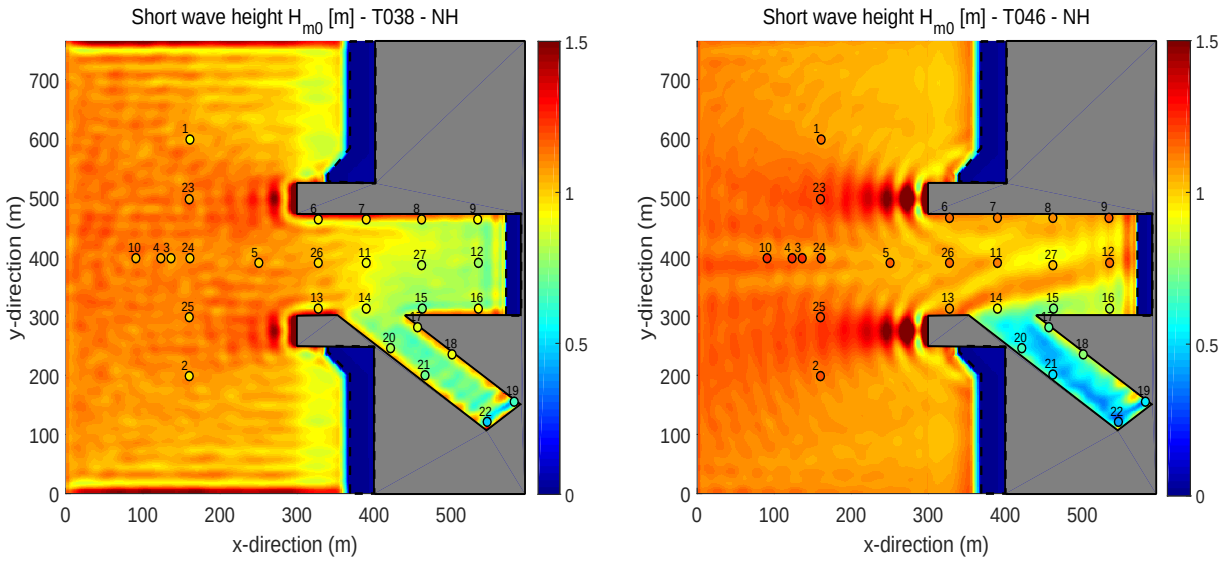

(a) Test T038

(b) Test T046

Figure 8.2: Significant wave heights as calculated by NH. The circles denote the measured wave heights.

8.3.2. Long waves

This subsection presents the XBeach results of the wave heights, wave periods for the long waves and the resonant frequencies in the side basin. The MAE indices in the main basin are generally smaller than 0.20 for SB, and in the order of 0.10 for the NH mode. The reader is referred to Appendix B for the results of the main basin.

The calculated wave heights are shown in Figure 8.3 and an overview plot is presented in Figure 8.4

(only for SB). Both NH and SB overestimate the wave heights, but based on the MAE indices the phase-resolving mode performs slightly better. It should be noted that relatively high MAE indices are easily obtained, because the considered wave heights are small and a small deviation results in a large relative difference (and thus MAE index). In absolute terms, the overestimations are in the order of 2 centimetres.

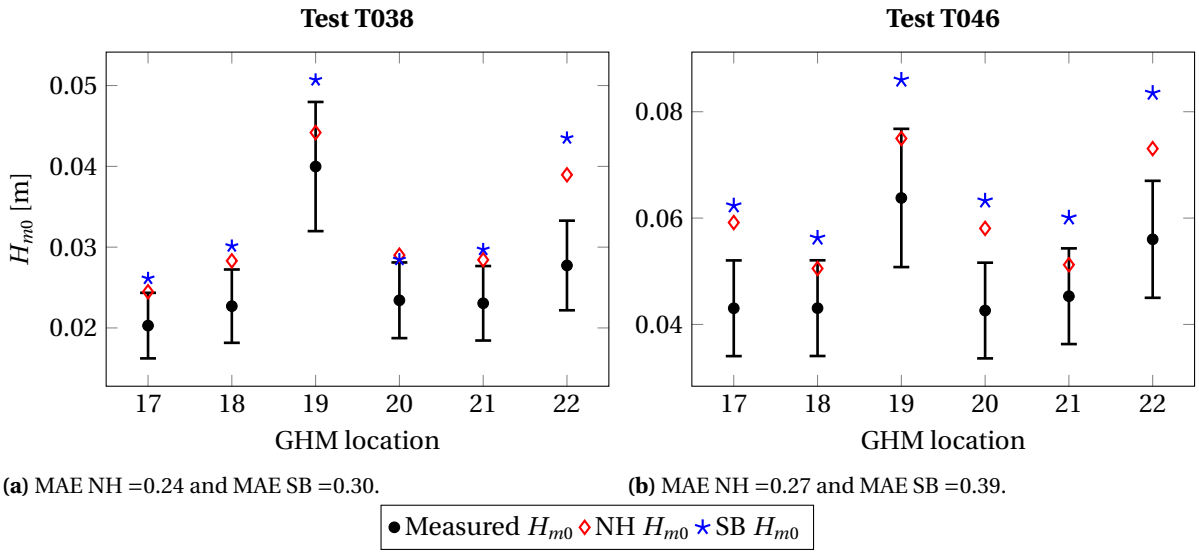

(a) MAE NH =0.24 and MAE SB =0.30.

(b) MAE NH =0.27 and MAE SB =0.39.

Figure 8.3: Significant wave heights of in the side basin. The vertical line indicates a 20% measurement deviation.

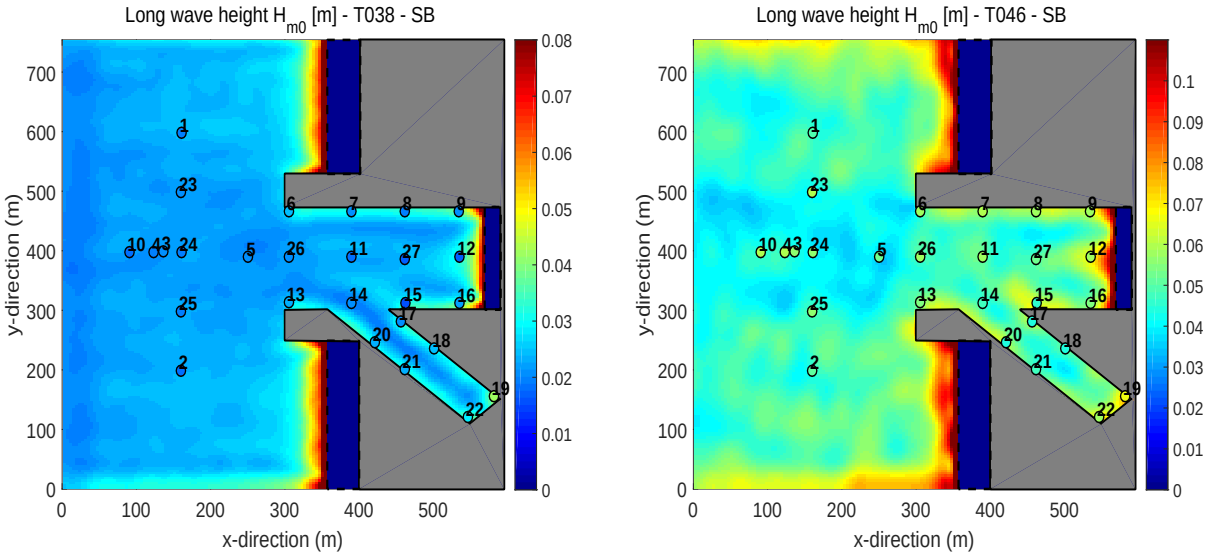

(a) Test T038.

(b) Test T046.

Figure 8.4: Significant wave heights as calculated by SB. The circles denote the measured wave heights.

NH calculates the wave heights with both short-crested (T038) and long-crested (T046) wave conditions reasonably with a MAE index of 0.24 to 0.27. SB overestimates the wave heights with the short-crested wave conditions on average with 30%, slightly more than NH. The overestimation is greater for SB with

the long-crested wave conditions where the long waves are not bounded to the short wave groups, with a MAE index of 0.40 which is considered as poor. This is in line with our findings with Case I in the Vinjè directional basin (see Chapter 6 and 7), where the role of the short waves was to minimise/control the amplification of the long waves. Although the MAE is relatively high with both wave conditions, it is clear that SB is more accurate in situations where short waves are present.

The results of this study is in line (qualitatively) with the study of *van Mierlo (2014)*. A comparison study with the same harbour layout and almost identical wave conditions as T046 (significant wave height was twice as high in his study) was carried out by *van Mierlo (2014)*, where the author showed with SWASH (same governing equations solved as in NH) that the overestimation in the side basin was also in the order of 20%.

The calculated wave periods, based on the energy spectrum with $f \leq 0.04$Hz, are in good agreement for both the SB and NH mode, see Figure 8.5. The MAE indices are in the order of 0.10, which are considered to be quite good. This is in line with the findings of Case I, where the calculated wave periods are quite accurate if the mean wave direction is not too oblique with respect to the harbour mouth. In this case, the harbour mouth is slightly less oblique than Case I.

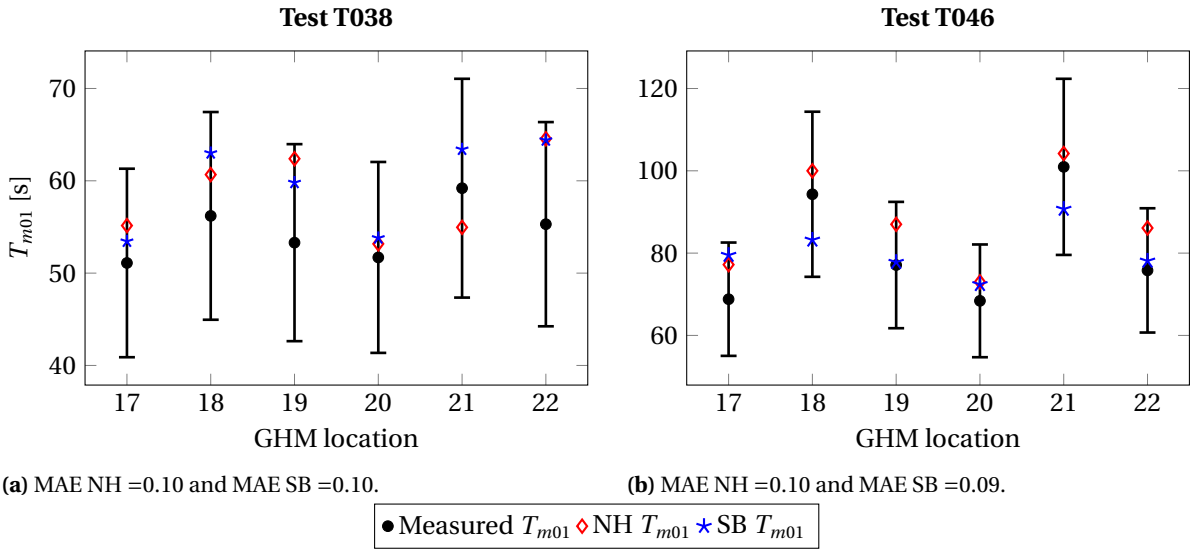

(a) MAE NH =0.10 and MAE SB =0.10. **(b)** MAE NH =0.10 and MAE SB =0.09.

Figure 8.5: Spectral wave periods of in the side basin. The vertical line indicates a 20% measurement deviation.

Further, Table 8.1 and Figure 8.6 show the resonant frequency and the energy spectrum at the corner of the side basin at location GHM19. The calculated Helmholtz frequency mode is in excellent agreement with the measurement and theoretical values for both NH and SB. Moreover, the energy spectrum of the two tests show that XBeach overpredicts the spectrum, which explains the overestimated wave heights. The NH mode reproduces the physics better, i.e., the energy distribution along the infragravity band is more accurate than SB. This trend was also found for Case I, where both modes within XBeach were able to identify the (theoretical) resonant frequencies, but there were some differences in the energy content.

Table 8.1: Resonant frequency at location GHM019 of Test T046. Biases (XBeach - measurement) of the Helmholtz mode are 0.04 and 0.02 for NH and SB, respectively.

Mode	NH (Hz)	SB (Hz)	Measured (Hz)	Theoretical (Hz)
Helmholtz	0.01075	0.011	0.0112	0.011

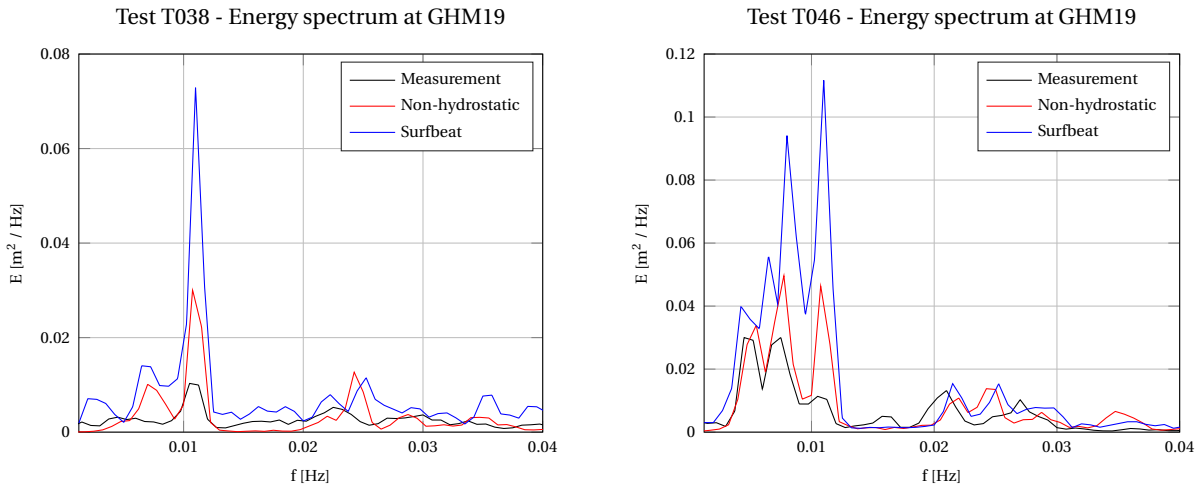

Figure 8.6: Energy spectrum of Tests T038 and T046 at location GHM019.

Further investigation on the energetic Helmholtz mode (0.0105 Hz - 0.0115 Hz) reveals that the energy level is overestimated in both tests: up to a factor 3 for SB, whereas NH overpredicts the energies up to a factor 2.25. The qualitative overestimation can be observed in Figure 8.6 and the significant wave heights of the Helmholtz mode are presented in Figure 8.7.

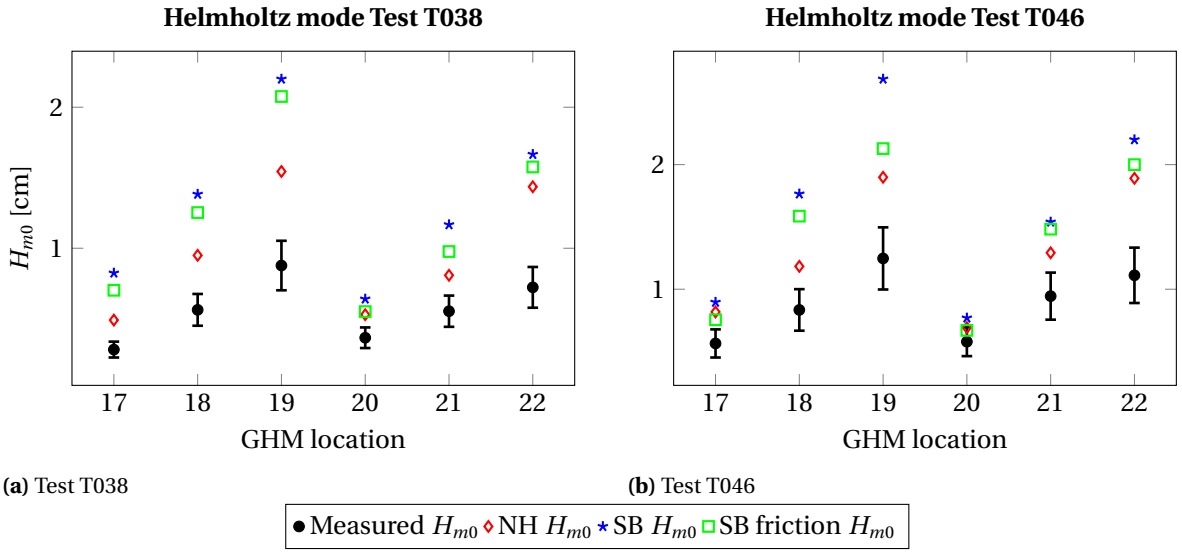

(a) Test T038 **(b)** Test T046

Figure 8.7: Significant wave heights of the Helmholtz mode. Overestimation up to factor 2.25 (NH) and 3 (SB). H_{m0} is determined by integrating over a narrow frequency band (0.0105 - 0.0115 Hz) and given in centimetres.

The overestimation is in line with the findings of *Monteban (2016)*. The author used MIKE21 BW and SWASH for Test T038, where the significant wave heights were overestimated with a factor 2.

Additional runs were carried out to reduce the overestimation in the Helmholtz mode of Test T046 with SB, see Figure 8.7 (□), by means of friction and directional spreading. The friction was increased up to an unrealistic (for this laboratory setting) manning coefficient of n = 0.075. The additional friction reduced the wave height of the Helmholtz mode in the order of 10%. This is in line with the theory that significant part of energy decay of the Helmholtz mode is by energy radiating out of the harbour mouth, rather than being dissipated by friction *(Rabinovich, 2009)*. Finally, the simulations with decreasing wave spreading did not show significant reduction of the energy in the Helmholtz mode.

8.4. Conclusion

This chapter presented an additional case to check whether the findings of Case I (the Vinjè directional basin) are generally applicable. The governing harbour processes in this chapter are similar to that of Case I and are diffraction, reflection and harbour oscillations. In order to assess the model performance, similar methodology is applied where the XBeach results have been compared with data obtained from physical modelling. The overall results are in line with the findings of the previous case in Chapters 6 and 7. Regarding the analysis, the following conclusions can be drawn:

Short waves

- SB cannot calculate the wave heights for the short waves in an area where the diffraction process is the main source of energy propagation into the harbour. This is because phase information is required, which is not considered in the SB mode (see also Chapter 3 and 7). The MAE indices are larger than 0.35 (MAE $\leq$ 0.20 is regarded as good, and MAE > 0.35 is poor).
- NH predicts the wave heights quite well with a MAE index in the order of 0.10 - 0.15.

Long waves

- The significant wave heights for the long waves are reasonably reproduced by both NH and SB with the short-crested wave condition (short waves spread into the harbour), with a MAE index of 0.25 - 0.30.
- The long-crested wave condition is only reasonably reproduced by NH. In SB, with these long-crested waves, the short wave energies cannot propagate into the harbour because there is no wave spreading. Consequently, the long waves cannot be 'controlled' by the short waves. The SB performs poor with a MAE index of 0.39.
- The periods of the long waves are well predicted with a MAE index not larger than 0.10.
- The frequency of the harbour oscillations are modelled correctly. The energetic Helmholtz mode is overestimated with factor 2 and 3 for NH and SB, respectively. This is in line with the findings of other studies where identical harbour layout was used (e.g. *Monteban (2016)* and *van Mierlo (2014)*).

The findings in the previous chapters of Case I apply here as well for both the short and long waves. This means that reproduction of the short waves is only correct with the NH mode in case similar method is used to derive the spectral wave height (method of circle). (Theoretical) resonant frequencies are always identified, whereas with respect to the wave period and wave height, more confidence is placed in the phase-resolving mode of XBeach. The MAE indices are for both cases quite similar.

Final Considerations

9

Conclusions & recommendations

9.1. Conclusions

The study examined the model skills to predict hydrodynamics in harbours with both XBeach non-hydrostatic and XBeach surfbeat. Two laboratory experiments, representing a fairly simple rectangular seaport, were reproduced in XBeach and compared in order to assess the model performance on mainly accuracy and also computational efficiency.

The main objectives of this study were:

1. To identify (theoretically) the possibilities and limitations of XBeach to reproduce hydrodynamics in harbours.
2. To examine predictive skills of the XBeach model by comparing the results with the measurements, as well as inter-model comparison.

The discussion of the results has been separated for the short and the long waves. For the former, these are derived from the energy balance equation, where the wave energy is proportional to the wave height squared (XBeach surfbeat). Also, short waves are defined as the energies above f > 0.04 Hz in the energy spectrum (XBeach non-hydrostatic). The long waves are the energies in the energy spectrum belonging to frequencies f ≤ 0.04 Hz in both XBeach non-hydrostatic and XBeach surfbeat.

9.1.1. Conclusions towards objective 1

The fundamental difference between non-hydrostatic and surfbeat is the type of numerical model. XBeach non-hydrostatic is a phase-resolving model, whereas XBeach surfbeat is a mix between phase-

averaged (short waves) and phase-resolving (long waves). Phase-resolving models provide phase information where the wave characteristics of the individual waves are calculated. These wave characteristics (e.g. wave heights and wave periods) can be, for instance, derived from the energy spectrum. Phase-averaged models do not calculate such information in detail, but are averaged over a wave group. Only the wave heights based on the wave energy can be obtained. Therefore, the governing equations are also different.

The literature review reveals that both the non-hydrostatic and surfbeat modes have challenges in predicting hydrodynamics in harbours. XBeach non-hydrostatic is theoretically able to resolve the harbour processes considered in this study (reflection, diffraction and harbour oscillations). The accuracy is limited by the dimensionless water depth kd of 1. Surfbeat, on the other hand, cannot resolve short wave processes such as reflection and diffraction, simply because there is no phase-information. The energy transfer from the short waves to the long waves makes it possible to resolve the long wave harbour processes, such as reflection of the long waves and harbour oscillations.

An additional disadvantage of both non-hydrostatic and surfbeat is that porous structures cannot be defined in the calculation model. These coastal structures are often present and have somehow influence on the wave climate in the harbour. For this reason, the case studies have been selected where the role of the porous structures is negligible.

9.1.2. Conclusions towards objective 2

In order to assess the predictive skills of the XBeach model, the results were compared with the measurements obtained from physical modelling with focus on the spectral wave heights, spectral wave periods and harbour oscillations.

A common objective method is introduced to compare and asses the XBeach model. The Mean Average Error index, which is the mean of the relative difference of each measurement point, indicates the model skill with the following scores: values below 0.20 are regarded as good. An index between 0.20 and 0.35 is sufficient and above 0.35 is regarded as poor.

The first case (hereafter: Case I) is a rectangular basin with only vertical walls with very oblique incidence waves. The second case (hereafter: Case II) is a rectangular main basin with an side basin attached and with normal incidence waves to the main basin. These cases allow us to reproduce the laboratory experiments where the governing wave processes are reflection, diffraction and harbour oscillations. The following conclusions can be drawn:

With regard to XBeach non-hydrostatic:

- The spectral wave heights for the short waves (f > 0.04 Hz) are generally well calculated. The Mean Average Error is, on average, in the order of 0.10 to 0.15. Care should be taken when a pronounced standing wave pattern is present in the harbour. In order to reduce this effect, it is recommended

to average the wave height over a certain area (e.g. circular area with diameter of a governing vessel).

- The periods for the short wave are well calculated, with a Mean Average Error of 0.10.
- The theoretical and measured resonant frequencies are always well identified.
- The wave heights for the long waves (f ≤ 0.04 Hz) are reasonably reproduced, with a Mean Average Error in the order of 0.10 to 0.25 for Case I. In Case II, the overestimation is mainly the energy in the Helmholtz mode with a Mean Average Error index of 0.25, which is in line with the findings of *van Mierlo (2014)* and *Monteban (2016)*. In their studies, similar harbour layout and wave conditions were used, though with different calculation models (SWASH and MIKE21BW)
- The periods for the long wave are well calculated, with Mean Average Error of 0.10 to 0.15.

With regard to XBeach surfbeat:

- The short wave field based on energy is not well modelled in the harbour. The Mean Average Error index is much larger than 0.35, which is considered as poor. In contrary to the non-hydrostatic mode, phase information is not considered and diffraction is therefore not included in the short wave module of XBeach surfbeat.
- The (theoretical) resonant frequencies are always identified in the calculation model.
- The wave heights for the long waves (f ≤ 0.04 Hz) are in all cases overestimated. However, the long waves are better reproduced if short wave energies are present in the harbour (Mean Average Error index 0.10 - 0.30). In other words, the long waves are still bounded to the wave groups, which prevents them to amplify freely. Without the presence of these short waves, the long waves are thus free and amplify too much with a Mean Average Error index up to 0.40. This is considered as poor.
- The energy in the Helmholtz mode is overestimated up to a factor of 3 in all cases.

It is concluded that the non-hydrostatic mode is more accurate than the surfbeat mode, for both short and long waves. Confidence is placed in surfbeat to calculate the wave heights for the long waves when short wave energies are able to penetrate into the harbour. Regarding the simulation time, surfbeat is at least 1 order of magnitude faster and the computational cost per grid cell is almost 20 times lower than non-hydrostatic.

9.1.3. Application boundaries and discussion

The remaining question that needs to be answered is as follows:

'To what extend is XBeach (Surfbeat & Non-hydrostatic) able to simulate hydrodynamics in harbours and under which circumstances and conditions can the numerical model be used?'

The considered governing wave processes were diffraction, reflection and harbour oscillations. Wave-structure interaction and depth-induced processes were not considered due to model limitation for the former and the lack of suitable data for the latter. The applicability and suitability of are given based on the considered wave processes and the two cases. Obviously, the application range is larger for XBeach non-hydrostatic than XBeach surfbeat.

Application limit(s) of XBeach non-hydrostatic:

- The applicability of XBeach non-hydrostatic is limited by the dimensionless water depth kd of 1. Below this limit, there seems to be no restriction in terms of accuracy and applicability for both the short (f > 0.04 Hz) and long (f ≤ 0.04 Hz) waves. Additionally, The Mean Average Error index is acceptable (generally less than 15%) for the wave heights and wave periods. The identification of the (theoretical) resonant frequencies can be done as well.

Application limit(s) of XBeach surfbeat:

- With regard to the short waves, XBeach surfbeat is strongly discouraged. This is because the basic common features found in harbours are not solved by the calculation model and hence resulting in inaccurate results.
- With regard to the long waves, the calculation model is applicable:
  - To identify the (theoretical) resonant frequencies. XBeach surfbeat gives always good results, regardless the imposed wave conditions and characteristics.
  - To predict the wave heights. Results are reasonably calculated, given that large amount of the long waves are bounded to the wave groups. If the long waves are completely free, i.e. not bounded to the wave groups, an estimation may be obtained from the XBeach surfbeat model. To allow long waves to be bounded to the wave groups in the harbour, directional spreading (short-crested waves) is recommended. Generally, the wave heights are overestimated. If accuracy plays an important role, the non-hydrostatic mode is preferred.
  - To calculate the wave periods. They are generally well calculated, but the wave periods are overestimated with extreme oblique waves (perpendicular to the harbour mouth). For the latter, more confidence is placed in XBeach non-hydrostatic.

Finally, general remarks are made on the model parameters of XBeach. The calculation model is quite limited in the possibilities to improve the modelling results. In this study, it was shown that mainly (flow)

friction (XBeach non-hydrostatic and surfbeat) and directional wave spreading (XBeach surfbeat) are able to affect the results. For example, it is not possible to use other numerical schemes, set reflection coefficients or define structure properties. Therefore, it is also questionable whether XBeach should be used for detailed design and/or calibration purposes.

A decision support chart is given in Figure 9.1. It provides a recommendation, based on accuracy and computational demand, which calculation model is preferred within XBeach. It should be noted that real harbours have a more complex shape where, for example, porous structures are often present. These aspects are not examined here and also not considered in Figure 9.1.

9.2. Recommendations

Attention to the model parameters

- In XBeach surfbeat, tuning of the directional spreading for the long-crested waves is recommended. The s value should not be set too large ($cos^{2s}\theta$ model is used in XBeach). An upper limit is approximately 500.
- Attention should be paid to the friction in XBeach surfbeat, especially when large amount of free long waves is expected. Some friction is required to dampen out these (amplifying) waves.
- In the phase-resolving mode, the calculation model performs quite well with the recommended settings in the user's manual. s =1000 is a good approximation for the long-crested waves.

Further research on the model performance

- Examine the effects of a varying bathymetry, e.g. refraction, with XBeach surfbeat. Modelling of the long waves are expected to improve, as short waves are able to refract into the harbour.
- Examine the model performance with a different and more complex harbour layout.
- Measures to reduce the overestimation in the Helmholtz mode of XBeach surfbeat.

Further model improvement and development

- Include possibilities to define structure properties for both non-hydrostatic and surfbeat.
- Include reflection and diffraction in the short wave module of XBeach surfbeat. By doing so, modelling of the short waves improves, which may result in higher accuracy for the long waves.
- Improve the lateral boundary issue in XBeach non-hydrostatic.

Figure 9.1: Decision support chart for XBeach, based on this study. The recommendation is based on accuracy and computational efficiency. NH denotes non-hydrostatic mode, SB is the surfbeat mode. The short waves are calculated from the energy balance equation, where the wave energy is proportional to the wave height squared (XBeach surfbeat). Additionally, short waves are defined as the energies above f > 0.04 Hz in the energy spectrum (XBeach non-hydrostatic). The long waves are the energies in the energy spectrum belonging to frequencies f ≤ 0.04 Hz in both XBeach non-hydrostatic and XBeach surfbeat. It should be noted that this decision support chart is based on the considered cases, where porous structures and depth-induced wave processes are not included.

Appendices & Bibliography

A

The Vinjè basin case

A.1. Model set-up Surfbeat

A.1.1. Computational grid and bathymetry

First, a computational grid is created. Grid settings should be chosen such that *stability* and *accuracy* requirements are satisfied.

The grid should fulfil accuracy for the low-frequency motions only as the short wave energies are resolved on the directional grid (Section 3.2.1). As rule of thumb, 20 to 30 grid points per wavelength are regarded sufficient to resolve the relevant wavelengths. This model set-up uses 30 grid points per wavelength. The grid spacing should not be too large as long waves may not accurately resolved due to numerical effects. From the frequency dispersion (Equation 2.1), the corresponding wavelength is 120 m for the peak period of 10 seconds and a water depth of 20 m (Test A1). If we then assume that the long waves are initially bounded to the wave group and each group consists of approximately 10 consecutive waves (or 1 order larger in magnitude compared to the short waves), the governing long wavelength is then 1200 m. This makes the computational grid rather coarse (50 m) and it cannot solve accurately the high-frequency waves in the infragravity band, especially in the harbour where free long waves are dominant with various wavelengths. To be on the safe side we choose a governing long wavelength of 600 m (5 times the short wavelength). One grid size is then in the order of 20 m.

A non-uniform grid is applied to compromise between computational effort and accuracy. In the harbour basin and near the harbour mouth the grid sizes are 10 m for both cross-shore and longshore direction, respectively. The grid size with a high resolution is such that it does not affect the results. Despite the higher grid resolution the computational time is still acceptable with a modern quad-core

i7-processor. Further away from the harbour basin grid sizes of 20 m are applied with a smooth transition between the grid cells.

Further, the nonlinear shallow water equations is discretised based on the explicit method of *Stelling and Duinmeijer (2003)*, indicating that there is a restriction on the time step and grid size which is represented by the *Courant-Friedrichs-Lewy Condition* (hereafter: CFL-condition) : $\sigma = u\Delta t/\Delta x \leq C_{max}$. An automatic optimised time step is applied by XBeach based on the user's defined C_{max}. So, stability is almost always satisfied. In 2D XBeach simulations, it is recommend to use a value smaller than 0.7.

The grid as discussed above should be amended if the area of interest, the harbour basin, is situated (partly) outside the area of the mean wave direction. Tests A2 and B2 have oblique incident waves coming from the offshore boundary with an angle of 30 degrees with respect to the x-axis. Waves that enter the domain obliquely introduce a shadow zone as in Figure A.1.

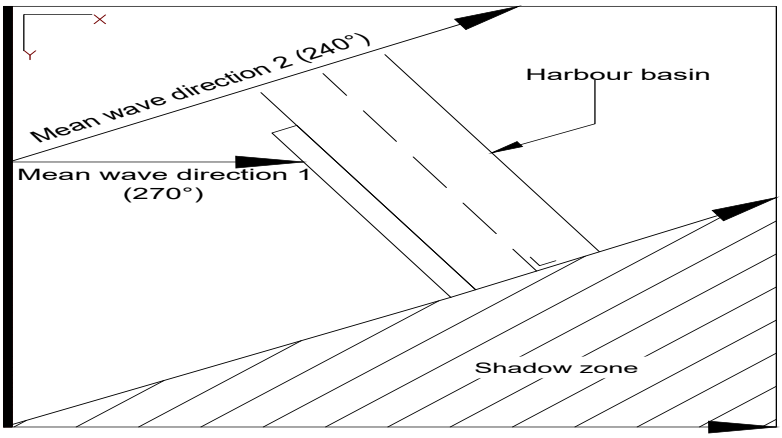

Figure A.1: Shadow zone problem.

In this particular case, it is not necessary to widen the model domain because the area of interest lies exactly inside the mean wave direction and outside the shadow zone. The effect of shadow zone on the calculated wave heights is, initially, assumed to be minimal.

With respect to the short waves, these are resolved on the directional grid and no separate grid file needs to be supplied. The mean direction, directional grid size and range need to be defined in the steering file of XBeach. Following the nautical convention, the incoming wave directions are 240 and 270 degrees and thus a range of 180 to 360 degrees is sufficient. By further increasing (decreasing) the directional range, the computational time will increase (decrease). Subsection 3.3.2 demonstrated the effect of increasing the number of energy bins and using a higher directional resolution.

The bathymetry is a integrated part of the grid which means that the harbour and the sloping structures are indicated as local bottom elevation. The bathymetry is fairly simple and already discussed in Section 4.2.1. Also discussed is the lack of structure property in the model (Section 3.3.2); the structure is modelled as impermeable and assumed to be reflective.

In addition, the side walls that were present in the laboratory experiments were not included in the following simulations for the following reasons:

- The calculation model became unstable. Possibly, a steep structure is placed too close to the offshore and lateral boundaries boundary. A gradual reduction in water level over time was observed
- In XBeach, the offshore forcing is along the entire offshore boundary. This is not the case in the laboratory experiments for the oblique incoming waves (perpendicular to the harbour axis). The wave paddles close to the side walls were deactivated in order to prevent excess reflection.

The absence of the side walls is fairly justified as the results (Section 7.3) show similar trend as *van der Molen (2006)*, where he did included the side walls.

A.1.2. Boundary conditions

The Surfbeat mode treats the short and long waves separately which means that different boundary conditions need to be supplied.

A.1.3. Waves

Similar to the measurement campaign, the XBeach model is forced with a parametrized JONSWAP spectrum where the spectrum parameters needs to be defined by the user. The model forcing parameters are recorded in Table 4.1. The spectrum is automatically converted to wave energy at the offshore boundary that propagates into the domain.

At the lateral boundaries a Neumann boundary condition is used in which there are no lateral gradients. The situation becomes complex if the waves are propagating obliquely into the domain as it introduces shadow zones in the modelThe effect of shadow zone on the hydrodynamics is regarded as small (see Figure A.1) since it is relatively far to affect the hydrodynamics in the harbour basin.

A.1.4. Flow

The long waves are generated by energy transfer from the short wave groups to the long waves. Therefore it is not necessary to supply information with regard to the long wave propagation at the boundary. It is important that the offshore water depth should be deep enough such that it can apply the bound wave theory at the boundary as described by *Longuet-Higgins and Stewart (1964)*. The short waves should enter the domain in deep or intermediate water. A rule of thumb is that the ratio c_g/c is smaller than 0.85 because it generate enormous waves at the boundary otherwise, which is unrealistic. An offshore depth in the order of 20 to 30 m is often regarded as 'deep' enough.

At the offshore boundary a weakly-reflective boundary condition is imposed where the reflected long

waves can pass through the offshore boundary with minimal reflection. At the gravel slope, there is actually no need to impose a boundary condition since the waves are reflected against the sloping structure.

Neumann boundary condition is used at the lateral sides such that there is no gradient in water level and velocities.

A.1.5. Other model settings

The wave-action balance (Equation 3.1) is kept default by only including dissipation due to wave breaking *(Roelvink, 1993)*. The short wave friction is considered later in this study, because too much bottom friction can lead to underestimation.

The function of the gravel slopes facing the wave board and at the back of the model domain is to partially dissipate wave energy. To mimic this effect, locally a higher friction coefficient is applied as the slopes does not have the ability to absorb wave energy. There are three choices to approximate the friction coefficient: Chézy, Manning and White-Colebrook. The latter two formulations are depth dependent and more appropriate in situations where water levels are highly variable (e.g. during storm conditions on a barrier island). Initially, we use Chézy for flow fiction via the formulation of the bed shear stress in the nonlinear shallow water equation (see Equation 3.10). Because the stone size diameter of the slopes is known, in the order of 3 meters, it is possible to estimate the friction based on the Nikuradse roughness k_s and stone diameter. The Chézy formula, applicable in a turbulent flow, reads:

$$C = 18log\frac{12h}{k_s}, \quad \text{where } k_s = n \cdot D_{90} \tag{A.1}$$

where n is a coefficient and is generally in the range of 1 to 5. XBeach calculates automatically the dimensionless friction coefficient c_f. For the slopes, the Chézy coefficient is 20 $m^{1/2}/s$, which is slightly higher than the calculated value with Equation A.1 to compensate for the absence of the structure property. For the uniform flat bed and the harbour basin, default value of 55 $m^{1/2}/s$ is used as the friction coefficient is unknown.

An overview of the general input parameters of XBeach is given in Table A.1. The model behaviour is not known beforehand and it is difficult to indicate the model parameters that may affect the results. For this reason, an extensive sensitivity analysis is carried out on the hydrodynamics parameters in Section 7.4, based on the initial results from Section 7.3.

Table A.1: General input parameters for the steering file in XBeach

Parameter	Definition	Value	Dimension
nx	No. of grid cells in x-direction	400	-
ny	No. of grid cells in x-direction	182	-
thetamin	Lower directional limit	180	degrees (°)
thetamax	Higher directional limit	360	degrees (°)
dtheta	Directional resolution	90	degrees (°)
singledir	Preserves wave groupiness	1 (on)	-
bedfriction	Flow friction (Chézy)	Variable	$m^{1/2}/s$
CFL	Courant-criterion	0.7	-
front, back	Flow boundary condition	weakly-reflective	-
lateralwave	Wave boundary condition, lateral	Neumann	-
left, right	Flow boundary condition, lateral	Neumann	-
break	Short wave breaking	Roelvink2	-

A.2. Model set-up Non-hydrostatic

A.2.1. Computational grid and bathymetry

This wave-resolving mode of XBeach solves the total surface elevation of the water motion. This implies that both the short and long waves are resolved on the computational grid. Now the accuracy and stability requirements are based on the primary wave characteristics. With a peak period of T_p = 10 s and 30 grid points per wavelength, one grid cell has a resolution of 4 x 4 m in the harbour area, and 10 x 10 m further away where the effect on the hydrodynamics is expected to be minuscule. This non-uniform grid is favourable in order to make a trade-off between computational cost and accuracy, because the computational time is quite large. Without MPI parallel computing, the computational time for a modern quad-core i7-processor is in the order of 5 days (Surfbeat computational time was in the orde of 4 hours). For typical large harbour applications, the effect of very short waves in the higher frequency band (T_p > 10 s) is limited with respect to the size of the vessels and thus the chosen grid resolution is regarded as sufficient[1].

The bathymetry differ slightly from the laboratory experiments for the same reason. Also, the effect of the rear gravel slope was small and therefore excluded from the model.

A.2.2. Boundary conditions

In contrast to the Surfbeat mode where two different types of boundary conditions need to be supplied (for both the short wave an flow module), the Non-hydrostatic mode only requires one type in order to

[1]For smaller applications such as Marina docks and fishing ports, where the size of the vessels are relatively small, the energy in the higher frequency band cannot be neglected.

have an unique solution satisfying the nonlinear shallow water equations.

The calculation model is forced with a parametrized JONSWAP spectrum and are listed in Table 4.1. The offshore boundary, based on the Sommerfeld radiation condition, is absorbing-generating and weakly reflective. The calculation model computes both the actual velocity based incoming velocity and the total surface elevation. One requirement in order to apply this boundary conditions is that the reflected waves are long and such that the waves are practically travelling perpendicular to the offshore boundary.

At the rear boundary, there is no gravel slope incorporated. This is done in order to reduce the grid cells in the computational domain. In chapter 7 the effect of the rear slope was examined, which was small and therefore excluded from the computational domain. An absorbing boundary is chosen for this purpose.

For the lateral boundary conditions, XBeach recommends the default Von Neumann where there is no gradient of velocity and water level. However, there are some issues related to this boundary condition. In Subsection 3.3.2, a relative simple bathymetry with a semi-infinite breakwater was used to investigate the basic features of diffraction using this boundary condition. As time proceeds, there is a gradual decrease in the water level observed. Applying a 'wall' as boundary condition (zero-velocity) does solve this problem, but causes too much reflection. An intermediate solution is the advective boundary condition, which lies between the Von Neumann (no gradient) and 'wall' (zero velocity). This boundary condition is elaborated further, since this is the only suitable substitution of Von Neumann if the calculations are relatively long ($>$ 1 hour).

The advective boundary condition calculates the velocity from the nonlinear shallow water equation, but takes only the advective terms into account if that term decreases the local velocity at the boundary. The advective terms read as follows:

$$u\frac{\partial v}{\partial x} + v\frac{\partial v}{\partial y} \tag{A.2}$$

The use of this advective boundary conditions has the problem that it causes reflection, although much less than the 'wall' boundary condition. The influence of reflection on the model results is minimised by enlarging the computational domain in both cross-shore and longshore direction with a coarse grid resolution in these extended regions. For this reason, the side walls are not included (which also causes numerical instabilities) and the computational time increases.

A.2.3. Other model settings

Other model settings are similar to that of the Surfbeat model. The reader is referred to Chapter 7, Subsection A.1.5 for a detailed explanation. An overview of the general input parameters of XBeach is given in Table A.2.

Table A.2: General input parameters for the steering file in XBeach Non-hydrostatic

Parameter	Definition	Value	Dimension
nx	No. of grid cells in x-direction	439	-
ny	No. of grid cells in x-direction	575	-
bedfriction	Flow friction (Chézy)	Variable	$m^{1/2}/s$
CFL	Courant-criterion	0.6	-
front	Flow boundary condition for nonh	weakly-reflective	-
back	Flow boundary condition	weakly-reflective	-
left, right	Flow boundary condition, lateral	no_advec	-

A.3. Split frequency

The results for the short and long waves are treated separately. To this end, a split frequency needs to be chosen that separates the long and short waves. The limit is set at $f = 0.04$ Hz, because above this limit in XBeach, it contains minimal amount of energy of the infragravity waves. In the measurements similar trend is observed: between $f = 0.04 - 0.05$ Hz there is very little energy present. This chosen split frequency is further supported by the fact that most of the resonance modes are below this frequency. Additionally, higher resonance modes are more sensitive for friction and thus resulting in relatively small amount of energy in the higher frequency region of the infragravity band. Figure A.2 shows the high frequency peak (Hz > 0.04) and low frequency tail (Hz ≤ 0.04), where the dashed line indicates the split frequency.

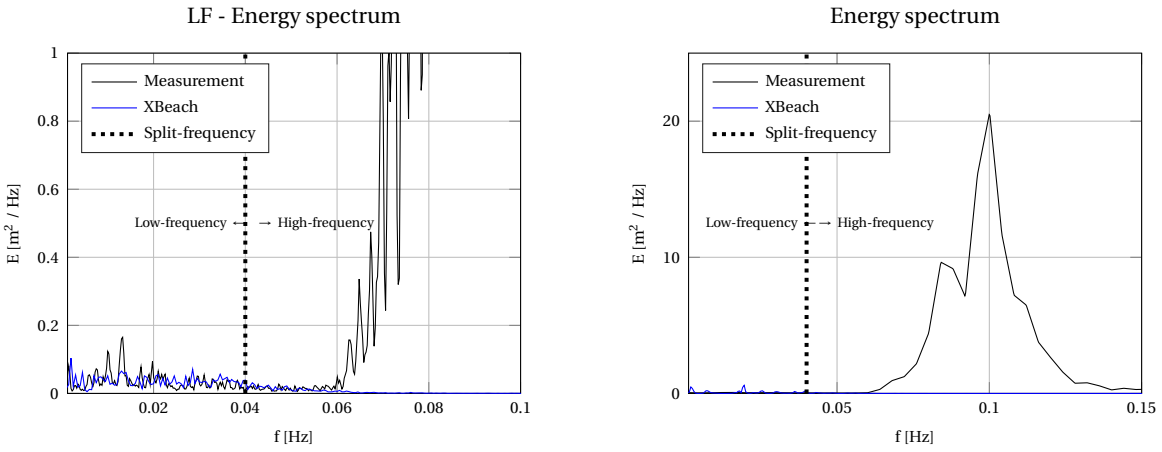

Figure A.2: Split frequency at $f = 0.04$ Hz indicated with dotted line.

A.4. Results in physical model scale Surfbeat

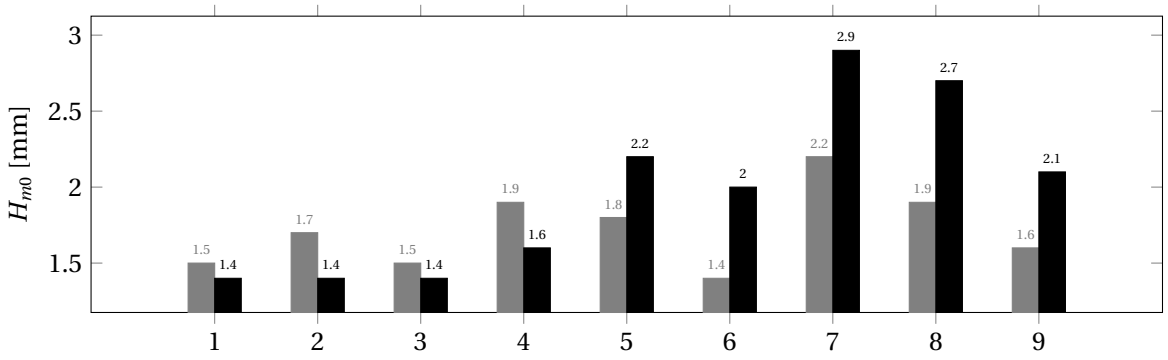

(a) Test A1: wave heights in physical model scale.

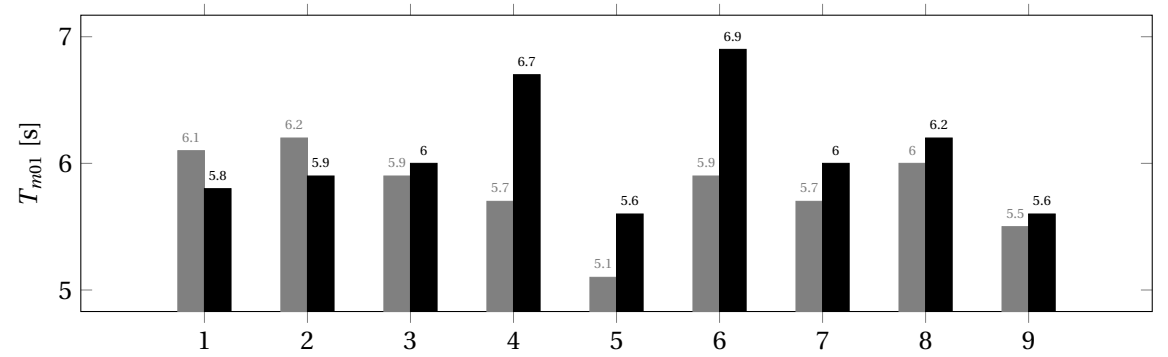

(b) Test A1: wave periods in physical model scale.

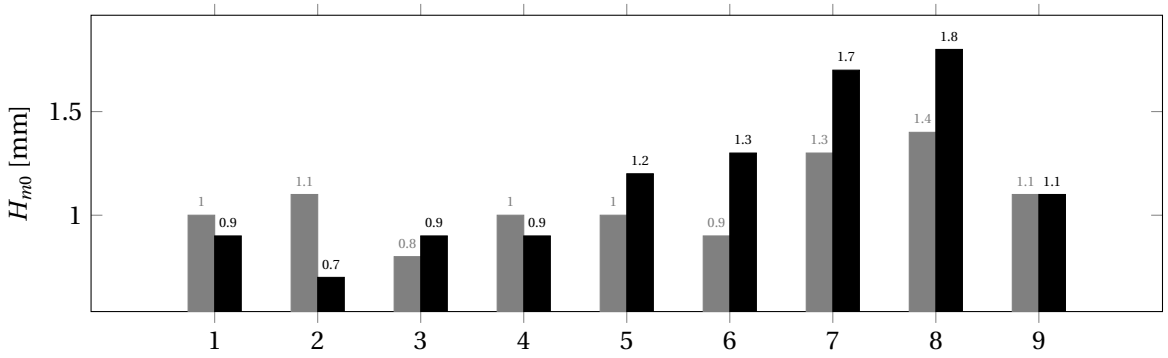

(c) Test B1: wave heights in physical model scale.

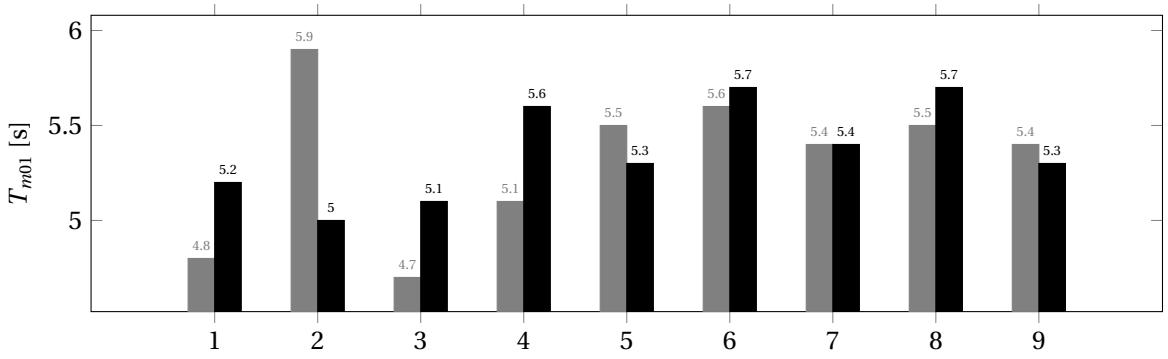

(d) Test B1: wave periods in physical model scale.

Figure A.3: Results in physical model scale of Test A1 and B1. (■) is the measured variable, (■) is the calculated variable.

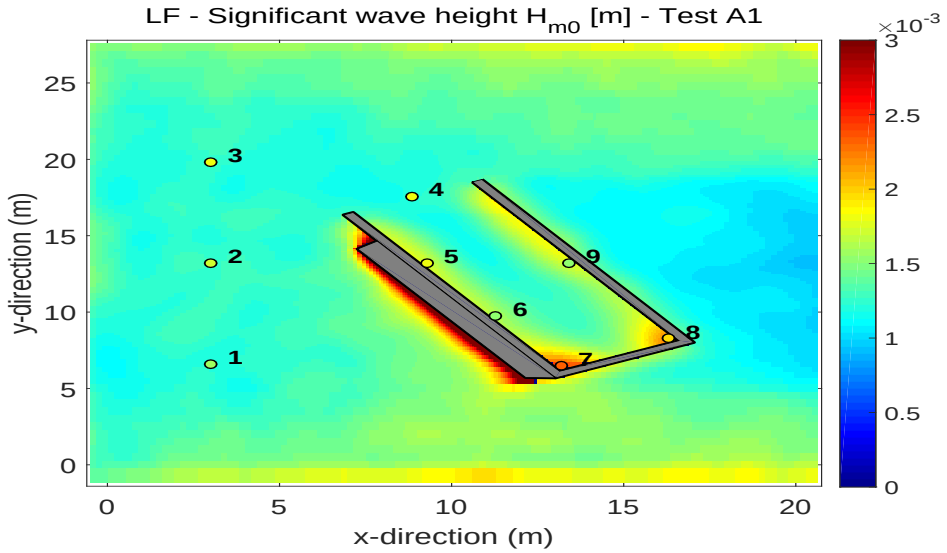

(a) Test A1

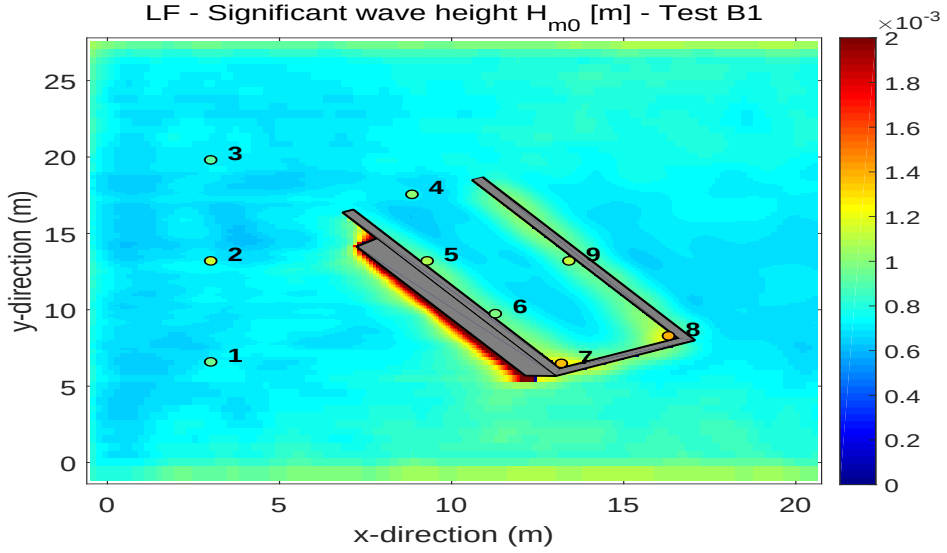

(b) Test B1

Figure A.4: Overview plots in physical model scale.

Table A.3: Numerical parameters in physical model scale for the SB mode. Froude scaling law 1:100.

Parameter	Prototype scale	Physical model scale
Spectral wave height H_{m0} (m)	3 / 6	0.03 / 0.06
Peak wave period T_p (s)	10	1
Peak frequency (Hz)	0.1	1
Water depth (m)	20	0.2
Grid resolution (m)	10 to 20	0.1 to 0.2
Grid points per wavelength	≈ 30	≈ 30
Cut-off frequency (Hz)	0.04	0.4

A.5. Results in prototype scale Surfbeat: Short waves

Table A.4: Wave heights. MAE A1 = 0.59, MAE A2 = 0.61, MAE B1 = 0.44 and MAE B2 = 0.53.

	Test A1			Test A2			Test B1			Test B2		
GHM	Lab	SB	Bias	Lab	SB	Bias	Lab	SB	Bias	Lab	SB	Bias
1	3.01	2.98	-0.01	6.08	6.01	-0.01	3.15	3.04	-0.04	5.81	5.71	-0.02
2	2.96	3.02	+0.02	6.65	6.11	-0.08	3.10	2.97	-0.04	6.10	5.73	-0.06
3	3.12	2.97	+0.05	6.01	5.86	-0.03	3.14	2.99	-0.04	6.28	5.69	-0.10
4	3.65	2.98	-0.18	3.87	5.18	+0.33	3.10	2.81	-0.10	5.33	5.03	-0.06
5	2.91	0	-1	2.84	0	-1	2.55	0.42	-0.84	4.14	0	-1
6	2.27	0	-1	2.47	0	-1	2.34	0.43	-0.84	3.81	0	-1
7	2.80	0	-1	2.67	0	-1	2.67	0.47	-0.80	3.98	0	-1
8	2.63	0	-1	2.57	0	-1	2.39	0.88	-0.63	3.93	0.55	-0.86
9	2.65	0	-1	2.60	0	-1	3.16	1.31	-0.59	4.48	1.30	-0.70

A.6. Results in prototype scale SB & NH

A.6.1. Test A1

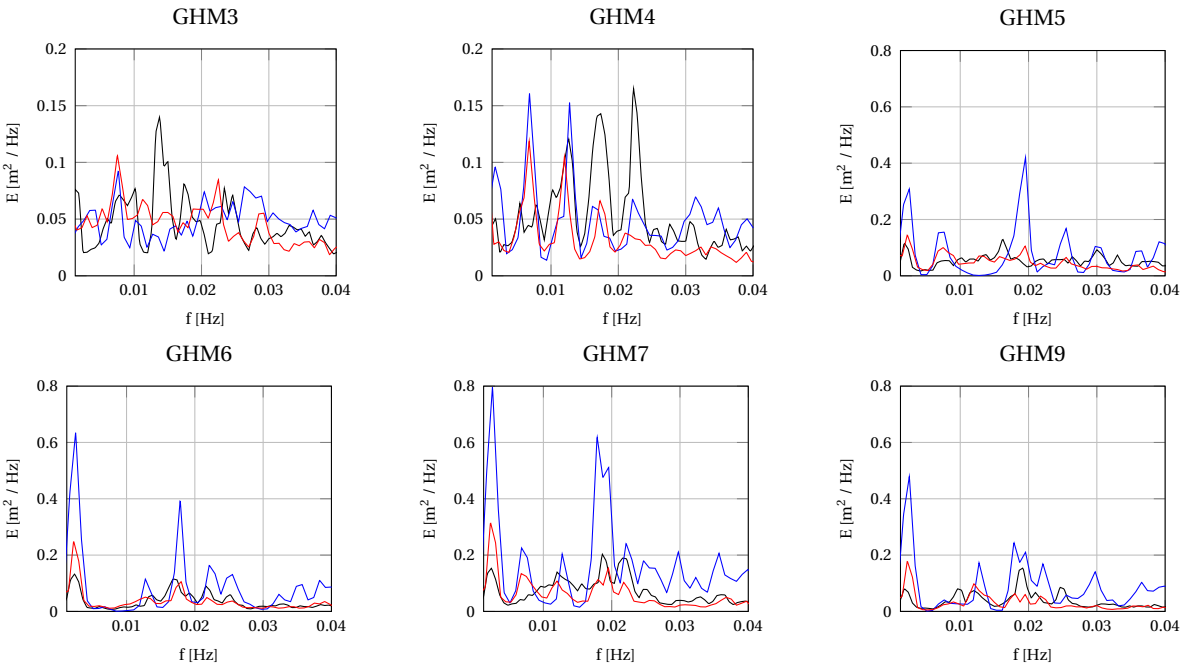

Figure A.5: Energy spectra of Test A1. Measured spectrum (–), SB spectrum (–), NH spectrum (–).

A.6.2. Test A2

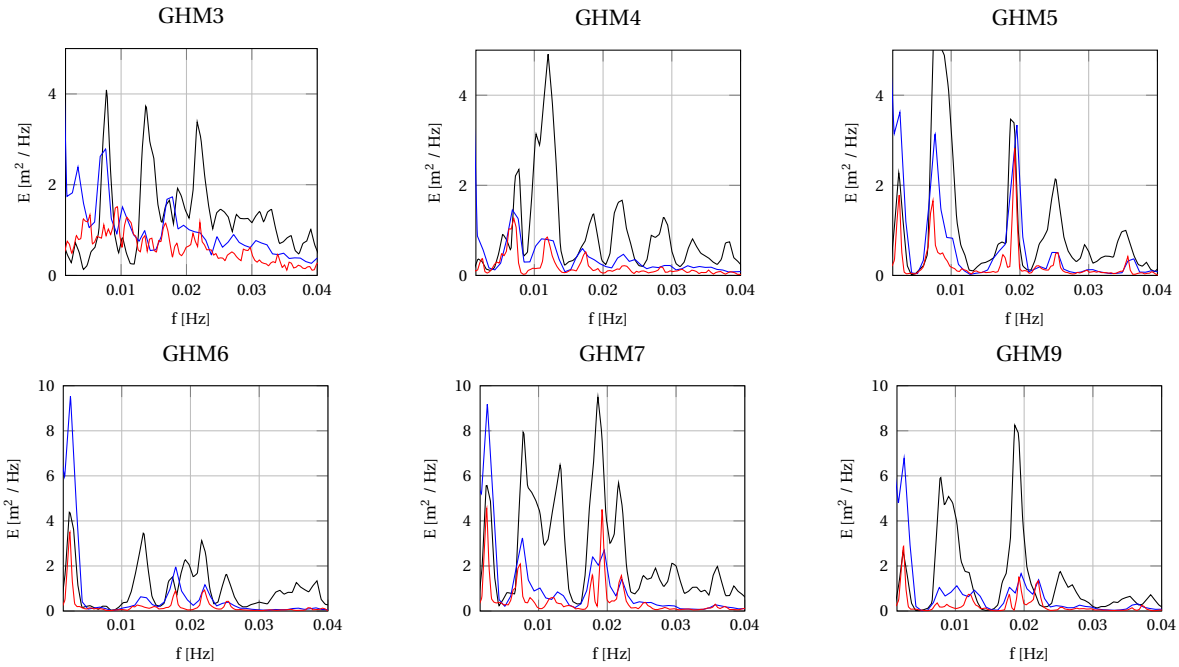

Figure A.6: Energy spectra of Test A2. Measured spectrum (–), SB spectrum (–), NH spectrum (–).

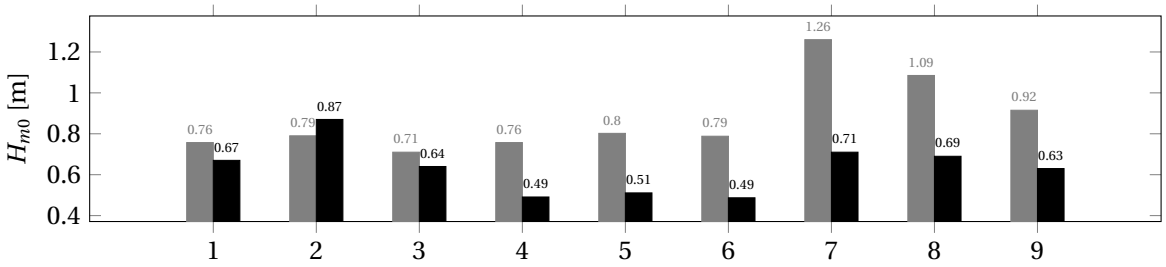

(a) Test A2: wave heights.

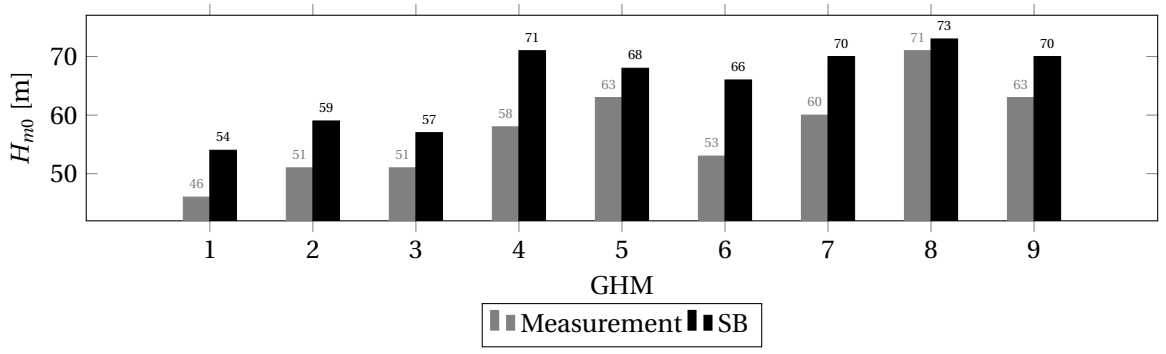

(b) Test A2: wave periods.

Figure A.7: Test A2

A.6.3. Test B1

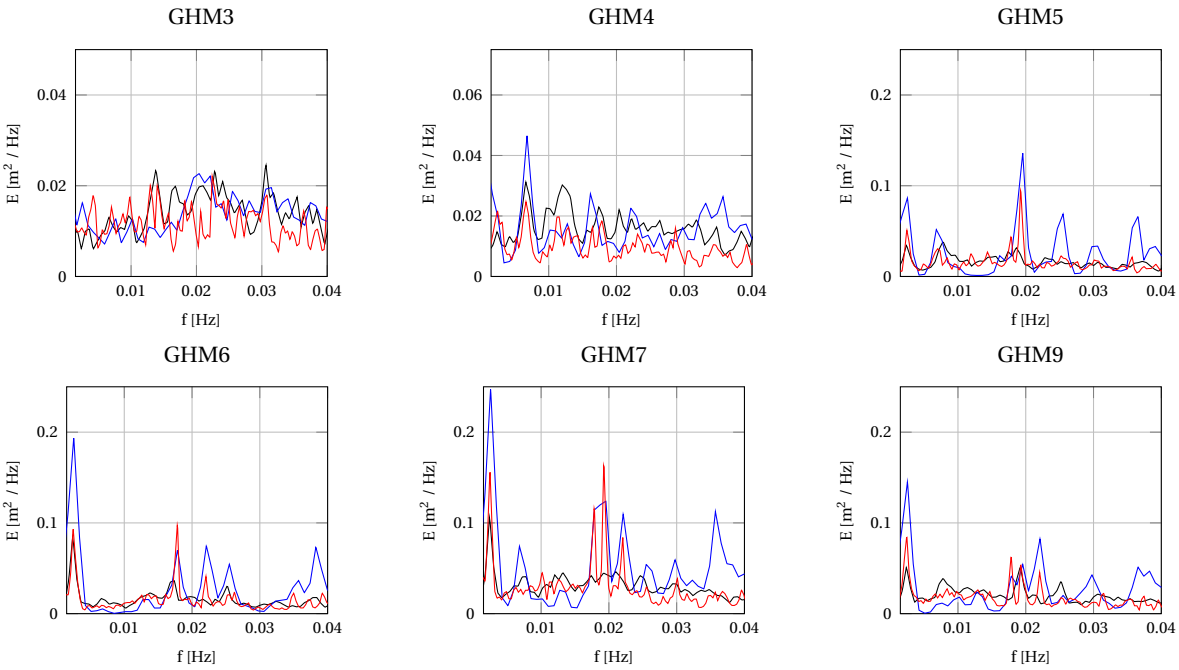

Figure A.8: Energy spectra of Test B1. Measured spectrum (–), SB spectrum (–), NH spectrum (–).

A.6.4. Test B2

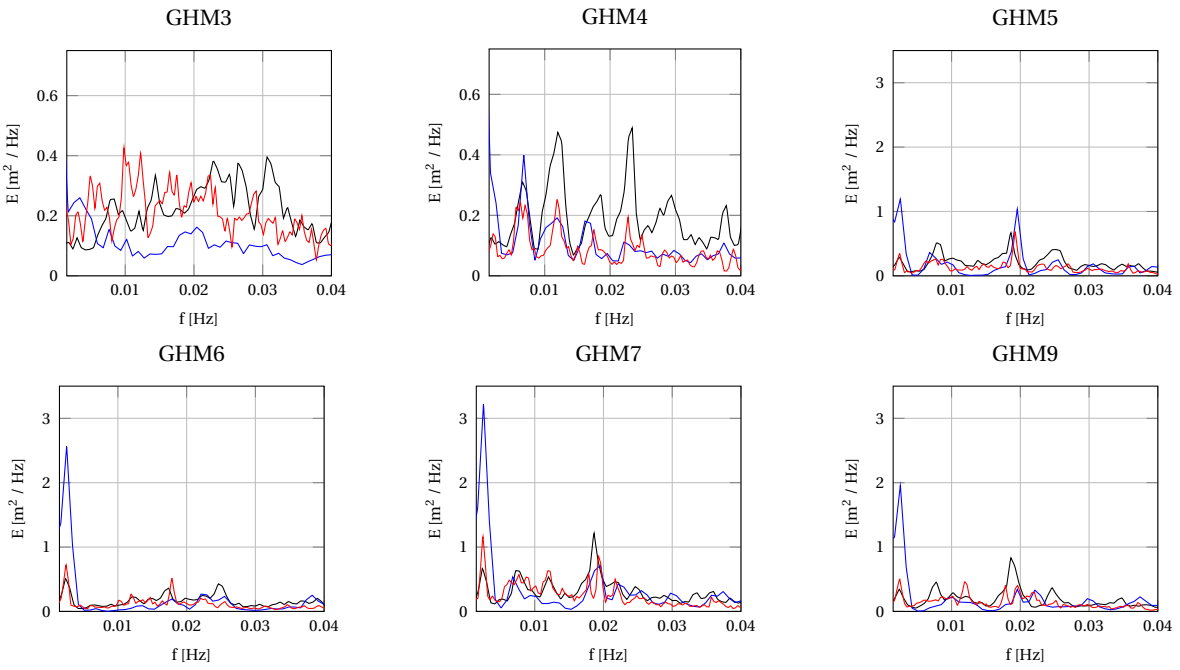

Figure A.9: Energy spectra of Test B2. Measured spectrum (–), SB spectrum (–), NH spectrum (–).

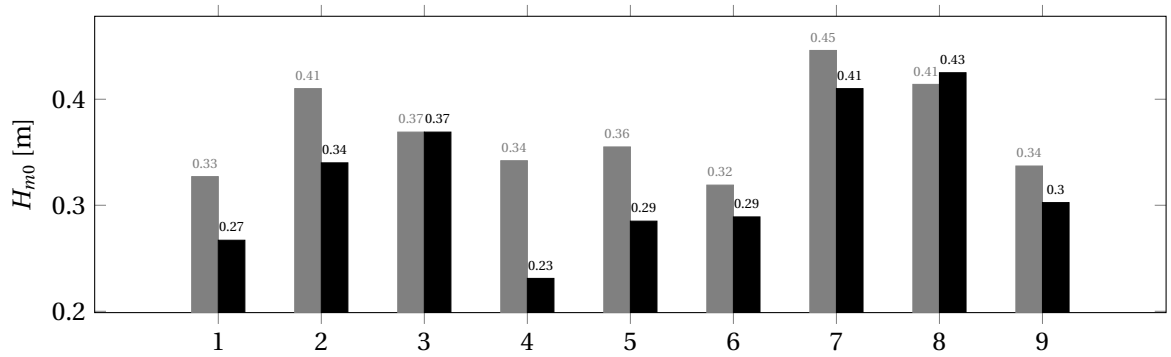

(a) Test B1: wave heights.

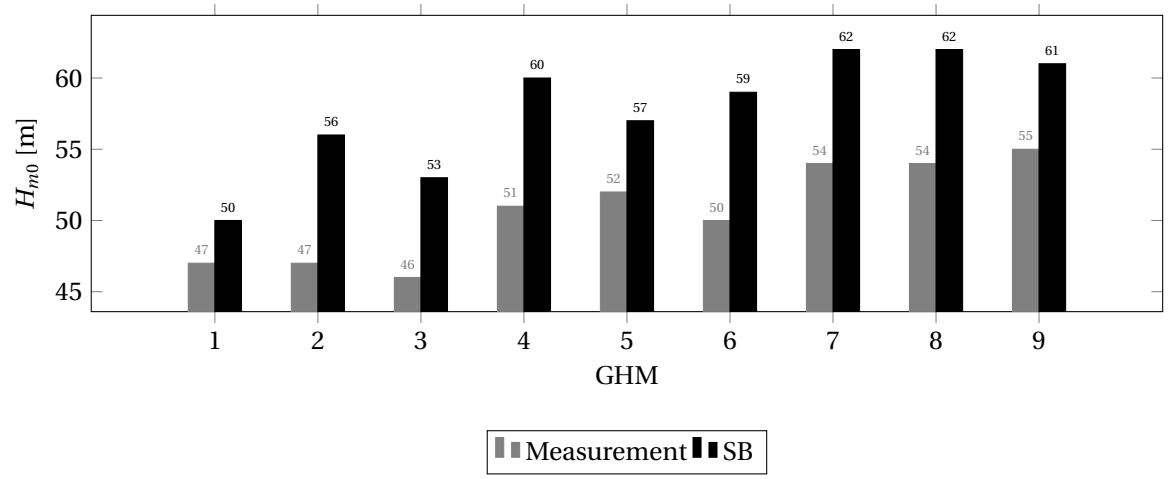

(b) Test B2: wave periods.

Figure A.10: Test B2

A.7. Bias scores

Table A.5: Wave height bias scores of the individual wave gauges.

	Test A1		**Test A2**		**Test B1**		**Test B2**	
GHM	SB	NH	SB	NH	SB	NH	SB	NH
1	0	-0.07	-0.09	-0.12	-0.05	-0.17	-0.12	-0.18
2	-0.06	+0.17	-0.14	+0.10	+0.20	-0.13	-0.32	-0.17
3	+0.06	-0.12	-0.03	-0.10	-0.06	-0.13	-0.14	0
4	-0.05	-0.33	-0.19	-0.36	0	-0.17	+0.09	-0.24
5	+0.16	-0.21	-0.09	-0.37	+0.2	+0.23	0	-0.11
6	+0.53	-0.13	-0.04	-0.37	+0.2	0	+0.16	-0.13
7	+0.53	-0.19	-0.21	-0.44	+0.21	0	+0.07	-0.11
8	+0.58	-0.10	-0.11	-0.37	+0.21	+0.07	+0.12	+0.05
9	+0.44	-0.25	-0.12	-0.46	+0.18	-0.01	+0.09	-0.12

Table A.6: Wave periods bias scores of the individual wave gauges.

	Test A1		**Test A2**		**Test B1**		**Test B2**	
GHM	SB	NH	SB	NH	SB	NH	SB	NH
1	-0.11	+0.05	+0.30	+0.24	-0.04	+0.04	+0.09	+0.06
2	-0.07	+0.03	+0.10	+0.17	-0.10	+0.04	+0.02	+0.19
3	-0.04	+0.14	+0.14	+0.14	-0.02	+0.10	+0.20	+0.15
4	-0.04	+0.16	+0.19	+0.22	-0.03	+0.17	+0.14	+0.18
5	+0.03	+0.21	+0.09	+0.08	-0.07	+0.09	+0.14	+0.10
6	+0.02	+0.17	+0.56	+0.45	-0.02	+0.05	+0.56	+0.22
7	-0.02	+0.07	+0.48	+0.20	-0.03	+0.10	+0.28	+0.19
8	+0.02	+0.10	+0.24	+0.03	+0.05	+0.10	+0.35	+0.20
9	-0.02	+0.09	+0.30	+0.11	-0.05	+0.13	+0.35	+0.11

A.8. Additional sensitivity analysis

A.8.1. Flow friction: Manning

Figure A.11 shows the effect of various Manning coefficient on the spectra and various period bands, for Test A1. The runs were carried out with values varying from n = 0.005 – 0.06 and values between n ≈ 0.015 – 0.04 are considered realistic in coastal engineering applications. Closer inspection on the lower plots of Figure A.11 in the range of n ≈ 0.015 – 0.04 show that the reduction of the wave heights for all period bands is quite small with increasing roughness. Overall the effect of the full range of Manning coefficients is similar to that of Chézy.

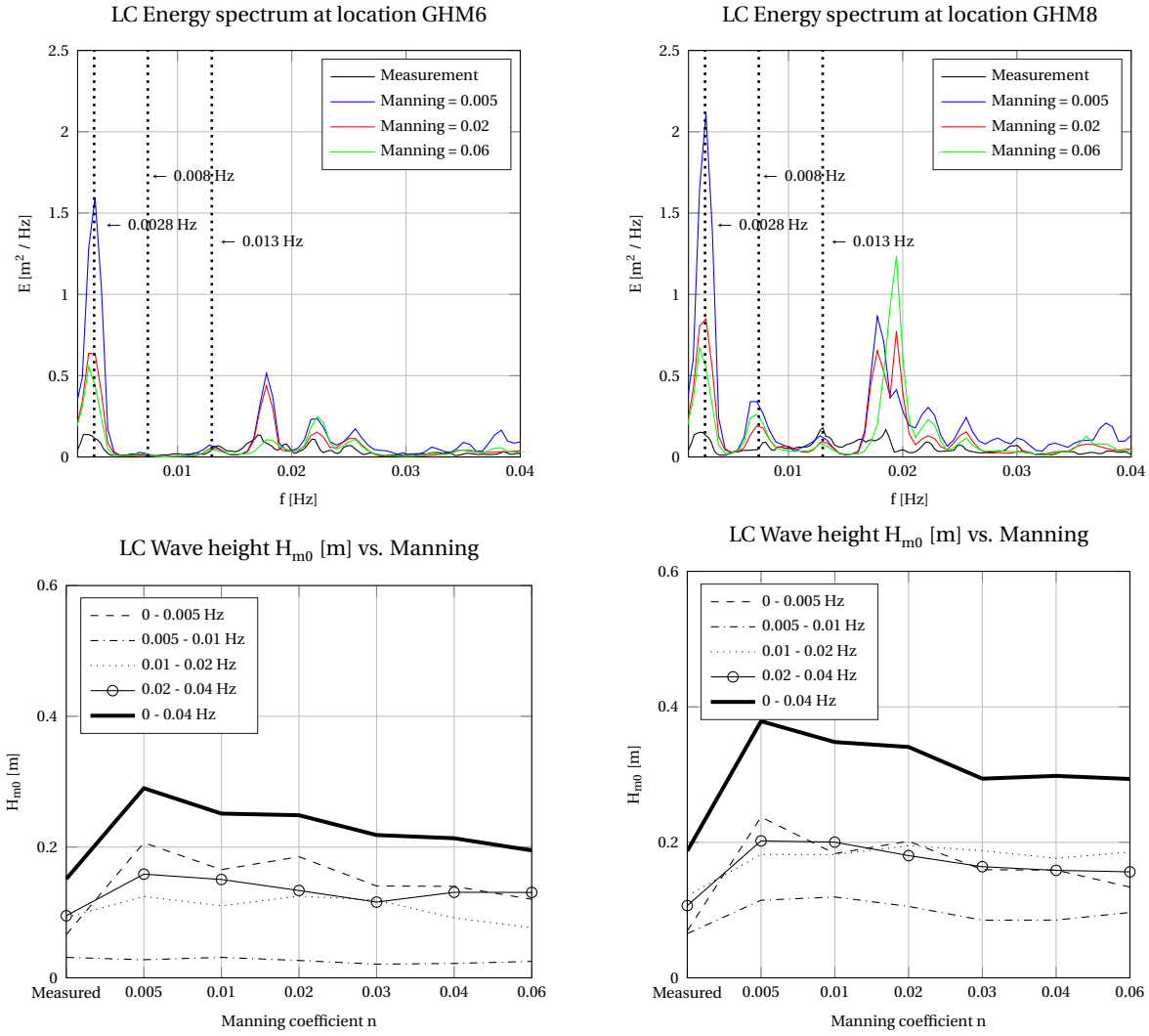

Figure A.11: Test A1: spectra for various Manning coefficient (upper) and long wave height as function of Manning coefficient (lower) for long-crested waves.

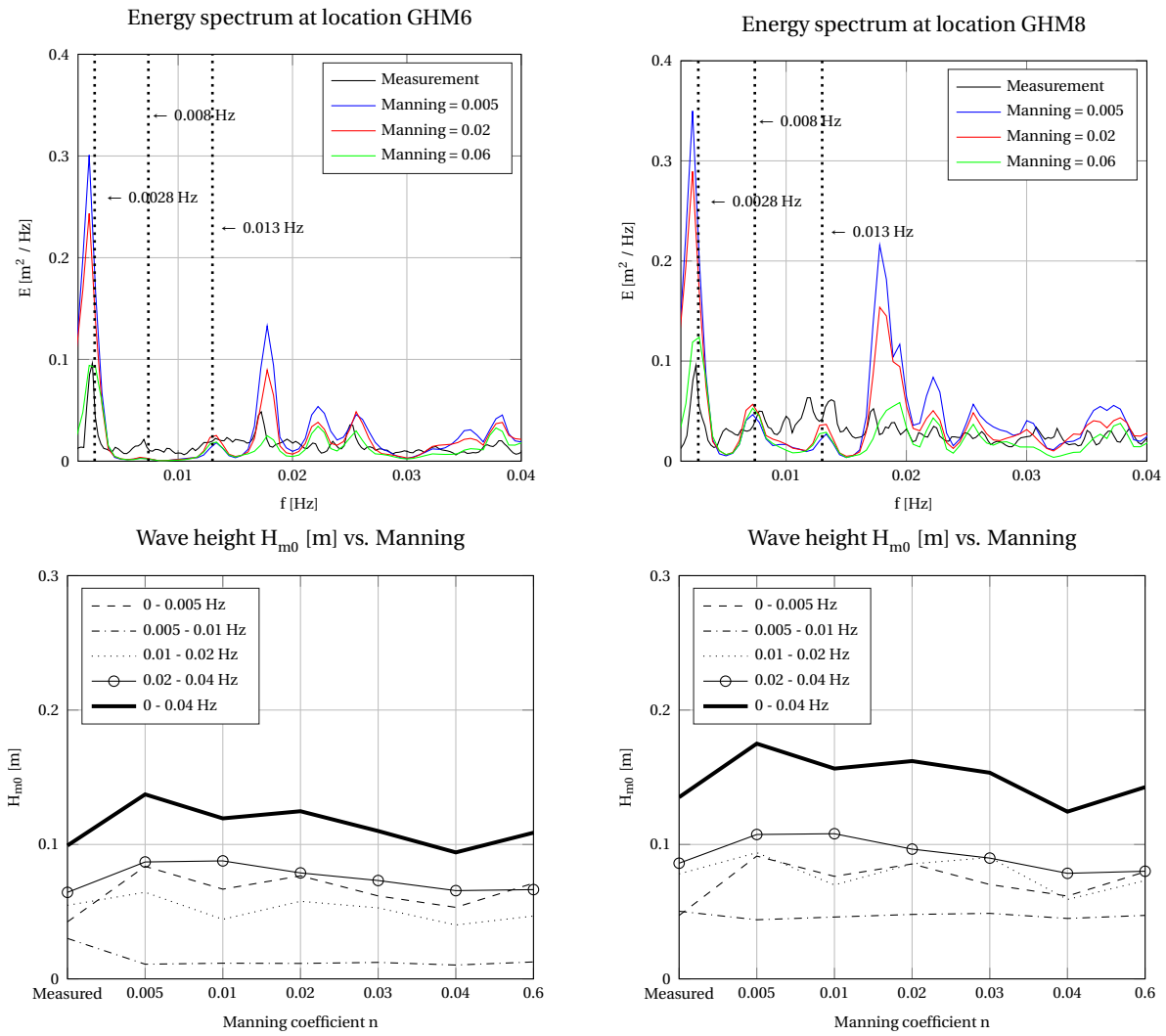

Figure A.12: Test B1: spectra for various Manning coefficient (upper) and long wave height as function of Manning coefficient (lower) for short-crested waves.

Similar results are obtained as Chézy if the friction formulation of Manning is used. The calculated wave heights with the Manning friction coefficient are also well modelled by XBeach, see Figure A.12. A Manning coefficient of $n \approx 0.035$ matches the calculated wave heights fairly.

A.8.2. Short wave friction

Wave friction in XBeach is referred to energy dissipation of the orbital movements and is unrelated to the flow friction as described in Subsection 7.4.2. The wave friction is described in Equation 3.1 with the term D_f and only dissipates the short wave energies.

In deep water the wave orbital motions does not experience bed resistance too much and can be often neglected. In shallow water however, a turbulent boundary layer between the wave motion and the bed arises which is essentially the transition from orbital motion to the bed. As a result, the large velocity

gradient incurs large shear stresses at this transition region which dissipates energy from the wave action above the layer. In general harbour application, we are neither in deep water nor shallow water, but in transitional water depth. The horizontal velocities of the wave motions near the bed are not negligible, but are also not as pronounced as it is in shallow water and therefore it has its contribution to wave energy dissipation. Generally speaking, the wave friction is mainly determined by the bed roughness and the orbital velocity close to the bed. Since phase information is not available in the short wave module, a parametrised dissipation term is used, according to *Jonsson (1966)*.

The decay of energy results in less energy transfer to the long waves and thus smaller wave heights. From the results with default XBeach settings we tend to say that the lack of short wave dissipation is not the main mechanism that causes the differences between the calculated and the measured wave heights. This dissipation term might be more interesting with extreme wave heights, such as Test A2 and B2. Nevertheless, it is worth to examine what the effect is of this dissipation term. In the sensitivity analysis for the wave spreading (Subsection 7.4.1) it was demonstrated that a small deviation in forcing could trigger amplification at the resonant mode(s), causing the wave heights to increase. It is possible that absent of small amount of energy could result in less amplification of the long waves.

In the laboratory basin with a smooth bed and in intermediate water depth, the typical friction factors f_w are in the order of (O)10^{-1} and (O)10^{-2} *(Jonsson, 1966)*. This sensitivity analysis is only carried out for Test A1, because it was shown in Subsection 7.4.2 that flow friction is able to dissipate energy for Tests B which is theoretically more sound. Several runs are carried out to examine the influence on the long wave height in the harbour basin.

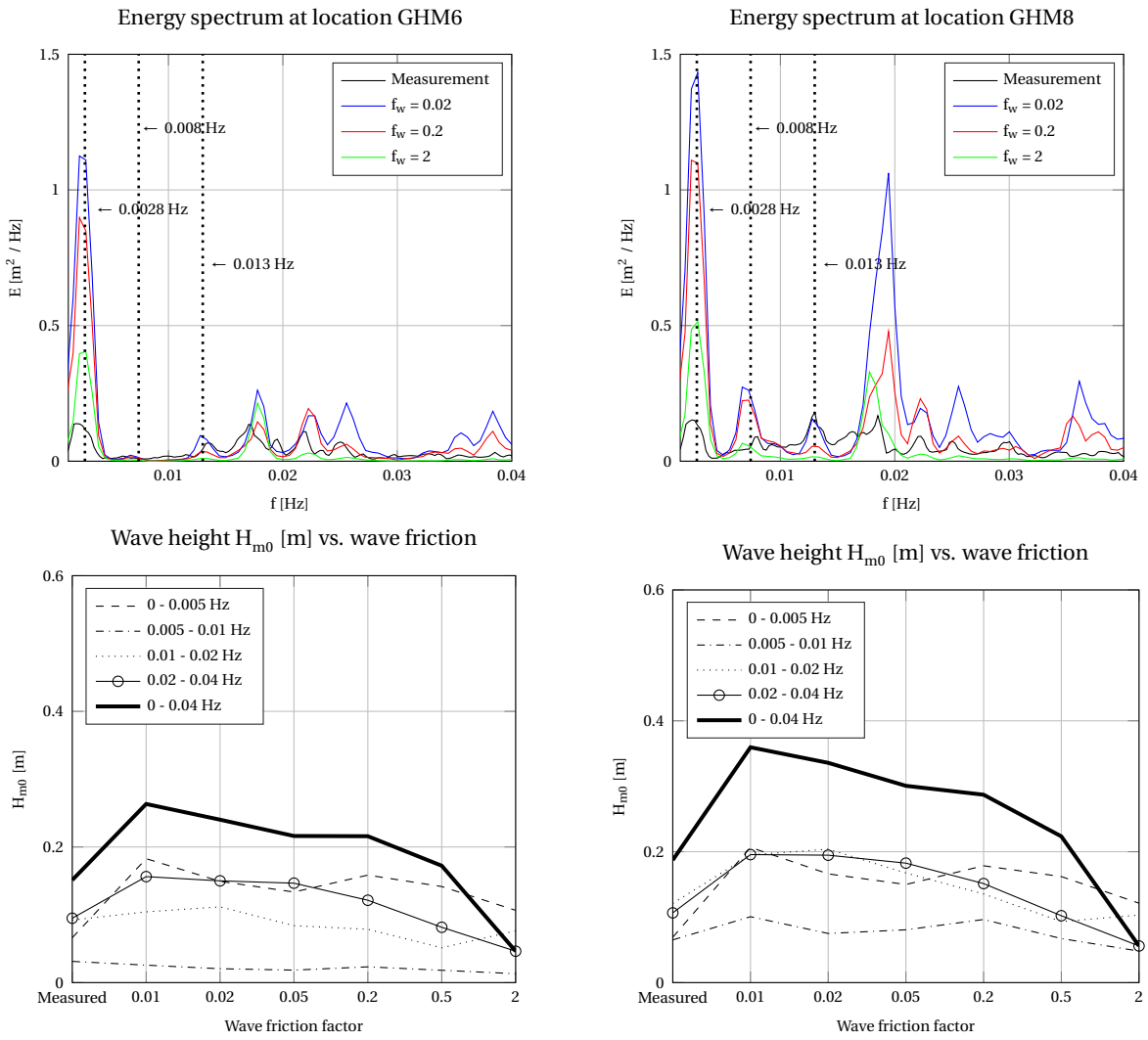

Figure A.13: Spectra for various wave friction factors (upper) and long wave height as function of friction coefficients (lower).

Figure A.13 shows the results of various wave friction factors on the spectral evolution and spectral wave heights. Realistic values in this laboratory setting are between $f_w = 0.02$ and 0.05. Generally, the results confirm the hypothesis that increasing friction factors leads to reduction of the wave heights. Values $f_w > 0.5$ matches the measurements, but it is questionable how realistic this is in a typical laboratory setting with a smooth bed in relative deep water. Although the wave heights inside the harbour corresponds better to the measurements, the offshore wave energy (both short and long) is too much dissipated. It can be concluded that short wave friction is not the determining factor and that the use of short wave friction is dubious in this setting.

A.8.3. Long wave periods

Additional analysis was done to examine the discrepancy with the wave periods. In Test A2 and B2, the wave periods increased with increasing obliquity of the waves with respect to the harbour mouth. This trend continues with increasing obliquity of the incidence waves. However, a physical sound explanation could not be given in this study.

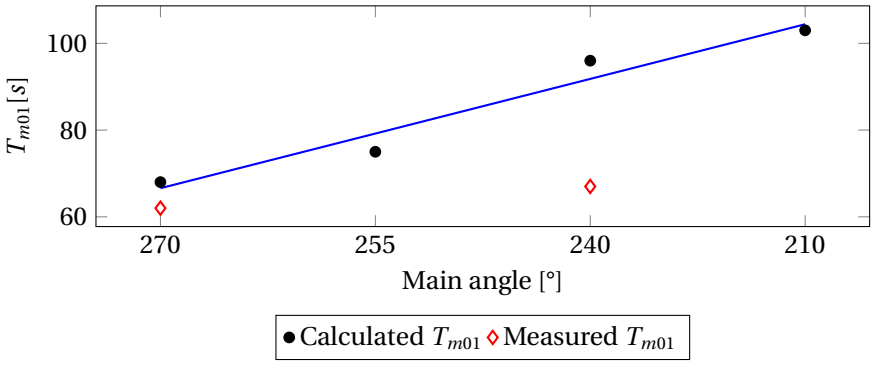

Figure A.14: Wave periods versus mean wave direction.

B

Benchmark tests for Harbour models

B.1. Model set-up non-hydrostatic and surfbeat

The model set-up is almost identical to that of the Vinjè basin case. For a detailed description of the model set-up, the reader is referred to Appendix A. For the differences between the model setup of Case I and Case II, the reader is referred to Section 8.2 of Chapter 8.

For a fair comparison, it is advised to use the initial dimensions of the data (i.e. no scaling effects). However, numerical instabilities occurred especially with the non-hydrostatic mode. This problem could be solved by running the simulations on prototype scale. Moreover, by scaling the laboratory experiments with 1:20 according to the Froude scaling law, it allows us to make a fair comparison with the study of *Monteban (2016)*. The hydraulic and numerical parameters are listed in Table B.1 for Tests T038 and T046.

Table B.1: Numerical parameters Test T038 / T046 of XBeach. Froude scaling law 1:20.

Parameter	Prototype scale	Physical model scale
Spectral wave height H_{m0} (m)	0.98 / 1.04	0.049 / 0.052
Peak wave period T_p (s)	6.67 / 6.67	1.49 / 1.49
Peak frequency (Hz)	0.15 / 0.15	0.67 / 0.67
Water depth (m)	8.8 / 8.8	0.44 / 0.44
Grid resolution SB (m)	4	N/A
Grid resolution NH (m)	1.4	N/A
Grid points per wavelength	≈ 40	N/A
Cut-off frequency (Hz)	0.04	0.4

B.2. Test T038

B.2.1. Results of the short waves

The significant wave heights H_{m0} are shown in Figures B.1a and B.1b for the SB mode and the NH mode, respectively. The absence of diffraction in the SB can be visually observed in Figure B.1a. In the side basin, the wave heights are underestimated with a factor of about 2. The NH mode shows better correspondence.

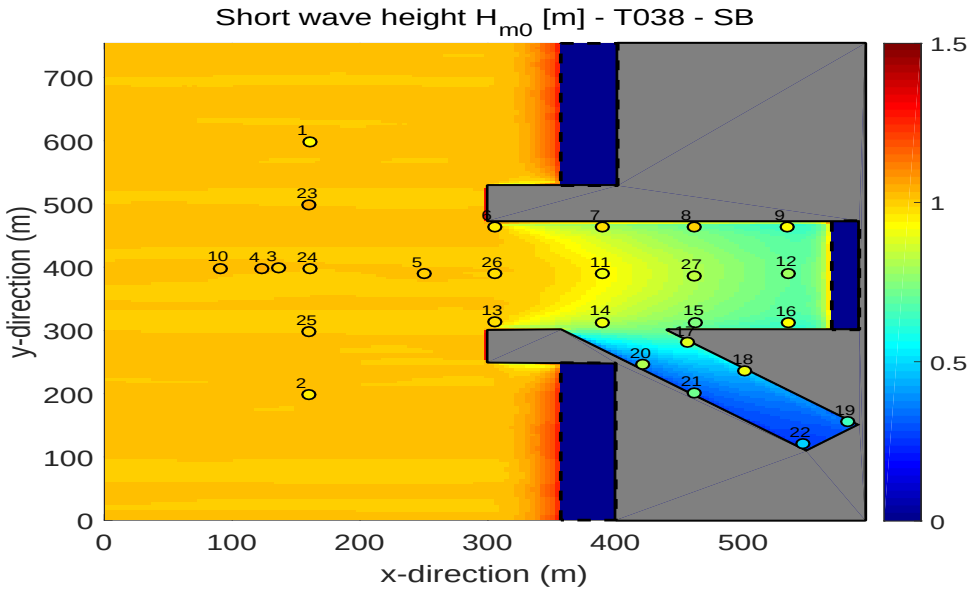

(a) Test T038: XBeach SB.

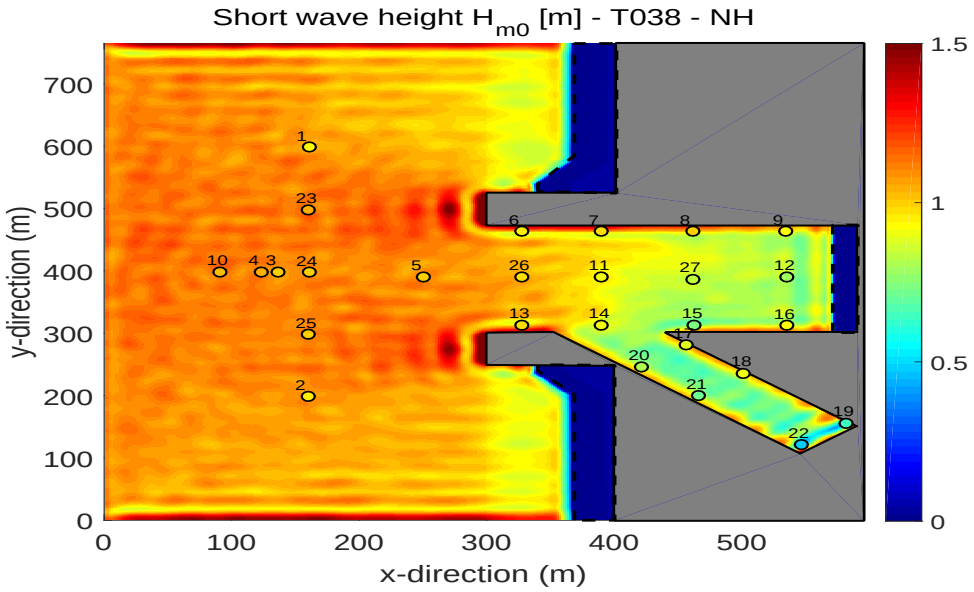

(b) Test T038: XBeach NH.

Figure B.1: Significant short wave heights H_{m0} of Test T038. The circles indicate the measured wave heights.

The NH mode shows good correspondence with the measurements. Generally at each measurement sensors, the calculated wave heights is within the 20% deviation band, as shown in Figure B.2. The calculated periods for the short waves are shown in Figure B.3. This allows us to say that XBeach NH is capable to reproduce the hydrodynamics in a fairly simple harbour basin for the short waves.

The SB mode shows larger differences for the calculated wave heights. Especially in the side basin, where diffraction is regarded as important, the SB mode cannot calculated the correct wave heights. The little amount of wave energy in the side basin is entirely due to directional spreading of the waves.

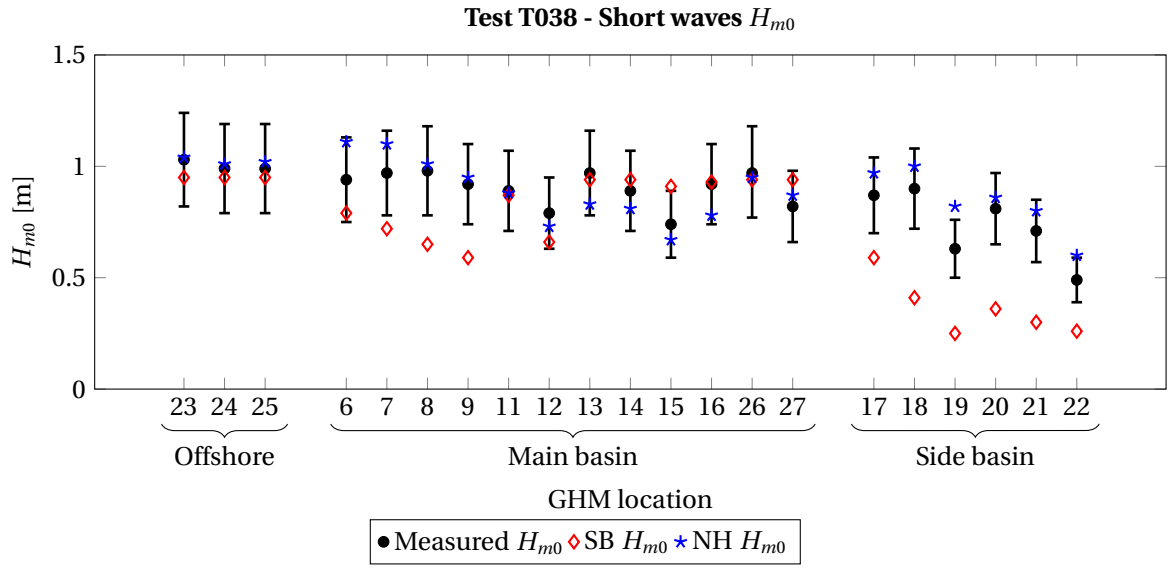

Figure B.2: Wave heights of the short waves of Test T038. MAE SB total = 0.34, MAE SB main basin = 0.17, MAE SB side basin = 0.51. MAE NH total = 0.11, MAE NH main basin = 0.10, MAE NH side basin = 0.15.

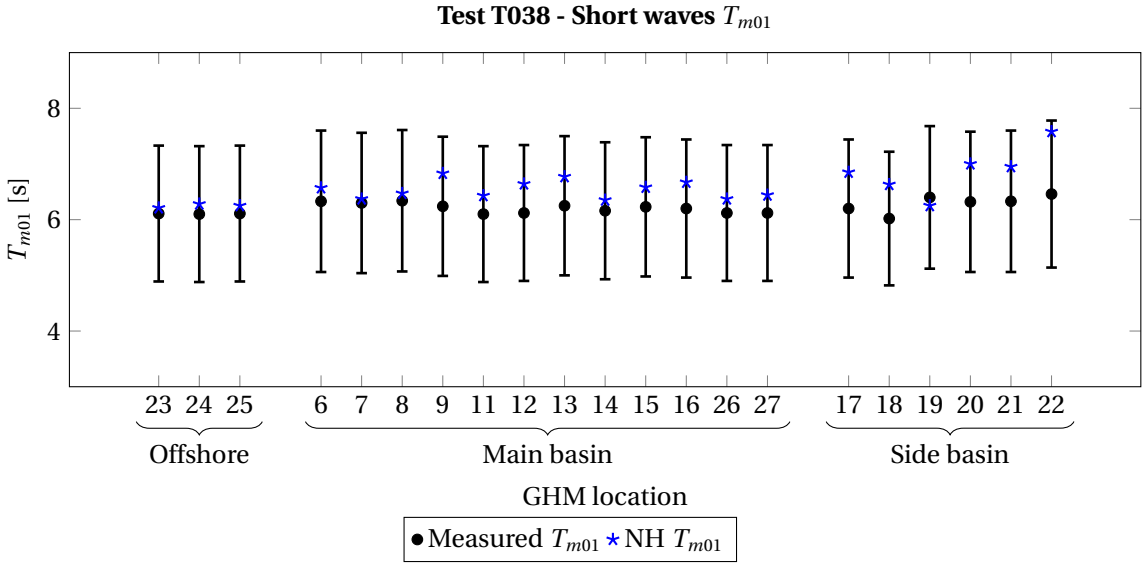

Figure B.3: Periods of the short waves of Test T038. MAE NH total = 0.06 MAE NH main basin = 0.07, MAE NH side basin = 0.08.

B.2.2. Results of the long waves

The wave heights and periods for the long waves are shown in Figures B.4 and B.5, respectively. In both modes, the wave heights are calculated in the same order of magnitude, but outside the 20% deviation band at some measurements locations. A possible explanation is insufficient friction of the quay wall. However, with MAE indices in the order of 0.10 - 0.20, the results are acceptable. The largest overestimations are to be found in the side basin.

The wave periods are generally well calculated, with MAE index in the order of 0.10.

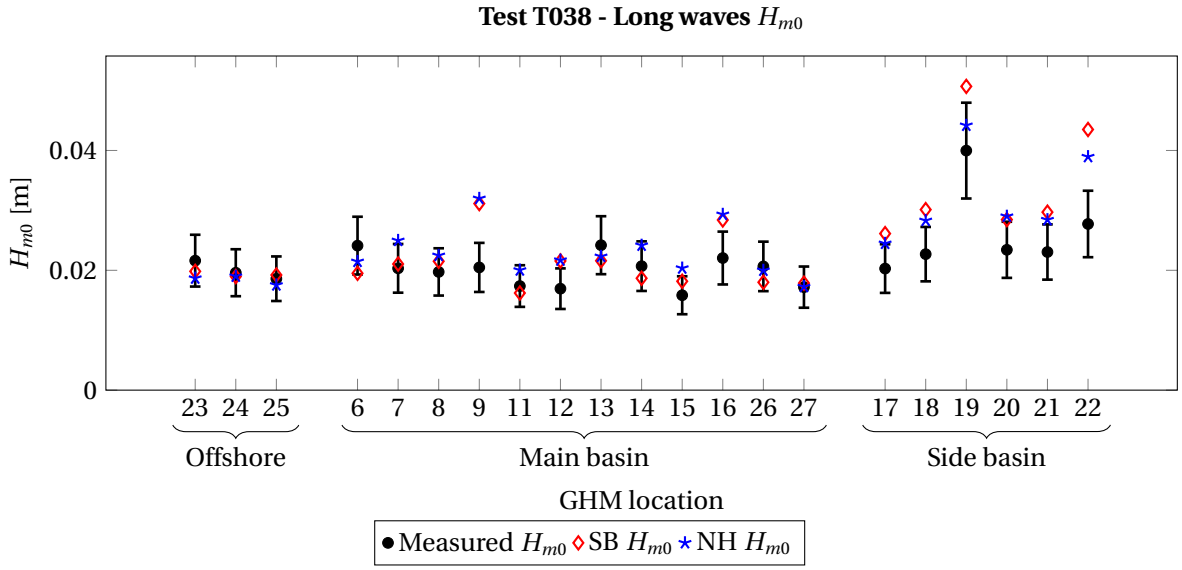

Figure B.4: Wave heights of the long waves of Test T038. MAE SB total = 0.16, MAE SB main basin = 0.17, MAE SB side basin = 0.30. MAE NH total = 0.17, MAE NH main basin = 0.20, MAE NH side basin = 0.24.

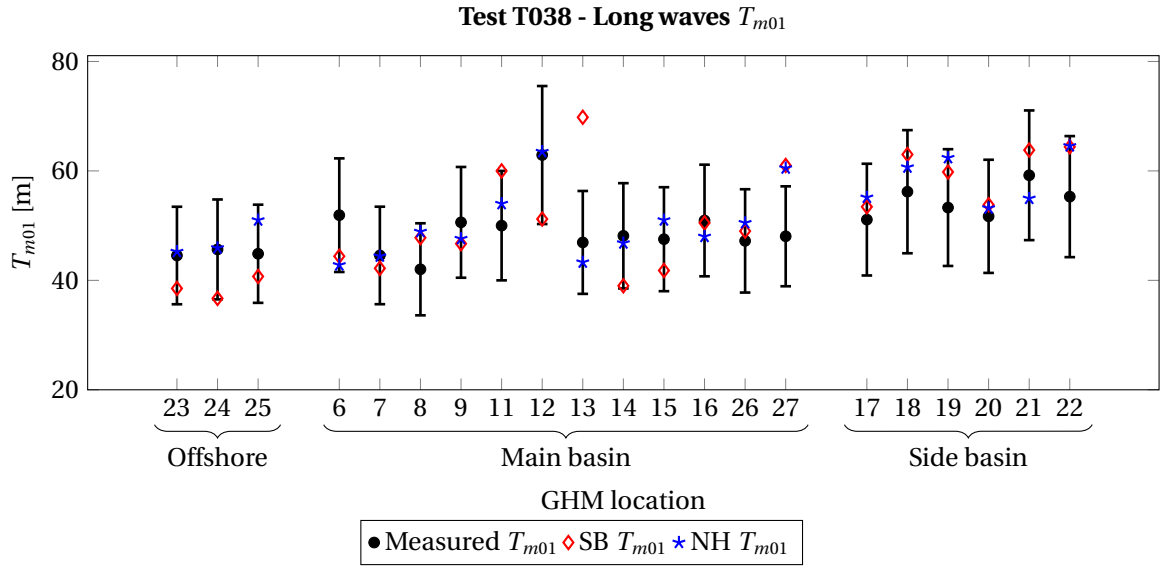

Figure B.5: Wave periods of the long waves of Test T038. MAE SB total = 0.09, MAE SB main basin = 0.10, MAE SB side basin = 0.10. MAE NH total = 0.08, MAE NH main basin = 0.09, MAE NH side basin = 0.10.

B.3. Test T046

B.3.1. Results of the short waves

The results of the significant short wave heights are shown in Figure B.6. The upper figure is the short wave field as calculated by SB and averaged over 2 hours. In the upper figure, there is hardly any energy in the side basin. In contrary to Test T038, where wave energies enter the side basin by means of directional spreading, wave energy is completely absent.

The lower figure of Figure B.6 is the significant short wave heights as calculated by NH.

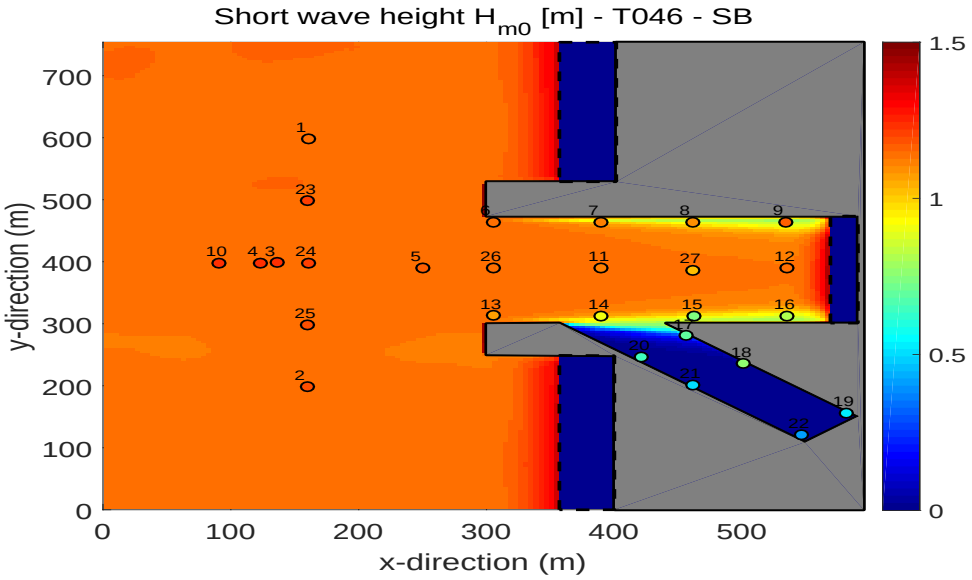

(a) Test T046: XBeach SB.

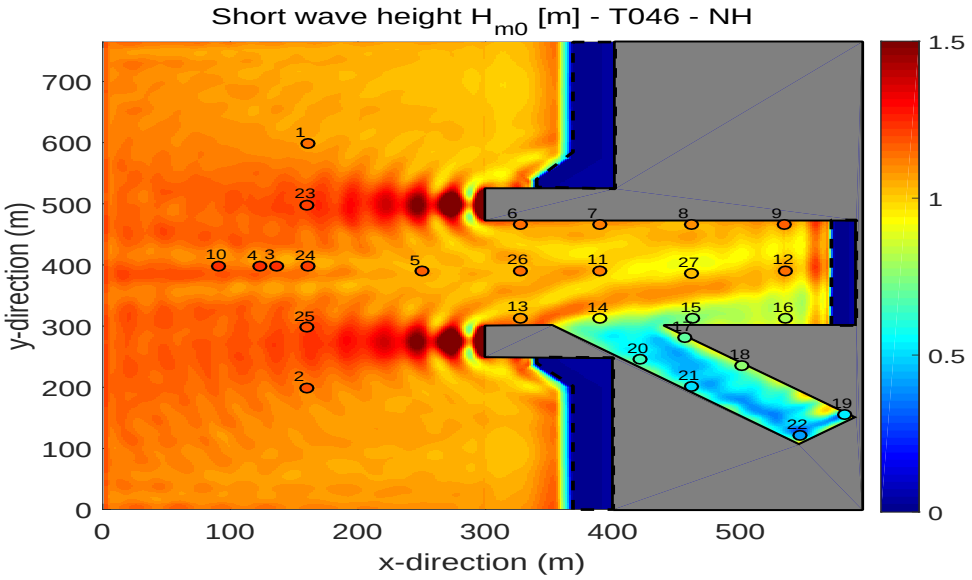

(b) Test T046: XBeach NH.

Figure B.6: Significant short wave heights of Test T046. The circles indicate the measured wave heights.

The calculated wave heights are presented in Figure B.7. The wave heights, both offshore and in the main basin are well calculated with the NH mode. The SB mode calculates the wave heights reasonably. The striking difference is to be found in the side basin. The NH mode predicts the wave heights quite well, whereas the SB underestimates the wave heights. This is expected as there is no diffraction included in the SB mode of XBeach. Based on the MAE index, the NH performs much better, especially where diffraction is not to be neglected (and also no directional spreading).

The calculated wave periods of the short waves are shown in Figure B.8 and is in good agreement with the measurements.

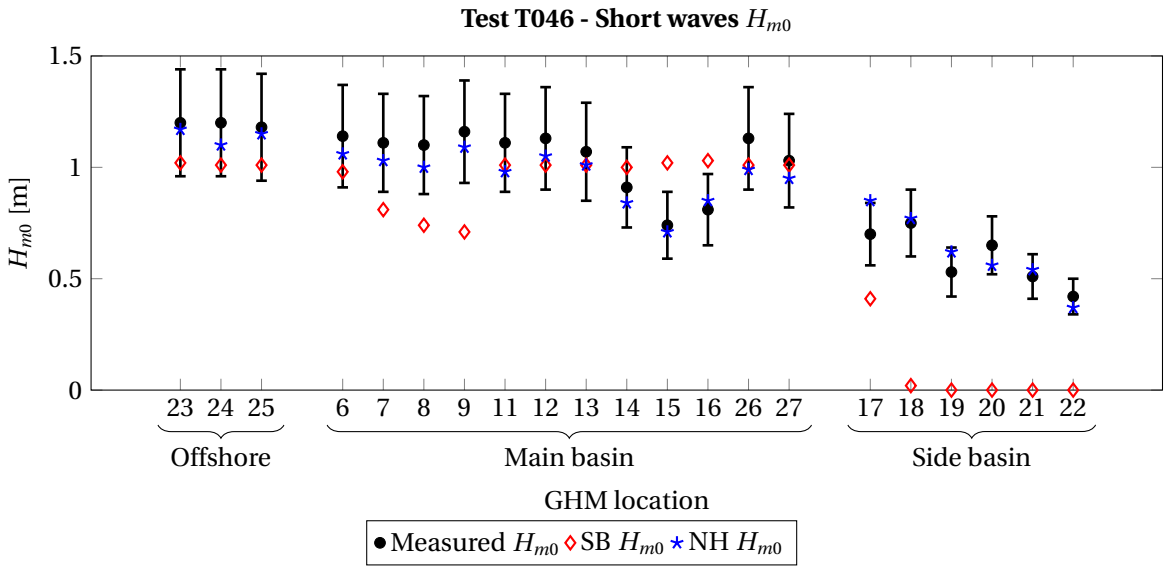

Figure B.7: Short wave heights of Test T046. MAE SB total = 0.34, MAE SB main basin = 0.31, MAE SB side basin = 0.89. MAE NH total = 0.11, MAE NH main basin = 0.10, MAE NH side basin = 0.11.

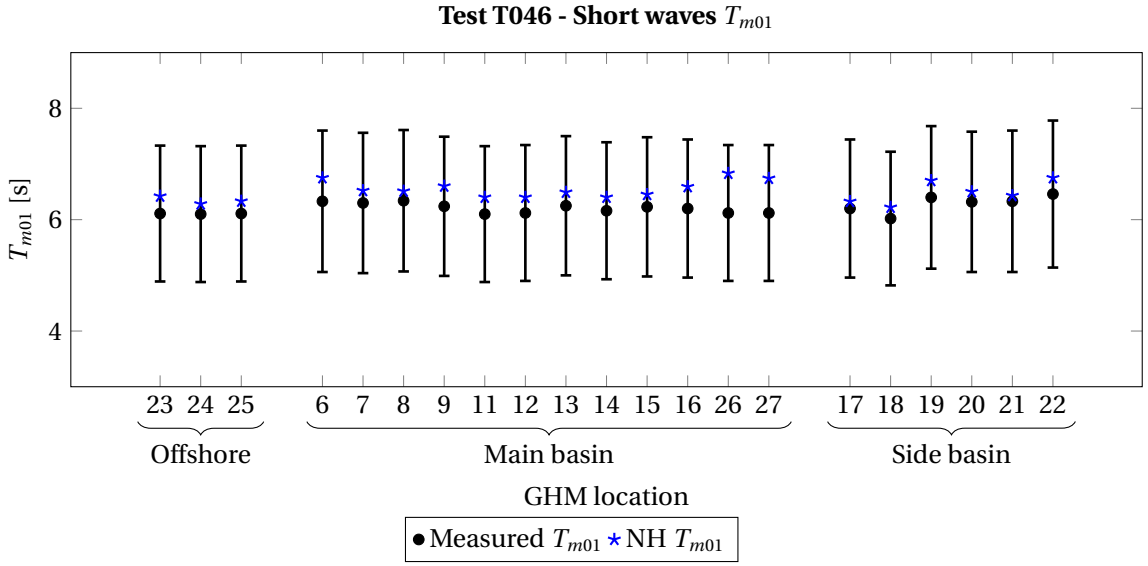

Figure B.8: Periods of the short waves of Test T038. MAE NH total = 0.07 MAE NH main basin = 0.07, MAE NH side basin = 0.07.

B.3.2. Results of the long waves

The wave heights of Test T046 are shown in Figure B.9. The striking difference is again to be found in the side basin. Both models overestimate the wave heights. However, NH is more accurate. The role of the short wave energies is demonstrated. The overestimation with these long-crested wave conditions (T038), because in this case the long waves are completely free.

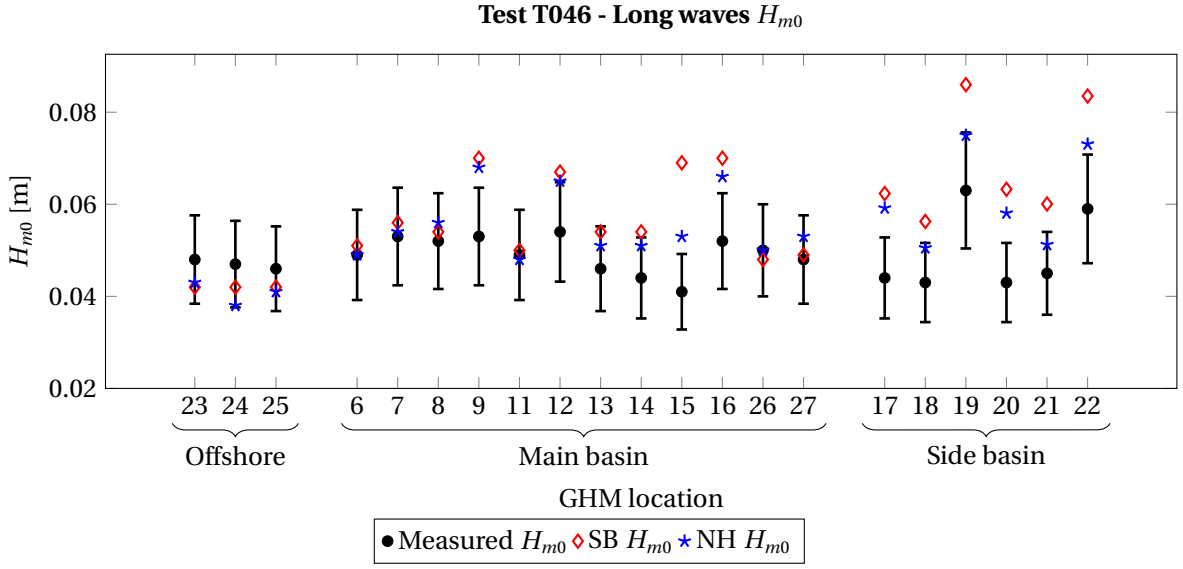

Figure B.9: Long wave heights of Test T046. MAE SB total = 0.22, MAE SB main basin = 0.17, MAE SB side basin = 0.39. MAE NH total = 0.18, MAE NH main basin = 0.11, MAE NH side basin = 0.27.

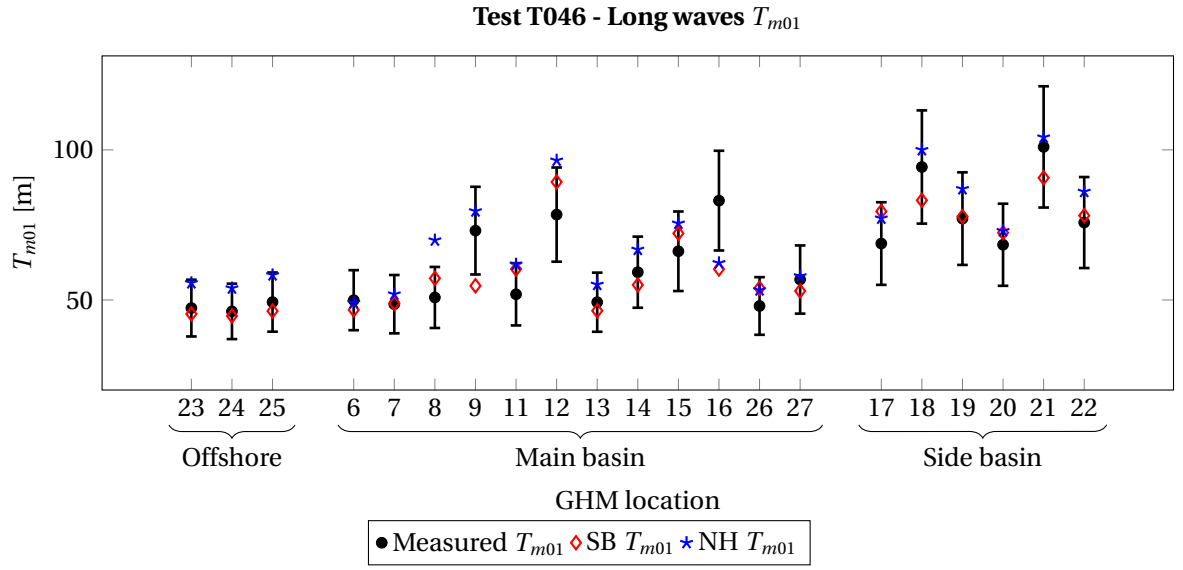

Figure B.10: Wave periods of the long waves of Test T046. MAE SB total = 0.09, MAE SB main basin = 0.10, MAE SB side basin = 0.10. MAE NH total = 0.08, MAE NH main basin = 0.09, MAE NH side basin = 0.10.

Bibliography

J Alabart, A Sanchez-Arcilla, and G P van Vledder. Analysis of the performance of swash in harbour domains. Number 1, pages 1–10 BT – Proceedings of the 3rd IAHR Europe cong, 2014. ISBN 978-989-96479-2-3.

J Battjes and J Janssen. Energy Loss and Set-Up Due To Breaking of Random Waves. *Proceedings of 16th Conference on Coastal Engineering, ASCE*, (1):569–587, 1978. ISSN 2156-1028. doi: 10.9753/icce.v16.

J A Battjes. Surf similarity. *Proceedings of ICCE*, (1):466–480, 1974. ISSN 2156-1028. doi: 10.1007/978-1-61779-361-5.

H. J. M. Bijleveld. Projectbeschrijving R&D Haves EZ-LIP: H3896.40 Validatie golfkrachten op schepen. Technical report, Delft Hydraulics, 2004.

Joas Boeyinga. Boussinesq-type wave modelling in port applications. Technical Report May, Delft University of Technology, 2010.

Margaret R Boshek. Reflection and Diffraction Around Breakwaters. Technical report, 2009.

G F Carrier and H P Greenspan. Water waves of finite amplitude on a sloping beach. *J. Fluid Mech.*, 4: 97–109, 1958. ISSN 0022-1120.

Christopher Daly. Low Frequency Waves in the Shoaling and Nearshore Zone A Validation of XBeach. Technical Report June, 2009.

Delft3D - FLOW User Manual. Delft3D - FLOW User Manual - Deltares. Technical report, 2014.

Deltares. XBeach Manual. Technical report, 2015a.

Deltares. XBeach Skillbed Report. Technical report, Deltares, Delft, 2015b.

J. P. H. Dobrochinski. A combination of SWASH and Harberth to compute wave forces on moored ships. (October), 2014. URL `http://repository.tudelft.nl/view/ir/uuid:a0b269f8-6dc3-4de0-b1bd-918577f1456f/`.

F Enet, Alphonse Nahon, Gerbrant Van Vledder, and David Hurdle. Evaluation of diffraction behind a semi-infinite breakwater in the SWAN Wave Model. pages 1–14, 2006. URL `ftp://www.wmo.int/Documents/PublicWeb/amp/mmop/documents/JCOMM-TR/J-TR-34-9th-waves-workshop/Papers/Enet.pdf`.

Matthijs Gawehn. Incident, infragravity and very low frequency wave motions on an atoll reef platform. Technical report, 2015.

Jr. G.J. Arcement and V.R. Schneider. Guide for Selecting Manning ' s Roughness Coefficients for Natural Channels and Flood Plains United States Geological Survey Water-supply Paper 2339. Technical Report 2339, 1989.

Yoshimi Goda, Tomotsuka Takayama, Suzuki, and Yasumasa. Diffraction Diagrams for Directional Random Waves. *Coastal Engineering*, pages 628–650, 1978.

L. Holthuijsen. *Waves in Oceanic and Coastal Waters*, volume 20. Cambridge University Press, Delft, 2007. ISBN 9780511618536. doi: http://dx.doi.org/10.1017/CBO9780511618536.

I Jonsson. Wave boundary layers and friction factors. *Coastal Engineering Proceedings*, pages 127–148, 1966. ISSN 2156-1028.

M.S. Longuet-Higgins and R.w. Stewart. Radiation stresses in water waves; a physical discussion, with applications. *Deep Sea Research and Oceanographic Abstracts*, 11(4):529–562, 1964. ISSN 00117471. doi: 10.1016/0011-7471(64)90001-4.

Dennis Monteban. Numerical modelling of wave agitation in ports and access channels. Technical Report June, 2016.

Ellen Quataert. Wave runup on atoll reefs. Technical Report January, 2015.

Alexander B. Rabinovich. Seiches and Harbour Oscillations. In *Handbook of Coastal and Ocean Engineering*, pages 193–236. 2009. ISBN 9789812819307. doi: 10.1142/9789812819307_0009.

B. Reijmerink. Golfrandvoorwaarden in havens. Technical Report september, 2012.

D. Rijnsdorp and M. Zijlema. Simulating waves and their interactions with a restrained ship using a non-hydrostatic wave-flow model. *Coastal Engineering*, 114:119–136, 2016. ISSN 0378-3839. doi: 10.1016/j.coastaleng.2016.04.018. URL `http://dx.doi.org/10.1016/j.coastaleng.2016.04.018`.

Dano Roelvink, Ad Reniers, Ap van Dongeren, Jaap van Thiel de Vries, Robert McCall, and Jamie Lescinski. Modelling storm impacts on beaches, dunes and barrier islands. *Coastal Engineering*, 56(11-12): 1133–1152, 2009. ISSN 03783839. doi: 10.1016/j.coastaleng.2009.08.006.

J. A. Roelvink. Dissipation in random wave groups incident on a beach. *Coastal Engineering*, 19(1-2): 127–150, 1993. ISSN 03783839. doi: 10.1016/0378-3839(93)90021-Y.

S. E. Sand. Long waves in directional seas. *Coastal Engineering*, 6, 1982. doi: 10.1016/0378-3839(82)90018-7.

P.b. Smit. Non-hydrostatic modelling of large scale tsunamis. Technical report, 2008.

G. S. Stelling and S. P A Duinmeijer. A staggered conservative scheme for every Froude number in rapidly varied shallow water flows. *International Journal for Numerical Methods in Fluids*, 43(12):1329–1354, 2003. ISSN 02712091. doi: 10.1002/fld.537.

Jas Sutherland, A. H. Peet, and R. L. Soulsby. Evaluating the performance of morphological models. *Coastal Engineering*, 51(8-9):917–939, 2004. ISSN 03783839. doi: 10.1016/j.coastaleng.2004.07.015.

G. Symonds, D. A. Huntley, and Anthony J. Bowen. Two-dimensional surf beat: Long wave generation by a time-varying breakpoint. *Journal of Geophysical Research*, 87(C1):492, 1982. ISSN 0148-0227. doi: 10.1029/JC087iC01p00492.

A.J. van der Hout, M.P.C. de Jong, F. Jaouen, and O.J. Waals. Long Waves in Intermediate Depths and Their Influence on Design of Nearshore Terminals. In *IAHR World Congress*, pages 1–12, 2015.

Wim van der Molen. *Behaviour of Moored Ships in Harbours*. PhD thesis, Delft University of Technology, 2006.

P.P.D. van der Ven. Benchmark tests of wave penetration in harbours. Technical report, Deltares, 2016.

A. van Dongeren, J. Battjes, T. Janssen, J. van Noorloos, K. Steenhauer, G. Steenbergen, and A. Reniers. Shoaling and shoreline dissipation of low-frequency waves. *Journal of Geophysical Research: Oceans*, 112(2):1–15, 2007. ISSN 21699291. doi: 10.1029/2006JC003701.

Pieter Van Geer, Bram De Vries, Ap Van Dongeren, and Jaap Van Thiel de Vries. Dune Erosion Near Sea Walls: Model-Data Comparison. *Coastal Engineering Proceedings*, 1(33):sediment.102, 2012. ISSN 2156-1028. doi: 10.9753/icce.v33.sediment.102.

F van Mierlo. Numerical Modelling of Wave Penetration in Ports. Technical Report November, Delft University of Technology, Delft, 2014.

G Watson and H Peregrine. Low frequency waves in the surf zone. *23rd Int. Conf. on Coastal Eng. ASCE*, 818:818–831, 1992.

Marcel Zijlema and Guus Stelling. Efficient computation of surf zone waves using the nonlinear shallow water equations with non-hydrostatic pressure. *Coastal Engineering*, 55(10):780–790, 2008. ISSN 03783839. doi: 10.1016/j.coastaleng.2008.02.020.

Marcel Zijlema and Guus S. Stelling. Further experiences with computing non-hydrostatic free-surface flows involving water waves. *International Journal for Numerical Methods in Fluids*, 48(2):169–197, 2005. ISSN 02712091. doi: 10.1002/fld.821.

Marcel Zijlema, Guus Stelling, and Pieter Smit. SWASH: An operational public domain code for simulating wave fields and rapidly varied flows in coastal waters. *Coastal Engineering*, 58(10):992–1012, 2011. ISSN 03783839. doi: 10.1016/j.coastaleng.2011.05.015.